

**INVESTIGATING INTRINSIC AND EXTRINSIC FACTORS THAT REGULATE
CANCER CELL MOTILITY**

by

LISA RACHELLE DECOTRET

B.Sc., Carleton University, 2015

A THESIS SUBMITTED IN PARTIAL FULFILLMENT OF
THE REQUIREMENTS FOR THE DEGREE OF

DOCTOR OF PHILOSOPHY

in

THE FACULTY OF GRADUATE AND POSTDOCTORAL STUDIES

(Pathology and Laboratory Medicine)

THE UNIVERSITY OF BRITISH COLUMBIA

(Vancouver)

June 2022

© Lisa Rachelle Decotret, 2022

The following individuals certify that they have read, and recommend to the Faculty of Graduate and Postdoctoral Studies for acceptance, the dissertation entitled:

Investigating intrinsic and extrinsic factors that regulate cancer cell motility.

submitted by Lisa Decotret in partial fulfillment of the requirements for

the degree of Doctor of Philosophy

in Pathology and Laboratory Medicine

Examining Committee:

Dr. Kevin Bennewith, Associate Professor, Department of Pathology and Laboratory
Medicine, UBC.

Co-supervisor

Dr. Catherine Pallen, Emeritus Professor, Department of Pediatrics, UBC.

Co-supervisor

Dr. Karla Williams, Assistant Professor, Faculty of Pharmaceutical Sciences, UBC.

Supervisory Committee Member

Dr. Christopher Maxwell, Associate Professor, Department of Pediatrics, UBC.

University Examiner

Dr. Andrew Minchinton, Associate Professor, Department of Pathology and Laboratory
Medicine, UBC.

University Examiner

Additional Supervisory Committee Members:

Dr. James Chinten Lim, Associate Professor, Department of Pediatrics, UBC.

Supervisory Committee Member

Dr. Stephen Yip, Associate Professor, Department of Pathology and Laboratory Medicine,
UBC.

Supervisory Committee Member

Abstract

Mechanisms of cellular motility are highly conserved and regulate many physiological processes including embryonic development, wound healing, and angiogenesis. Cancer cells can exploit normal mechanisms of cellular motility to facilitate invasion and metastasis, the process by which cancer cells disseminate to distant organs. Invasion can be triggered by a host of intrinsic and extrinsic factors, many of which remain unknown. Here, I investigate the role of one intrinsic factor (receptor-type protein tyrosine phosphatase alpha) and one extrinsic factor (ionizing radiation) in facilitating cancer cell invasion.

Receptor-type protein tyrosine phosphatase alpha (PTP α) is a widely expressed transmembrane-bound protein that has been implicated in integrin signaling, focal adhesion formation, and normal cell migration. During normal cell migration, cells use focal adhesions to facilitate cycles of cell adhesion to, and release from, the extracellular matrix (ECM). Focal adhesion structures bear resemblance to invadopodia, which are dynamic actin-based protrusions that form on the plasma membrane of cancer cells. In this study, I hypothesized that PTP α promotes invadopodia-mediated triple-negative breast cancer (TNBC) cell invasion. My work involving the depletion of PTP α in TNBC reveals PTP α as a regulator of ECM degradation and invasion *in vitro* and *in vivo*. My studies suggest that PTP α is an intrinsic regulator of TNBC cell invasion.

Radiation therapy is among the most common treatments for cancer. While radiation is an effective treatment option, there have been reports showing the surviving fraction of cells may exhibit increased invasiveness. Since the precise mechanisms that modulate ionizing radiation (IR)-induced invasion remain largely unknown, the goal of this study was to investigate the role

of IR in upregulating key signaling mechanisms associated with invadopodia activity. Our studies revealed IR upregulates a key invadopodium protein, TKS5, expression while decreasing Glioblastoma multiforme (GBM) cell invasion *in vitro*, suggesting GBM cells invade independently of invadopodia. I then developed an *ex vivo* brain slice invasion assay to investigate mechanisms of GBM cell invasion into brain tissue. Using this model, I found a subset of GBM spheroids exhibited increased invasion post-irradiation. These studies suggest IR is a potential extrinsic regulator of GBM invasion when cells are within the brain microenvironment.

Lay Summary

It was reported in 2021 that cancer is the leading cause of death accounting for 30% of all deaths in Canada. The primary cause of cancer-related mortality is metastasis, the process by which cancer cells break free from the original tumour and spread to other sites in the body allowing for new tumours to grow. Metastasis remains poorly understood. A further understanding of the mechanisms of metastasis is critical for finding ways to limit or prevent the spread of cancer.

Here, my research focuses on investigating various ways cancer cells spread throughout the body. I explore (i) the role of a widely expressed transmembrane molecule called receptor-like protein tyrosine phosphatase alpha ($PTP\alpha$) in breast cancer cell invasion and (ii) the effects of radiation therapy on brain cancer cell invasion.

Preface

Chapter 1: I created the chapter outline, conducted the literature search, and wrote 95% of the text in the Introduction section. Dr. Catherine Pallen and Dr. Kevin Bennewith assisted with editing this chapter. This work is currently unpublished.

Chapter 2: A version of Chapter 2 has been published. Dr. Brennan Wadsworth assisted with tumour implantation. Ling Vicky Li performed the MMP14 flow cytometry experiments. Katie Milne from the Deeley Research Center in Victoria, BC performed all immunohistochemical staining. Dr. Brennan Wadsworth, Ling Vicky Li, and Dr. James Lim edited the final versions of the manuscript. Dr. Kevin Bennewith assisted with experimental design and editing the published manuscript. Dr. Catherine Pallen conceptualized the project, secured funding, and assisted with experimental design, and editing the published manuscript. I performed 90% of all experiments presented in Chapter 2, analyzed all data, and wrote the published manuscript.

Decotret, L.R., Wadsworth, B.J., Li, L., Lim, C.J., Bennewith, K.L., and Pallen, C.J. (2021). Receptor-type protein tyrosine phosphatase alpha (PTP α) influences MMP14 localization and facilitates triple-negative breast cancer cell invasion. *Molecular Biology of the Cell*, 32(7):567-578.

Chapter 3: The work presented in Chapter 3 was conceptualized in collaboration with Dr. Kevin Bennewith. I designed the experiments with input from Dr. Kevin Bennewith, performed 90% of all experiments, analyzed and interpreted all data presented herein, and wrote all text. Rachel Cederberg performed and analyzed the PI flow cytometry experiments. Monica Hsu assisted

with cell culture maintenance, generating tumour spheroids, and performing western blot experiments. Che-Min Lee generated cDNA samples for qPCR and Ling Vicky Li performed the qPCR experiments.

Chapter 4: The work presented in Chapter 4 was conceptualized in collaboration with Dr. Kevin Bennewith. I performed all experiments, analyzed and interpreted the data presented herein, and wrote the entire chapter. Che-Min Lee assisted with cryosectioning, staining, and imaging hypoxia in tumour spheroids. Rocky Shi developed the ImageJ macro for analyzing *ex vivo* brain slice invasion. Kiersten Thomas assisted with the brain slice fixation protocol.

Decotret L.R, Shi, R., Thomas, K.N., Hsu, M., Pallen, C.J., and Bennewith K.L.

Development and validation of an advanced *ex vivo* brain slice invasion assay to model glioblastoma cell invasion into the complex brain microenvironment. *In Preparation.*

Chapter 5: Unpublished material written by me.

Ethics Approval Information: All animal experiments were performed in accordance with the Canadian Council on Animal Care guidelines under the UBC research ethics certificates A17-0231 – “Promotion of metastasis by tumour hypoxia and immune cells” and A21-0266 - “Immune cells and tumour hypoxia affect primary and metastatic tumour growth”.

Table of Contents

Abstract.....	iii
Lay Summary.....	v
Preface.....	vi
Table of Contents	viii
List of Tables	xiii
List of Figures.....	xiv
List of Symbols	xvii
List of Abbreviations	xviii
Acknowledgements	xxii
Dedication	xxiv
Chapter 1: Introduction	1
1.1 Overview of cellular motility.....	1
1.1.1 Aberrant cell migration and invasion.....	1
1.2 Mechanisms of cancer cell motility	2
1.2.1 Overview of invadosomes.....	3
1.2.2 Overview of matrix metalloproteases (MMPs).....	6
1.2.3 Signaling mechanisms that modulate invadopodia formation and function.	7
1.3 Investigating intrinsic regulators of cancer cell invasion.	11
1.3.1 Overview of the PTP superfamily.....	11
1.3.1.1 Oncogenic roles of PTPs.....	12
1.3.1.2 Protein tyrosine phosphatase alpha (PTP α).....	13

1.3.1.3	Physiological roles of PTP α	15
1.3.1.4	Role of PTP α in oncogenic signaling and cancer cell invasion.	18
1.4	Investigating extrinsic regulators of cancer cell invasion.....	19
1.4.1	Electromagnetic radiation.	19
1.4.2	Radiation therapy.....	20
1.4.3	Biological responses of cancer cells to ionizing radiation.....	22
1.4.4	Ionizing radiation-induced cancer cell invasion.	24
1.4.5	Role of IR in invadopodia-associated signaling mechanisms.....	26
1.5	Rationale and hypotheses.....	30
1.5.1	Role of PTP α in breast cancer invasion.....	30
1.5.2	Role of ionizing radiation in Glioblastoma cell invasion.	31
1.5.3	Cell lines	32

Chapter 2: Receptor-type protein tyrosine phosphatase alpha mediates MMP14

	localization and facilitates triple-negative breast cancer cell invasion.	33
2.1	Rationale and Hypothesis	33
2.2	Materials and Methods.....	35
2.2.1	Cell culture.....	35
2.2.2	Transfection (siRNA and plasmids).....	36
2.2.3	Lentiviral Transfection (shRNA).....	36
2.2.4	Antibodies and reagents.....	37
2.2.5	Matrix degradation assay	38
2.2.6	Immunoblotting.....	38
2.2.7	IncuCyte chemotaxis assays	39

2.2.8	MMP antibody array	39
2.2.9	ELISAs.....	39
2.2.10	Flow cytometry	40
2.2.11	Immunofluorescence.....	40
2.2.12	Orthotopic xenograft tumour model	41
2.2.13	Immunohistochemistry	41
2.2.14	Statistical analysis.....	42
2.3	Results.....	42
2.3.1	Depletion of PTP α does not affect PTP ϵ expression.....	42
2.3.2	PTP α mediates matrix degradation.....	43
2.3.3	Expression of PTP α is important for TNBC invasion.....	45
2.3.4	Knockdown of PTP α does not impact the secretion of soluble MMPs.....	47
2.3.5	PTP α mediates MMP14 localization to the membrane.....	50
2.3.6	PTP α localizes to endosomes but does not localize to invadopodia.....	52
2.3.7	Depletion of PTP α inhibits tumour growth.....	61
2.3.8	PTP α knockdown upregulates <i>in vivo</i> apoptotic signaling.....	63
2.3.9	Depletion of PTP α decreases the aggressiveness of breast tumour xenografts....	65
2.4	Discussion.....	68

Chapter 3: Ionizing radiation upregulates TKS5 expression in GBM cells *in vitro*

independent of invadopodia activity and cellular invasion.....	74
3.1 Rationale and Hypothesis	74
3.2 Materials and Methods.....	76

3.2.1	Cell culture.....	76
3.2.2	Antibodies and reagents.....	77
3.2.3	Immunoblotting.....	77
3.2.4	Matrix degradation assay	78
3.2.5	Immunofluorescence.....	78
3.2.6	Cell Survival Assays.....	78
3.2.6.1	Clonogenic survival assay.....	78
3.2.6.2	Flow Cytometry	79
3.2.7	Real time qPCR.....	79
3.2.8	<i>In vitro</i> chemotaxis invasion assays.....	80
3.3	Results.....	80
3.3.1	TKS5 and Src expression in glioma cell lines.	80
3.3.2	GBM cells primarily utilize focal adhesions to degrade ECM.	81
3.3.3	LN229 and LN18 cells respond to irradiation.	84
3.3.4	Ionizing radiation upregulated TKS5 mRNA and protein expression levels.	87
3.3.5	Focal adhesion-mediated gelatin degradation is upregulated by IR.	93
3.3.6	Ionizing radiation decreases <i>in vitro</i> GBM cell invasion.....	95
3.4	Discussion.....	98
Chapter 4: Development and validation of an advanced <i>ex vivo</i> brain slice invasion assay to model glioblastoma cell invasion into the complex brain microenvironment.....		103
4.1	Rationale and Hypothesis	103
4.2	Materials and Methods.....	106
4.2.1	Cell culture.....	106

4.2.2	Detection of spheroid hypoxia	106
4.2.3	<i>In vitro</i> spheroid invasion assay	107
4.2.4	Generation of organotypic brain slices	107
4.2.5	Alamar blue metabolic assay	108
4.2.6	<i>Ex vivo</i> brain slice spheroid invasion assay	108
4.2.7	Antibodies	109
4.2.8	Immunofluorescence	109
4.3	Results	110
4.3.1	Ionizing radiation decreases GBM spheroid invasion <i>in vitro</i>	110
4.3.2	Development of an advanced <i>ex vivo</i> brain slice invasion assay	115
4.3.3	Optimization of deep tissue imaging strategies.	117
4.3.4	GBM cells exhibit different patterns of invasion <i>in vitro</i> versus <i>ex vivo</i>	119
4.3.5	Quantifying tumour cell invasion into brain slices.	121
4.3.6	Organotypic brain slices from adult C57BL/6J mice exhibit increased viability in serum-containing media	123
4.3.7	Ionizing radiation alters GBM cell invasion into <i>ex vivo</i> brain slices.	130
4.4	Discussion	132
	Chapter 5: Conclusions and Future Directions.....	137
5.1	Summary	137
5.2	Future Directions	138
	References	149
	Appendix: Supplemental Tables.....	167

List of Tables

Table 1.1 Oncogenic roles of protein tyrosine phosphatases (PTPs).....	14
Table A1. List of investigated cell lines.....	167
Table A2. Troubleshooting guide for the <i>ex vivo</i> brain slice spheroid invasion assay.....	168

List of Figures

Figure 1.1 Pathways involved in invadopodia initiation, stabilization, and activation	8
Figure 1.2 Categorization of protein tyrosine phosphatases (PTPs) into receptor-like PTPs or non-transmembrane PTPs	16
Figure 1.3 Mechanisms of DNA double strand break repair	23
Figure 2.1 Small interfering RNA (siRNA)-mediated PTP α knockdown does not alter PTP α expression or cellular proliferation <i>in vitro</i>	44
Figure 2.2 Depletion of PTP α reduces extracellular matrix (gelatin) degradation	46
Figure 2.3 Generation of shRNA-expressing MDA-MB-231 cells stably depleted of PTP α	48
Figure 2.4 PTP α regulates migration and invasion of TNBC cells	49
Figure 2.5 Depletion of PTP α does not alter the secretion of soluble MMPs	51
Figure 2.6 PTP α knockdown decreases MMP14 localization to plasma membrane protrusions	53
Figure 2.7 PTP α does not localize to TKS5-positive invadopodia structures	57
Figure 2.8 PTP α localizes to caveolin-1-positive and early endosome antigen-1-positive endosomal structures	60
Figure 2.9 Depletion of PTP α reduces primary tumour growth of MDA-MB-231 breast xenografts	62
Figure 2.10 Depletion of PTP α upregulates intratumoural cleaved caspase-3 expression levels <i>in vivo</i>	64
Figure 2.11 Depletion of PTP α decreases the aggressiveness of breast tumour xenografts	66
Figure 3.1 TKS5 and Src protein expression levels do not predict GBM cell invasion.	82

Figure 3.2 Gelatin degradation can occur at sites of invadopodia or focal adhesions in glioma cells.	83
Figure 3.3 Analysis of LN229 and LN18 cell survival following exposure to ionizing radiation.	85
Figure 3.4 Exposure to ionizing radiation upregulates TKS5 mRNA and protein expression in LN229 cells.	88
Figure 3.5 Ionizing radiation minimally alters invadopodia formation.....	91
Figure 3.6 Focal adhesion-mediated ECM degradation is upregulated by ionizing radiation.....	94
Figure 3.7 Ionizing radiation reduces <i>in vitro</i> GBM cell invasion through Matrigel.	96
Figure 4.1 Assessment of spheroid size and levels of hypoxia prior to irradiation.....	111
Figure 4.2 Ionizing radiation inhibits GBM spheroid invasion in a dose-dependent manner	113
Figure 4.3 <i>Ex vivo</i> brain slice spheroid invasion assay workflow	116
Figure 4.4 Confocal imaging techniques to improve depth of imaging	118
Figure 4.5 Different invasive phenotypes of GBM cells when embedded into Matrigel versus murine brain tissue.....	120
Figure 4.6 Workflow of a semi-automated ImageJ macro used to quantify invasion into <i>ex vivo</i> brain slice cultures	122
Figure 4.7 Time course of LN229 and LN18 GFP-tagged GBM spheroids invading into brain tissue <i>ex vivo</i>	124
Figure 4.8 Assessment of brain slice viability in culture.....	126
Figure 4.9 Spheroid placement does not impact invasiveness.....	129
Figure 4.10 Ionizing radiation minimally impacts GBM spheroids invasion into brain tissue <i>ex vivo</i>	131

Figure 5.1 Preliminary data shows PTP α knockdown decreases caveolin-1 phosphorylation at tyrosine position 14 (cav-1-pY14).....140

Figure 5.2 Representative images displaying interactions between GFP-expressing GBM cells and alpha-smooth muscle actin (α SMA)-positive vasculature or glial fibrillary acidic protein (GFAP)-positive astrocytes within the surrounding brain environment.....146

List of Symbols

α alpha

β beta

ε epsilon

List of Abbreviations

α SMA	alpha smooth muscle actin
ADAMs	a disintegrin and metalloproteinases
ADP	adenosine diphosphate
Arp2/3	actin related protein 2/3
BBB	blood-brain barrier
BSA	bovine serum albumin
CAFs	cancer-associated fibroblasts
Cav-1	caveolin-1
CC3	cleaved caspase 3
CDC42	cell division control protein 42 homology
cDNA	complementary DNA
DAPI	4',6-diamidino-2-phenylindole
DIV	days <i>in vitro</i>
DMEM	Dulbecco's Modified Eagle's Medium
DMSO	dimethyl sulfoxide
DNA	deoxyribonucleic acid
DSB	double-strand breaks
EEA1	early endosome antigen 1
ELISA	enzyme-linked immunosorbent assay
EM	electromagnetic
FA	focal adhesions
FBS	fetal bovine serum

FGF	fibroblast growth factor
GBM	Glioblastoma multiforme
GFAP	glial fibrillary acidic protein
Gy	gray
H&E	hematoxylin and eosin
HIF-1 α	hypoxia-inducible factor 1-alpha
HI-HS	heat-inactivated horse serum
HR	homologous repair
IDH1/2	isocitrate dehydrogenase $\frac{1}{2}$
KDa	kilodalton
MBP	myelin basic protein
MEFs	mouse embryonic fibroblasts
Mena ^{INV}	mena invasive
MMP	matrix metalloproteinase
mRNA	messenger RNA
mSv	millisievert
NADPH	nicotinamide adenine dinucleotide phosphate
NHEJ	non-homologous DNA end joining
NOD	nonobese diabetic
NOX	NADPH oxidase
NSG	NOD SCID gamma
N-WASP	neural wiskott-aldrich syndrome protein
PARP	poly (ADP-ribose) polymerase

PDGF	platelet-derived growth factor
Pen-Step	penicillin-streptomycin
PI(3)P	phosphatidylinositol 3-phosphate
PI(3,4)P ₂	phosphatidylinositol 3,4-bisphosphate
PBS	phosphate buffered saline
PBST	0.2% tween-20 in PBS
PFA	paraformaldehyde
PRL	phosphatases of regenerating liver
PSP	protein serine/threonine phosphatase
PTK	protein tyrosine kinase
PTP	protein tyrosine phosphatase
PTP α	receptor-type protein tyrosine phosphatase alpha
PTP1B	protein tyrosine phosphatase 1B
PVDF	polyvinylidene difluoride membrane
RhoA	ras homolog family member A
RIPA	radioimmunoprecipitation assay
RNA	ribonucleic acid
ROCK	rho-associated protein kinase
ROS	reactive oxygen species
RT	room temperature
SCID	severe combined immunodeficiency
SD	standard deviation
SDS	sodium dodecyl sulfate

SEM	standard error of the mean
siRNA	small-interfering RNA
shRNA	short hairpin RNA
SSB	single-strand breaks
STS	Staurosporine
TGF β	transforming growth factor beta
TIMP	tissue inhibitors of matrix metalloproteinases
TKS	tyrosine kinase substrate
TKS5	tyrosine kinase substrate with 5 SH3 domains
TNBC	triple-negative breast cancer
TMZ	temozolomide
UV	ultraviolet
VEGF	vascular endothelial growth factor
WT	wild-type
ZEB1/2	Zinc Finger E-Box Binding Homeobox 1 or 2

Acknowledgements

It has been an honour to complete my PhD degree at the BC Cancer Research Center. First and foremost, thank you to my supervisors Dr. Catherine Pallen and Dr. Kevin Bennewith for their mentorship, unwavering support and guidance, and always believing in my abilities as a scientist. A special thank you goes to my current supervisor Dr. Kevin Bennewith for always being available to discuss my data, plan future experiments and setting an example of how to maintain a healthy work-life balance. Thank you to my committee members (Dr. James Lim, Dr. Karla Williams, Dr. Stephen Yip, and Dr. William Lockwood) for thoughtful discussions and advice on how to keep pushing forward.

I would also like to thank the previous members of the Pallen Lab (Dr. Jing Wang, Dr. Philip Ly, Dr. Dominik Sommerfeld, and Cassandra Dawson) for endless support, guidance and lots of laughs over the years. Thank you to all members of the Bennewith lab (Dr. Liz Halvorsen, Dr. Elizabeth Franks, Dr. Brennan Wadsworth, Dr. Natalie Firmino, Rachel Cederberg, Rocky Shi, Che-Min Lee, Kiersten Thomas, Michael Hall, and Monica Hsu), for welcoming me into the lab, lending an ear to listen, and always sharing a booth with me at Rouge. I would also like to thank my collaborators Ling Vicky Li and Dr. James Lim at the BC Children's Research Institute for their assistance with my experiments, as well as Dr. Amanda Harvey and Dr. Neil Cross from the University of Sheffield in Sheffield, UK for welcoming me into their lab for the summer and teaching me how to culture organoids. Finally, thank you to Dr. Michael Lizardo and Dr. Philip Ly for sharing your confocal microscopy expertise.

This dissertation would not have been possible without the help of some key members of the Department of Pathology and Laboratory Medicine including Dr. Hayden Pritchard, Dr. Dana Devine, Dr. H  l  ne C  t  , and Heather Cheadle for ensuring my success in graduate school.

Thank you to the staff at the BC Cancer Research Cancer, particularly Gayle Paquette and Tara MacDonald in the Animals Resource Center, and to Katy Milne at the Deeley Cancer Research Center in Victoria, BC for completing our immunohistochemical staining at rocket speeds.

Thank you to my amazing friends (Hung, Kat, Alice, Paul, Jill, Brycen, Sophy, Jacob, Lu, Dustin) for being my Vancouver family and always being there through the highs and lows of graduate school. I would like to thank my family for their constant support through my graduate school endeavors. Finally, thank you to my husband for your daily encouragement and being an enormous help over the past 7 years. This is for you.

To my loving husband.

Chapter 1: Introduction

1.1 Overview of cellular motility

Cellular motility plays a central role in many normal physiological processes including embryonic development, muscle contractions, wound healing, and the movement of immune cells throughout the body (Lauffenburger and Horwitz, 1996). In a developing embryo, cells collectively migrate as sheets to form three germ layers, which eventually give rise to various tissues and organs (Keller, 2005). Furthermore, leukocytes exit the vasculature via diapedesis and migrate to sites of injury or infection to initiate an immune response (Geng, 2001). Cellular migration is a complex process by which cells can move individually or as collective groups in the form of clusters, strands, or sheets often in response to external stimuli from neighboring cells or the surrounding microenvironment (Stuelten et al., 2018).

1.1.1 Aberrant cell migration and invasion

Aberrant regulation of cellular migration can drive the progression of several diseases including cancer cell invasion and metastasis. Metastasis, the movement of cancer cells throughout the body, is initiated when cancer cells break free from the primary tumour mass, invade through the surrounding tissue, intravasate into the vasculature or lymphatic system, extravasate from these vessels, and colonize new tissue (Fares et al., 2020; Karaman and Detmar, 2014; Stuelten et al., 2018; van Zijl et al., 2011). Despite being a highly inefficient process, at least 66% of all cancer-related deaths are due to metastasis (Dillekås et al., 2019). Thus, a better understanding of the complex mechanisms of cancer cell motility is important for limiting the spread of cancer.

1.2 Mechanisms of cancer cell motility

During the initial stages of the metastatic cascade, tumour cells detach from the primary tumour mass and invade into the surrounding extracellular matrix (ECM) (Stuelten et al., 2018). The ECM is a complex component of the microenvironment comprised of a cross-linked network of fibrous proteins (*i.e.* collagens and fibronectin) and proteoglycans (Walker et al., 2018). Increased matrix cross-linking leads to a stiffer ECM, which has been shown to induce the invasiveness of cancer cells (Gkretsi and Stylianopoulos, 2018). Increased matrix stiffness has also been shown to induce epithelial to mesenchymal transition (EMT) in mammary epithelial cells resulting in increased breast cancer cell invasion (Chen et al., 2013; Wei et al., 2015). EMT is a dynamic process by which epithelial cells undergo morphological and functional alterations to become mesenchymal cells, marked by enhanced invasiveness, increased resistance to apoptosis, and elevated levels of ECM-degrading proteinases (Kalluri and Weinberg, 2009).

It has been established that cancer cells may utilize protease-dependent (Fisher et al., 2006; Hotary et al., 2006; Sabeh et al., 2009, 2004) or protease-independent (Sabeh et al., 2009; Sahai and Marshall, 2003; Wolf et al., 2003) mechanisms of cellular invasion depending on the structural properties of the surrounding ECM. Protease-dependent mechanisms of cellular invasion rely heavily on matrix metalloproteinase-14 (MMP14) to enzymatically degrade surrounding ECM. Protease-independent mechanisms are thought to be driven by RhoA- and ROCK-dependent contractility that involves cancer cells adopting an amoeboid-like mechanism of motility in order to squeeze through pores in the matrix (Poincloux et al., 2009; Sabeh et al., 2009). More recently, Wisdom *et al.* assessed the role of matrix plasticity on cancer cell motility and found that cells in highly plastic matrices first utilize protease-dependent, invadopodia-

mediated mechanisms of invasion to enzymatically degrade the matrix and then generate contractile forces to move through the “holes” previously generated by invadopodia in a protease-independent manner (Wisdom et al., 2018). Others have reported that stromal cells within the tumour microenvironment, such as cancer-associated fibroblasts (CAFs), possess invadopodia-independent degradative properties that can promote the invasion of tumour cells (Cao et al., 2016). Importantly, both protease-dependent and -independent mechanisms of cancer cell dissemination may result in the formation of metastases.

In sections 1.2.1 and 1.2.2, I will describe a group of structures that facilitate protease-dependent invasion collectively referred to as “invadosomes”.

1.2.1 Overview of invadosomes

Invadosomes, a term referring to both podosomes and invadopodia, are key structures involved in facilitating cellular invasion (Linder, 2009). Podosomes were first discovered and isolated from macrophages in 1977 (Davies and Stossel, 1977). Shortly after, invadopodia were described as proteolytically active protrusions that form on the plasma membrane of chicken embryo fibroblasts transformed with Rous sarcoma virus (Chen, 1989; David-Pfeuty and Singer, 1980; Tarone et al., 1985). While podosomes and invadopodia share a similar function, they differ in cell of origin, stability, size, shape, and protein composition. Podosome formation occurs in normal cells, such as vascular smooth muscle cells, endothelial cells, and immune cells, have a relatively short turnover time of a few minutes, and form ring-like protrusive structures called “rosettes” (Eddy et al., 2017; Murphy and Courtneidge, 2011). Invadopodia primarily form in Src-transformed and malignant cancer cells, are relatively stable structures with a turnover time on the order of hours, and are often longer protrusions than podosomes (Eddy et

al., 2017; Murphy and Courtneidge, 2011). Notably, there are several other structures that facilitate cell-matrix adhesions and cellular motility including focal adhesions, lamellipodia, and filopodia that do not fall under the umbrella term of 'invadosomes' due to their lack of proteolytic activity (Paterson and Courtneidge, 2018).

Invadopodia form at the plasma membrane of highly invasive cancer cells and mediate multiple stages of metastasis including initial invasion into the ECM, intravasation, and extravasation (Eckert and Yang, 2011; Gligorijevic et al., 2012; Leong et al., 2014). The presence of invadopodia on invasive cells is often identified by the formation of proteolytically active TKS5 (tyrosine kinase substrate with 5 SH3 domains)-rich puncta (Abram et al., 2003; Seals et al., 2005). TKS5 is a scaffolding protein that belongs to the family of tyrosine kinase substrate (TKS) adaptor proteins and consists of a N-terminal phospho homology (PX) domain, five Src homology 3 (SH3) domains, and several proline-rich regions (Kudlik et al., 2020; Saini and Courtneidge, 2018). Unlike other invadopodia-associated proteins that localize to various cellular structures, TKS5 is considered highly specific to invadopodia structures (Abram et al., 2003; Seals et al., 2005). TKS5 is also a direct substrate of Src and was found to be constitutively phosphorylated at tyrosine positions 552, 557 and 619 in Src-transformed fibroblasts (Lock et al., 1998). This Src-mediated phosphorylation of TKS5 promotes binding of the PX domain to phospholipid PI(3,4)P₂ on the plasma membrane, which allows other proteins to bind to TKS5 creating multi-protein complexes and initiating the formation of invadopodia (Abram et al., 2003; Oikawa et al., 2012). Thus, TKS5 plays a critical role in the formation and stabilization of invadopodia precursor structures (Sharma et al., 2013).

Invadopodia have been found to have an outer invasive ring positive for focal adhesion-associated proteins such as vinculin, paxillin, and integrins (Branch et al., 2012; Mueller et al., 1999). Thus, some reports suggest focal adhesions are precursor structures to invadopodia. Other data suggest focal adhesions and invadopodia are distinct structures that form independently of one another. Depletion of focal adhesion kinase (FAK) was found to increase invadopodia activity and results in the preferential localization of active, phosphorylated Src from focal adhesions to invadopodia (Chan et al., 2009; Kolli-Bouhafs et al., 2014). Future work is required to determine the precise relationship between focal adhesions and invadopodia structures, and how these structures either work together or in competition to facilitate cancer cell motility.

Extensive research has been conducted to characterize invadopodia in a variety of malignant cancer cell lines using two-dimensional *in vitro* ECM degradation assays (Paz et al., 2014). Despite a large body of pre-clinical data, invadopodia have only recently been observed *in vivo*. Initial *in vivo* studies identified invadopodia-like protrusive structures degrading naïve basement membrane isolated from rat peritoneum (Schoumacher et al., 2010), in the intestine of zebrafish (Seiler et al., 2012) and by following anchor cell invasion in *C. elegans* (Hagedorn et al., 2013). More recently, a chicken embryo model has been used to study invadopodia-mediated invasion across the chorioallantoic membrane (CAM) using high resolution intravital microscopy (Leong et al., 2014; Williams et al., 2019). In 2019, TKS5-positive structures were identified in paraffin-embedded human pancreatic tumour specimens as well as paraffin-embedded tissue collected from malignant tumours within stomach, colon, rectal, gallbladder, breast, and brain tissue (Baik et al., 2019; Chen et al., 2019a, 2019b). Although clinical data is limited, the identification of TKS5-positive structures in patient samples suggests the presence of

invadopodia within human tumours and highlights the importance of therapeutically targeting invadopodia to block cancer cell invasion and metastasis.

1.2.2 Overview of matrix metalloproteases (MMPs)

The proteolytic activity of invadopodia is primarily mediated by matrix metalloproteinases (MMPs), which are a group of zinc-dependent enzymes that remodel tissue and have been implicated in many normal physiological processes including angiogenesis, wound healing, and embryogenesis (Cui et al., 2017). Since the initial discovery of MMP1 in 1962, there have been 28 MMPs identified in vertebrates, of which 24 are expressed in human tissue (Iyer et al., 2012; Laronha and Caldeira, 2020). MMPs can be subdivided into six groups based on structure and substrate specificity (Cathcart et al., 2015; Cui et al., 2017): collagenases (MMP1, MMP8, MMP13, MMP18), gelatinases (MMP2, MMP9), stromolysins (MMP3, MMP10, MMP11), Matrilysins (MMP7, MMP26), membrane-type (MMP14, MMP15, MMP16, MMP17, MMP24, MMP25), and other (MMP12, MMP19, MMP20, MMP21, MMP22, MMP23, MMP27, MMP28). The MMP family of proteases also includes 8 closely related ADAMs (a disintegrin and metalloproteinases) and 4 TIMPs (tissue inhibitors of metalloproteinases) (Cathcart et al., 2015).

MMP2, MMP9, and MMP14 have been found to localize to invadopodia, and are considered necessary for enzymatic activity of invadopodia and cancer cell invasion (Artym et al., 2006; Chen and Wang, 1999; Clark et al., 2007; Jacob and Prekeris, 2015; Monsky et al., 1993; Nakahara et al., 1997; Poincloux et al., 2009). MMP2 and MMP9 are secreted gelatinases that primarily recognize and cleave gelatin (denatured collagen) while MMP14 is a transmembrane-bound protease that has a broader recognition for various substrates that can also

activate certain soluble MMPs (Cathcart et al., 2015; Poincloux et al., 2009). As such, the combined activity of MMP2, MMP9, and MMP14 is critical for the function of invadopodia. The precise signaling mechanisms involved in targeting MMPs to invadopodia are further discussed in section 1.2.3.

1.2.3 Signaling mechanisms that modulate invadopodia formation and function.

Invadopodia formation is a highly complex process that occurs in three stages that involve multiple signaling pathways: initial precursor formation, precursor stabilization, and invadopodia maturation (Beatty and Condeelis, 2014; Eddy et al., 2017) (Figure 1.1).

Initiation: Invadopodia precursor formation is initiated by several stimuli including growth factors, epithelial to mesenchymal transition (EMT), and hypoxia (Eddy et al., 2017). Growth factors known to induce invadopodia formation in several human cancer cell lines include epithelial growth factor (EGF), transforming growth factor- β (TGF- β), platelet-derived growth factor (PDGF), and hepatocyte growth factor (HGF) (Beatty and Condeelis, 2014; Eddy et al., 2017; Jacob and Prekeris, 2015; Yamaguchi et al., 2005). EGF stimulation promotes activation of the epithelial growth factor receptor (EGFR) to facilitate the binding and activation of Src, which induces downstream signaling pathways critical for invadopodia precursor formation (Mader et al., 2011) (Figure 1). Twist1, Twist2, Snail, Slug, ZEB1, and ZEB2 transcription factors are known activators of EMT (Dongre and Weinberg, 2019). Twist1-induced PDGFR α expression in response to TGF- β stimulation has been shown to mediate Src-induced invadopodia formation outlining the role of EMT in stimulating invadopodia formation and function (Eckert and Yang, 2011). Hypoxic conditions have also been shown to increase the expression of neural Wiskott-

Aldrich syndrome protein (N-WASP), an actin regulatory protein important for cytoskeleton reorganization in invadopodia precursors (Salvi and Thanabalu, 2017) (Figure 1.1). Invadopodia precursor initiation involves the recruitment of several proteins: cortactin, N-WASP, cofilin, Arp2/3, and F-actin (Eddy et al., 2017). TKS5 is then recruited to the precursor complex and acts as a scaffold protein to stabilize the entire protein complex (Sharma et al., 2013). Since many of these proteins are also found in lamellipodia, filopodia, and podosomes, the colocalization of TKS5 with actin cytoskeletal proteins (*i.e.*, cortactin, actin, *etc.*) is currently used to identify invadopodial structures.

Stabilization: Following initiation, the precursor structures become stabilized and anchored to the plasma membrane. MENA interacts with SHIP2, which aids in the conversion of the phosphoinositide PI(4,5)P to PI(3,4)P₂ (Beaty and Condeelis, 2014) (Figure 1.1). It has been proposed that the precursor structures weakly bind to PI(3,4)P₂ enriched sites on the plasma membrane via the phox homology (PX) domain on TKS5 (Abram et al., 2003; Sharma et al., 2013). The invadopodia precursors are then further stabilized by β 1 integrin-mediated adhesion (Beaty and Condeelis, 2014) (Figure 1.1). Notably, α 2, α 3, α 5, α 6, and β 1 integrins have been reported to localize to invadopodia (Beaty et al., 2013; Beaty and Condeelis, 2014; Branch et al., 2012; Peláez et al., 2019). It is known that β 1 integrin interacts with Arg, a tyrosine kinase, resulting in Arg phosphorylation. However, β 1 integrin activation is not sufficient to fully activate Arg (Beaty and Condeelis, 2014). EGFR-mediated activation of Src results in Arg and subsequently cortactin phosphorylation, which mediates the recruitment of Nck1 to precursor structures inducing actin polymerization via the Arp2/3 complex (Jacob and Prekeris, 2015; Stylli et al., 2009; Yamaguchi et al., 2005) (Figure 1.1). Thus, the EGFR–Src–Arg pathway is important to induce actin

polymerization in invadopodia precursors (Mader et al., 2011). Hypoxia is also thought to induce signaling pathways critical for invadopodia precursor stabilization and maturation. Diaz *et al.* showed the induction of hypoxia in BxPC3 pancreatic cells increased invadopodia formation and function through HIF1 α -dependent activation of Notch signaling (Díaz et al., 2013).

Maturation: Stabilization is followed by invadopodia maturation, which involves actin polymerization and MMP recruitment. Invadopodium elongation occurs via increased actin polymerization, which is partially regulated by Arg kinase activity (Mader et al., 2011). Arg mediates cortactin phosphorylation, which regulates cofilin-dependent actin polymerization required for invadopodia maturation (Beaty et al., 2013; Beaty and Condeelis, 2014; Eddy et al., 2017) (Figure 1.1). Mena^{INV} (Mena invasive) promotes actin polymerization and invadopodia maturation by inhibiting protein tyrosine phosphatase 1B (PTP1B)-mediated dephosphorylation of cortactin (Weidmann et al., 2016). Mature invadopodia function by secreting matrix metalloproteinases (MMP2, MMP9) and utilize membrane-bound MMP14 to enzymatically degrade ECM and facilitate cancer cell invasion. The delivery of MMP14 to invadopodia is thought to be regulated by RhoA and Cdc42 signaling mechanisms (Eddy et al., 2017; Jacob and Prekeris, 2015; Sakurai-Yageta et al., 2008). Depletion of MMP14 from MDA-MB-231 breast cancer cells does not alter invadopodia precursor formation; however, the invadopodial structures are unable to degrade the ECM (Artym et al., 2006). Rab40b has been found to regulate MMP2 and MMP9 trafficking to invadopodia (Jacob et al., 2013). The recruitment and activation of MMPs to invadopodia remains an active area of research.

1.3 Investigating intrinsic regulators of cancer cell invasion.

Cellular invasion can be triggered by a diverse array of intrinsic and extrinsic factors. Intrinsic regulators of cancer cell invasion may include genetic aberrations that induce invasiveness such as the induction of oncogenic signaling pathways. While extrinsic regulators of cancer cell invasion may include stimuli from the surrounding microenvironment or interactions between cancer cells and stromal cells (*i.e.* cancer-associated fibroblasts, immune cells, etc.).

In Section 1.3, I will discuss the role of a potential oncogene, protein tyrosine phosphatase alpha (PTP α), in facilitating cancer cell invasion. The role of an extrinsic factor, ionizing radiation, in mediating cancer cell invasion will be discussed in Section 1.4.

1.3.1 Overview of the PTP superfamily.

Protein phosphatases are a group of enzymes that function by dephosphorylating tyrosine and/or serine/threonine residues, commonly referred to as protein tyrosine phosphatases (PTPs) or protein serine/threonine phosphatases (PSPs), respectively. PTPs and PSPs often oppose the functions of protein tyrosine kinases (PTKs) and serine/threonine kinases (STKs), enzymes that catalyze protein phosphorylation (Alonso et al., 2004). The coordination between kinases and phosphatases is key in regulating many cellular processes including cellular proliferation, metabolism, apoptosis, and motility. Thus, aberrant regulation of protein phosphorylation has been implicated in the pathogenesis of many diseases including diabetes and cancer (Du and Grandis, 2015; Hale et al., 2017).

Here, we will focus on protein tyrosine phosphatases (PTPs), which belong to a family of enzymes consisting of over 110 phosphatases (Tonks, 2006; Tonks et al., 1988). PTPs can be classified into four groups: Class I cysteine-based PTPs, Class II cysteine-based PTPs, Class III cysteine-based PTPs, and Class IV Asp-based PTPs (Alonso et al., 2004). Class I PTPs, which contains “classical” PTPs as well as dual-specific protein phosphatases (DSPs), is the largest and best characterized group of PTPs. Within the Class I PTP group, there are 38 “classical” PTPs that can be further subdivided into receptor-like (RTPTPs) and intracellular non-receptor enzymes (NRPTPs) (Andersen et al., 2004) (Figure 1.2). Class II PTPs represent one low molecular weight PTP (LMPTP), Class III defines Cdc25 phosphatases (cdc25A, cdc25B, and cdc25C), and Class IV describes four EyA genes shown to have phosphatase activity (Alonso et al., 2004).

1.3.1.1 Oncogenic roles of PTPs.

Since phosphorylation activates many signaling pathways, kinases traditionally act as oncogenes while phosphatases act as tumour suppressor genes. The first phosphatase recognized as a tumour suppressor was Phosphatase and Tensin Homolog (PTEN), which is frequently lost or mutated in various tumour types and found to promote tumorigenesis (Bollu et al., 2017). It has become more widely accepted that phosphatases can also dephosphorylate an inhibitory site on kinases to activate the protein (Tonks, 2013). Accumulating evidence suggests that the dysregulation of phosphatases can result in increased tumour formation and metastasis indicating PTPs may act as oncogenes. The oncogenic roles of various PTPs have been extensively reviewed (Du and Grandis, 2015; Hardy et al., 2018; Motiwala and Jacob, 2006; Östman et al., 2006; Tonks, 2006), which is further summarized in Table 1 (Table 1.1).

Protein tyrosine phosphatase non-receptor 11 (PTPN11), also known as Src homology region 2 domain-containing phosphatase-2 (SHP2), was the first phosphatase to be accepted as an oncogene in leukemia (Chan and Feng, 2007; Tartaglia et al., 2003; Tonks, 2006). PTP1B has also been recognized as a positive regulator of tumorigenesis (Bentires-Alj and Neel, 2007; Julien et al., 2007; Zhu et al., 2007). The phosphatase of regenerative liver (PRL) PTP family consists of PRL-1, PRL-2, and PRL-3 phosphatases, of which PRL-3 has been found to promote oncogenesis (Cramer et al., 2014; Hardy et al., 2018; Q. Zeng et al., 2003; Zimmerman et al., 2013). Interestingly, the oncogenic role of protein tyrosine phosphatase alpha (PTP α) seems varied and appears to be tumour-specific (Table 1.1). Whether PTP α plays a tumour-promoting or tumour-limiting role in other tumour types remains elusive and warrants further investigation.

1.3.1.2 Protein tyrosine phosphatase alpha (PTP α).

Protein tyrosine phosphatase alpha (PTP α) is a ubiquitously expressed transmembrane protein with particularly high expression in the brain and kidney (Sap et al., 1990). Receptor-type PTPs (RTPTPs) can be classified into eight distinct subtypes (R1 – R8) based on catalytic domain sequence similarities (Figure 1.2). PTP α , along with homolog protein tyrosine phosphatase epsilon (PTP ϵ), define the R4 RTPTP subtype. Unique features of PTP α are the presence of two intracellular catalytically active domains (D1 and D2) and a short extracellular domain. The majority of enzymatic activity occurs in the D1 domain with minor activity detected in the D2 domain (Wang and Pallen, 1991). Post-translational modifications involve extensive N- and O-linked glycosylation of the extracellular domain of the precursor protein (100 KDa) giving rise to the mature form of PTP α (130 KDa) (Daum et al., 1994).

Table 1.1 Oncogenic roles of protein tyrosine phosphatases (PTPs).

PTP	Technique	Tumour Type/ Cells	Observations	References
SHP2	Knockdown	Leukemia	Reduced apoptosis and growth.	(Tartaglia et al., 2003; Xu et al., 2005)
	Knockdown	Breast	Loss of growth.	(Zhou et al., 2008)
PTP1B	Knockout	Breast	Reduced tumorigenicity.	(Bentires-Alj and Neel, 2007)
	Overexpression	Gastric	Increased proliferation, colony formation, and tumorigenicity.	(Wang et al., 2011)
	Overexpression	Breast	Induced tumorigenesis.	(Julien et al., 2007)
PRL-3	Knockdown	Colon	Reduced tumour growth.	(Zhu et al., 2007)
	Overexpression	Colon	Increased invasion and metastasis.	(Q. Zeng et al., 2003)
	Knockout	Colon	Reduced clonogenicity and tumour formation.	(Cramer et al., 2014)
PTPRE	Knockdown	Colon	Reduced tumour formation and metastasis.	(Jiang et al., 2011; Zimmerman et al., 2013)
	Overexpression	Breast	Increased hyperplasia and tumour development.	(Elson, 1999; Elson and Leder, 1995)
	Overexpression	Fibroblasts	Cellular transformation and Src activation.	(Zheng et al., 1992)
PTPRA	Overexpression	Colon	Increased invasion.	(Krndija et al., 2010)
	Overexpression	Breast	Reduced metastasis.	(Ardini et al., 2000)

1.3.1.3 Physiological roles of PTP α

PTP α has been implicated in a number of normal physiological processes including neuronal differentiation and development, integrin signaling, as well as focal adhesion formation and cellular migration (Pallen, 2003).

Neuronal Differentiation and Development: PTP α is highly expressed in brain tissue (Sahin et al., 1995; Sap et al., 1990). The mRNA expression of PTP α was found to increase during neuronal differentiation of murine P19 embryonic cells and N1E-115 neuroblastoma cells (den Hertog et al., 1993). Genetically modified mice lacking PTP α remain viable but exhibit varied phenotypes including decreased anxiety and locomotor activity as determined by a Morris water maze (Skelton et al., 2003), as well as reduced body weight and adiposity (Cohen-Sharir et al., 2019). PTP α knockout mice have been found to have impaired learning capabilities as well as altered brain morphology with a smaller cerebellum compared to control mice (Petroni, 2003). Previous work from our lab has shown that oligodendrocyte precursor cells (OPCs) isolated from PTP α -null mouse embryos displayed enhanced OPC proliferation and defects in OPC differentiation, which correlated with an overall reduction in myelination (Shih et al., 2017; Wang et al., 2012, 2009).

Integrin Signaling: PTP α plays a dual role in integrin signaling as an upstream activator and downstream effector of proto-oncogene c-Src (Ponniah et al., 1999; Su et al., 1999). Mouse c-Src contains 533 amino acids while human c-Src contains an additional 3 amino acids resulting in 536 amino acids in total. Human Src contains a conserved tyrosine residue (Tyr⁴¹⁹) that activates Src upon autophosphorylation (Tyr⁴¹⁶ in mice) and an inhibitory tyrosine site at tyrosine residue

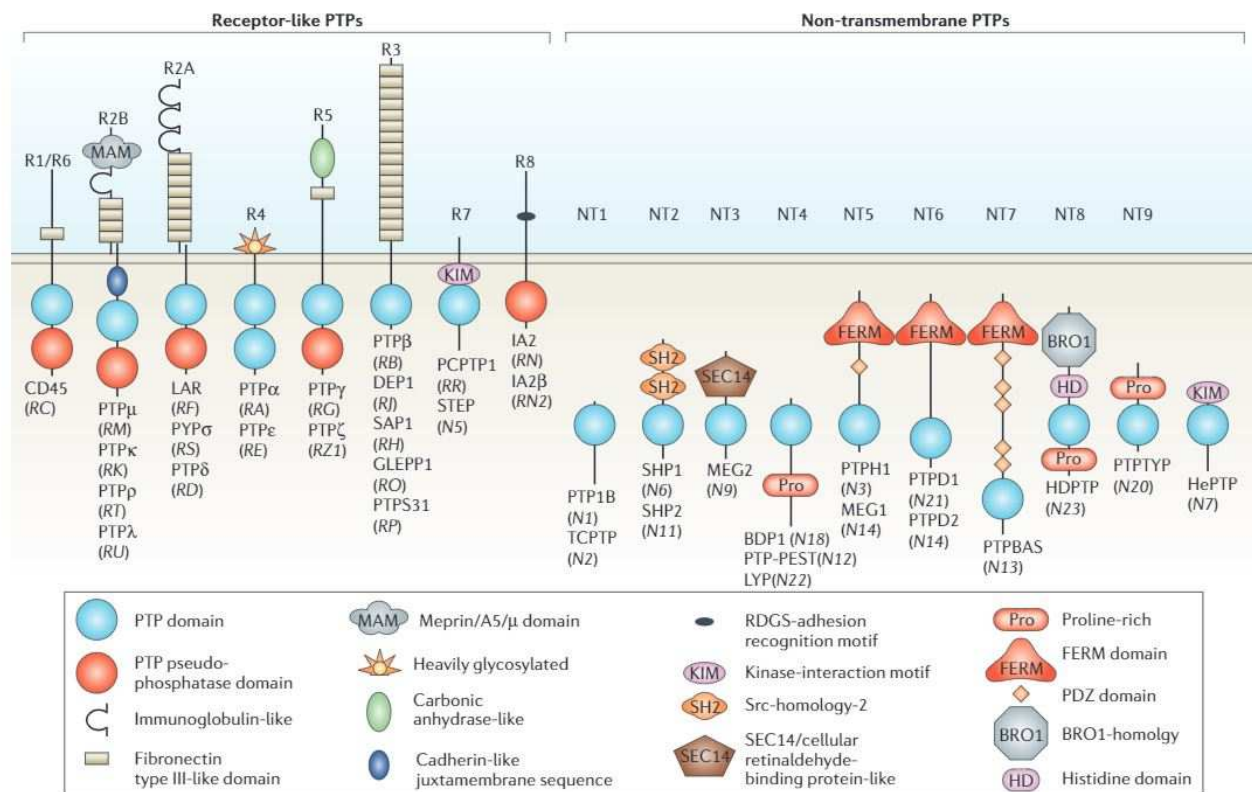


Figure 1.2. Categorization of protein tyrosine phosphatases (PTPs) into receptor-like PTPs or non-transmembrane PTPs.

Protein tyrosine phosphatases (PTPs) are classified as receptor-like PTPs (R1, R2A, R2B, R3, R4, R6, R7, R8) or non-transmembrane PTPs (NT1, NT2, NT3, NT4, NT5, NT6, NT7, NT8, NT9). PTPs are assigned to each subtype based on catalytic domain sequence similarities. For instance, PTP α and PTP ϵ are classified as receptor subtype R4 since both PTPs are receptor-bound, have two intracellular PTP domains and an extracellular heavily glycosylated region. Figure used with permission from N.K. Tonks *Nature Reviews Molecular Cell Biology* 7, 833-846 (2006).

530 (Tyr⁵²⁷ in mice) (Bjorge et al., 2000). It is currently known that PTP α acts proximal to integrins to activate c-Src via dephosphorylation at the C-terminal regulatory site (Tyr⁵³⁰), promoting the formation of the Src-FAK tyrosine kinase complex (Chen et al., 2006; L. Zeng et al., 2003). Activated Src in the Src-FAK complex then phosphorylates PTP α at Tyr⁷⁸⁹, which facilitates cellular migration (Chen et al., 2006; L. Zeng et al., 2003). In fact, fibroblasts derived from the embryos of PTP α knockout mice display enhanced Src phosphorylation at Tyr⁵²⁷ accompanied by reduced Src activity (Su et al., 1999; Ponniah et al., 1999). However, little is known about the role of PTP α in cancer cell motility and it is possible that that PTP α / PTP α -pTyr⁷⁸⁹ are important in Src-mediated signaling mechanisms that regulate invadopodia formation and function to promote the invasive motility of malignant cells.

Cellular migration: As previously mentioned, PTP α has been shown to regulate cellular migration. PTP α was found to colocalize with integrins at the leading edge of the cell and was required for the formation of focal adhesion complexes during initial stages of adhesion and cell spreading (Von Wichert et al., 2003). A wound healing migration assay revealed that mouse embryonic fibroblasts (MEFs) lacking PTP α displayed impaired cell migration into the wound (L. Zeng et al., 2003). Furthermore, MEFs lacking PTP α showed reduced cell spreading, actin stress fiber assembly, and focal adhesion formation, which could be rescued upon the re-introduction of WT-PTP α but not the inactive mutant (PTP α -Y789F) (Chen et al., 2006). In zebrafish, PTP α -knockdown results in defective cell migration that is essential during gastrulation and development (van Eekelen et al., 2010). PTP α also plays an important role in radial neuronal migration (Petroni, 2003). To summarize, PTP α / PTP α -pTyr⁷⁸⁹ expression play an important role in regulating cellular adhesions, focal adhesion formation, and cell migration.

1.3.1.4 Role of PTP α in oncogenic signaling and cancer cell invasion.

Few studies have focused on the role of PTP α in cancer cell invasion; however, of the data published, the role of PTP α in oncogenesis remains controversial. In 1992, Zheng *et al.* overexpressed PTP α cDNA in Fischer rat embryo fibroblasts. These PTP α overexpressing cells were transformed in culture compared to control cells that became quiescent, exhibited increased Src kinase activity, and formed tumours in immunodeficient mice suggesting PTP α -mediated oncogenic transformation when overexpressed (Zheng *et al.*, 1992). In 1995, Tabiti *et al.* report elevated PTP α mRNA levels in 10/14 late-stage colorectal tumours compared to normal adjacent tissue, and suggest that overexpression of PTP α enhances tumorigenicity (Tabiti *et al.*, 1995). Others have reported PTP α upregulation in human gastric cancer (Wu *et al.*, 2006) and squamous cell lung cancer (Gu *et al.*, 2017), which were associated with lymph node metastasis and clinical stage. The expression of PTP α has also been investigated in human breast cancer (Ardini *et al.*, 2000; Meyer *et al.*, 2014). Ardini *et al.* report that while PTP α expression levels varied greatly among tumour samples, high PTP α expression significantly correlated with low tumour grade and positive estrogen receptor status (Ardini *et al.*, 2000). Meyer *et al.* found PTP α contributes to tumour maintenance and initiation of estrogen receptor positive breast cancer; however, depletion of PTP α had no effect on metastasis (Meyer *et al.*, 2014). More recently, Krndija *et al.* report upregulated PTP α expression in colon cancer compared to normal tissue, and that PTP α regulates focal adhesion formation, cellular contractility, and *ex vivo* invasion into the chorioallantoic membrane (CAM) (Krndija *et al.*, 2010).

1.4 Investigating extrinsic regulators of cancer cell invasion.

In addition to the intrinsic factors discussed in Section 1.3 (pg. 11), invadopodia activity can also be regulated by several extrinsic signals from the tumour microenvironment including hypoxia or stromal cell interactions. For instance, others have shown that a hypoxic tumour microenvironment and HIF-1 α stabilization induces invadopodia formation through the NOTCH-EGFR signaling axis (Díaz et al., 2013; Md Hashim et al., 2013). ECM stiffness or rigidity is known to stimulate invadopodia maturation and activity in cancer cells (Alexander et al., 2008). Cell-cell contact between cancer cells and tumour-associated macrophages, for instance, has also been found to stimulate invadopodia maturation in cancer cells (Pignatelli et al., 2016). Another well described extrinsic regulator of cancer cell invasion is ionizing radiation (IR); however, the precise signaling mechanism that mediate IR-induced invasion remain relatively unknown (Moncharmont et al., 2014; Sundahl et al., 2018; Wank et al., 2018b). Since greater than 50% of all cancer patients will receive radiation therapy (*i.e.* ionizing radiation) during the course of their treatment, we chose to further investigate the signaling mechanisms that facilitate IR-induced invasion.

In Section 1.4, I will discuss the role of IR as a potential extrinsic regulator of invadopodia activity and cancer cell invasion.

1.4.1 Electromagnetic radiation.

Electromagnetic (EM) radiation is produced when an atom absorbs energy resulting in one or more electrons moving to a higher orbit away from the nucleus. When the electron(s) returns to its original position, this results in the release energy in the form of EM waves. Multiple EM waves traveling through space at the speed of light is collectively referred to as a

photon. The EM spectrum encompasses a variety of EM waves that vary based on wavelength and frequency, which are inversely related. From lowest to highest energies, the seven types of EM waves are radio waves, microwaves, infrared, visible light, ultraviolet (UV), x-rays, and gamma rays (Donya et al., 2014).

Radiation is characterized as either ionizing or non-ionizing. Non-ionizing radiation includes the lower frequency electromagnetic waves such as microwaves, radio waves, and visible light, which do not have enough energy to remove electrons from atoms (Han and Ngok Yu, 2009). Ionizing radiation is defined as radiation that has sufficient energy to remove one or more electrons thus converting a neutral molecule to an electrically charged molecule (Han and Ngok Yu, 2009). The different types of ionizing radiation include alpha, beta, neutron, gamma, or x-rays (Donya et al., 2014). Alpha radiation is classified as two protons and two neutrons emitted from an atom (*i.e.*, a helium nucleus) and is not able to penetrate clothing or skin. Beta radiation is generated when fast moving electrons are ejected from an atom, which has enough energy to penetrate human skin up to the germinal layer. Gamma radiation and x-rays readily penetrate most materials including the human body. The major difference between gamma radiation and x-rays is that gamma radiation is produced inside the nucleus following radioactive decay while x-rays are often produced artificially when electrons strike a target. Lastly, neutron radiation occurs during nuclear fission reactions (Donya et al., 2014). In terms of medical radiation, the two most commonly used types of radiation are x-rays and gamma rays.

1.4.2 Radiation therapy.

Approximately 50% of all cancer patients will receive radiation therapy either alone or in combination with other treatment modalities including surgery and chemotherapy (Baskar et al.,

2012; Delaney et al., 2005). The two types of radiation treatment delivered to cancer patients are external beam radiation or internal radiation, also known as brachytherapy.

External beam radiation is the most common type of radiation therapy and uses a machine called a linear accelerator to deliver ionizing radiation to patients. The amount of radiation delivered to patients is determined in three ways: (1) absorbed dose is the energy absorbed by the human body following exposure to radiation and is measured in gray (Gy), (2) equivalent dose is the energy absorbed by each organ specifically calibrated to the type of radiation delivered and is measured in millisievert (mSv), and (3) effective dose is the amount of energy absorbed by the whole body used for protective measures and is also measured in mSv (Fisher and Fahey, 2017). The conventional fractionation schedule for cancer patients receiving radiation is 60 Gy delivered in 30 fractions of 2 Gy. More recently, hyper- and hypo-fractionation schedules have been developed. Hyperfractionation radiation schedules often deliver the same total dose of radiation as conventional radiation therapy but given in smaller doses (*i.e.*, less than 1.8 Gy) delivered multiple times each day. Hypofractionation radiation involves delivering higher doses of radiation (*i.e.*, greater than 2 Gy) over a shorter period of time. For instance, elderly GBM patients may receive 40 Gy IR in 15 fractions rather than the traditional 60 Gy in 30 fractions (Roa et al., 2004).

Brachytherapy includes the use of radioactive isotopes (^{60}Co and ^{137}Cs) and involves the implantation of radioactive “seeds” inside the body close to the tumour (Borrego-Soto et al., 2015). Prostate cancer patients are often administered brachytherapy either alone or in combination with external beam radiation, which allows for the delivery of high doses of radiation specifically to the prostate (Strouthos et al., 2022). While both external beam radiation

and brachytherapy are considered effective treatment options, novel strategies to further improve the efficacy of radiation therapy are currently being explored.

1.4.3 Biological responses of cancer cells to ionizing radiation.

Direct Effects:

The direct role of IR is to induce DNA damage and cause cell death. Radiation can induce several types of DNA lesions including damage to nucleotide bases, single strand breaks (SSBs) and double strand breaks (DSBs). Of these DNA lesions, DSBs are the most difficult to repair and thus most lethal (Ward, 1991). In general, there are three mechanisms of DNA DSB repair: non-homologous end joining (NHEJ), homologous recombination (HR), and single strand alignment (SSA) (Figure 1.3). With NHEJ, the two fragments of DNA are joined together without the requirement of extensive sequence homology, which tends to be a highly error-prone process (Jackson, 2002; Khanna and Jackson, 2001; Moynahan and Jasin, 2010). With HR, the 3' ends of the DSB site are cleaved and then invasion of a sister chromatid occurs to act as a template for repair (Moynahan and Jasin, 2010). Either synthesis-dependent strand annealing (SDSA) or DSB repair (DSBR) may occur, each using the donor sequence to repair the damaged site (Figure 1.3). Another form of HR may occur, called single strand alignment (SSA), which uses homologous repeats to bridge the DNA DSBs (Moynahan and Jasin, 2010). HR is often less error-prone than NHEJ, allowing the surviving fraction of cells to survive with few mutations (Biau et al., 2019).

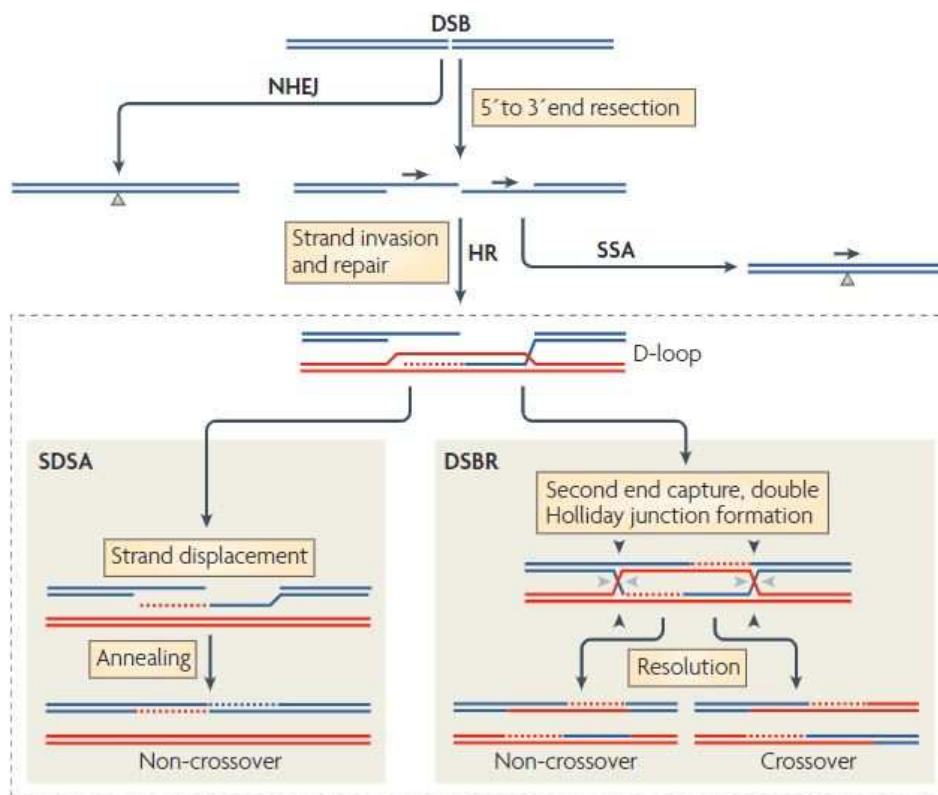


Figure 1.3. Mechanisms of DNA double strand break repair.

Double stranded breaks (DSBs) in mammalian cells are typically repaired via non-homologous end joining (NHEJ) or homologous recombination (HR). NHEJ simply joins the non-homologous DNA ends. HR is more complex and uses a template strand (red) to initiate repair via two alternative pathways: synthesis-dependent strand annealing (SDSA) or double stranded break repair (DSBR). SDSA results in a non-crossover outcome such that the newly synthesized strands (dotted lines) are displaced and anneal to the original strand of DNA leaving the template strand unchanged. DSBR results in either non-crossover or crossover outcomes such that the resultant strands are a mix of original and template strands. Figure used with permission from M.E. Moynahan and M. Jasin, *Nature Reviews Molecular Cell Biology* 11, 196-207 (2010).

Indirect Effects:

In addition to directly damaging DNA, radiation can also indirectly interact with water molecules within the cell to generate radical oxygen species (ROS). ROS is a collective term that includes both free radicals and non-free radical oxygen containing molecules - a free radical being defined as a molecule with one or more unpaired electrons. When water is first exposed to IR, H₂O is converted to H₂O⁺ and a free electron. Then, H₂O⁺ can react with another water molecule to generate ROS including O₂⁻, H₂O₂ and ·OH, which can indirectly damage DNA (Desouky et al., 2015; Han and Ngok Yu, 2009; Kim et al., 2019).

Radiation has also been found to have unpredictable, indirect effects on signaling mechanisms that regulate tumour recurrence, distant tumour growth (known as the abscopal effect), and invasion/metastasis (Camphausen et al., 2003; Vilalta et al., 2016; von Essen, 1991). There is a need to further understand the indirect effects of radiation, and how these effects impact clinical outcomes. In sections 1.4.4 and 1.4.5, I will further describe the precise mechanisms that facilitate IR-induced cancer cell invasion.

1.4.4 Ionizing radiation-induced cancer cell invasion.

The concept of ionizing radiation (IR)-induced metastasis was first reported by H.S. Kaplan and E.D. Murphy in 1949 (Kaplan and Murphy, 1949). Mammary carcinoma cells were subcutaneously implanted into the hind legs of mice and irradiated once the tumours reached 1 cm in diameter. Pulmonary metastases were found in 27/96 mice (43.5%) from the irradiated group and in 5/52 mice (9.6%) from the control group, suggesting IR increased the incidence of metastasis. Strong *et al.* (1978) performed a randomized clinical trial to determine if radiation

therapy combined with surgery would increase the survival rate of late-stage head and neck cancer patients compared to surgery alone. While there was no difference in outcome between the two treatment groups, it was found that patients who received adjuvant radiation therapy had an increased incidence of distant metastases (Strong et al., 1978). Other than these initial observations being made over 50 years ago, clinical studies reporting the incidence of radiation-induced distant metastases are limited.

Four possible mechanisms of IR-induced metastasis were previously proposed by C.F. von Essen: *i*) IR induces direct cellular changes to cancer cells resulting in increased metastasis, *ii*) IR alters distant tissue resulting in increased recruitment of cancer cells and metastases, *iii*) IR increases the ability of cancer cells to enter circulation and *iv*) IR increases the life expectancy of cancer patients resulting in more time for cancer cells to metastasize (von Essen, 1991). However, von Essen postulated accelerated entrance into circulation is the most likely explanation of IR-induced metastasis, which has been studied in recent years. Martin *et al.* (2014) used fluorescent microscopy to detect circulating tumour cells (CTCs) in blood samples collected from 27 patients with non-small cell lung carcinoma (NSCLC) undergoing radiation therapy, which detected CTCs in 17/27 patient samples by visualizing cytokeratin 8/18-positive and CD45-negative cells. It was found that 7/9 (77%) patients receiving palliative radiation and 4/8 (50%) of patients receiving curative radiation displayed increased CTCs post-IR (Martin et al., 2014). These findings corroborate the previously suggested theory that IR releases tumour cells into circulation increasing the risk of distant metastases and recurrence (Martin et al., 2017; Vilalta et al., 2016). Others have reported a role of IR in attracting non-irradiated tumour cells, either from a tumour or within circulation, towards irradiated tissue sites (Vilalta et al., 2014).

Despite limited clinical observations, there is a large body of work exploring IR-induced invasion and metastasis using *in vitro* and *in vivo* mouse models. Multiple groups have previously reviewed the effect of radiation on cancer cell motility (Moncharmont et al., 2014; Sundahl et al., 2018; Wank et al., 2018b). Thus, I will further summarize the most recent *in vitro* and *in vivo* reports of radiation-induced cancer cell motility particularly focusing on glioblastoma data in section 1.4.5.

Recently, sublethal doses of IR in combination with temozolomide (TMZ) treatment have been found to increase ECM degradation in U118, U87-MG, and LN229 GBM cells (Mao et al., 2018; Whitehead et al., 2018). Since invadopodia play a key role in facilitating ECM degradation, it seems plausible that IR may upregulate invadopodia activity to mediate GBM cell invasion.

1.4.5 Role of IR in invadopodia-associated signaling mechanisms.

As previously discussed in section 1.2.3, the mechanisms that modulate invadopodia formation and function are quite complex and involve many molecular players. For instance, interactions between EGFR-Src-Arg are important for initiating invadopodia formation, while matrix metalloproteinases (MMPs) are critical for maturation and function. Several groups have found that IR upregulates multiple factors associated with invadopodia signaling, such as EGFR, integrin, Src, and MMP signaling mechanisms.

EGFR: Irradiating GBM cells increased phospho-EGFR expression levels 15 minutes post-IR in a dose-dependent manner (Martinou et al., 2011). Park *et al.* state that pharmacologically inhibiting EGFR signaling blocked IR-induced MMP2 secretion and invasion of PTEN-functional GBM (U251 and U373) cells by inhibiting Src/EGFR-mediated Akt phosphorylation (Park et al., 2006).

In 2017, Kegelman *et al.* intracranially injected luciferase-tagged U1242 cells into nude mice and administered a single dose of 2.5 Gy IR per day for 4 days. Immunohistochemical analysis of tumour sections revealed IR increased the expression of pEGFR, pFAK, and pSrc, which was prevented by inhibiting EGFRvIII, a common mutation found in high grade gliomas, via PDZli treatment (Kegelman et al., 2017). Together, these reports highlight the role of radiation in promoting EGFR signaling mechanisms.

Integrins: Ionizing radiation has been found to increase the surface expression of $\beta 1$ and $\beta 3$ integrin in GBM cells as determined by flow cytometry (Cordes et al., 2003). Wild-Bode *et al.* analyzed the role of integrins in mediating IR-induced GBM cell invasion. The expression of $\alpha v\beta 3$ integrin, but not $\alpha v\beta 1$, was enhanced 4 hours post-IR and inhibition of $\alpha v\beta 3$ integrin blocked IR-induced motility of GBM cells (Wild-Bode et al., 2001). Goetze *et al.* investigated the role of two types of ionizing radiation (x-ray versus ^{12}C heavy ion radiation) on integrin expression and cell migration. Immunoblotting for $\beta 1$ and $\beta 3$ integrins in U87 GBM cells following x-ray or ^{12}C heavy ion radiation revealed a dose-dependent increase in expression levels, while $\beta 1$ expression increased in response to x-ray radiation but decreased post- ^{12}C heavy ion radiation exposure in colon cancer HCT116 cells (Goetze et al., 2007). Similarly, Rieken *et al.* showed that inhibition of $\alpha v\beta 3$ and $\alpha 5\beta 5$ integrins inhibits photon induced migration of U87 and LN229 GBM cells (Rieken et al., 2011). Reiken *et al.* followed this study up by later investigating the role of carbon ion radiation on integrin expression and glioma cell migration. It was found that exposure to 2 Gy or 10 Gy photon-IR increased $\alpha v\beta 3$ and $\alpha 5\beta 5$ integrin expression and increased the migration of U87 and LN229 GBM cells while carbon ion radiation caused the opposite effect (Rieken et al., 2012). Yao *et al.* found that exposure to 2 - 3 Gy IR induced $\alpha 5\beta 1$ integrin expression in Panc-1,

MiaPaCa-2, and BxPC-3 pancreatic cancer cells and tumour xenografts (Yao et al., 2011). Furthermore, Parthymou *et al.* showed $\alpha 5$ integrin mRNA expression levels increased in glioma cells post-exposure to 10 Gy and 40 Gy IR (Parthymou et al., 2004).

Src: Multiple reports have shown IR induces Src-signaling mechanisms. Exposure to a single dose to 2 Gy IR significantly increased the levels of activated Src (Kegelman et al., 2017). Similarly, exposure to fractionated doses of IR (2 Gy per day for 3 days) induces EMT via the activation of Src in MCF-7 and SKBR3 breast cancer cells. Genetic and pharmacological depletion of Src inhibited IR-induced invasiveness (Kim et al., 2015). More recently, Yoo *et al.* found exposing U87 GBM cells with 2 Gy IR per day for 3 days increased invasiveness and induced EMT *in vitro* and *in vivo* (Yoo et al., 2018). U87 cells were orthotopically injected into mice and the tumours were treated with IR. Immunohistochemical staining showed increased phospho-Src expression post-radiation, which was ameliorated via CD44 depletion. These data indicate radiation indirectly acts through the CD44 membrane-bound receptor to activate Src signaling mechanisms, induce EMT, and increased invasiveness of GBM cells (Yoo et al., 2018). Interestingly, CD44 has been shown to localize to invadopodia and mediate invadopodia activity, highlighting the need to further investigate the role of IR on invadopodial biology (Zhao et al., 2016). One group explored the use of 20 FDA-approved agents in combination with radiation and TMZ treatment to determine their potential to block therapy-induced GBM cell motility. The authors found that pre-treating LN229 GBM cells with IR and TMZ and then exposing the cells to either bosutinib (a Src inhibitor), vinorelbine tartrate or paclitaxel (both target microtubules), decreased ECM degradation (Whitehead et al., 2018). Lastly, Park *et al.* found exposing U251 and U373 GBM cells to a single dose of 5 Gy IR increased pSrc levels, which could be inhibited by treating cells with PP2, a Src

inhibitor. The authors report treating GBM cells with various kinase inhibitors targeting EGFR, Src, p38, PI3K, or AKT reduced the effect of radiation-induced cellular invasion (Park et al., 2006).

MMPs: Previous studies have shown IR increased the secretion and activity of MMP2 via the PI3K/Akt signaling pathway in U251 and U373 GBM cells in a dose-dependent manner (Park et al., 2006). Cordes *et al.* analyzed the effect of a single dose of 6 Gy IR on MMP2 and MMP14 expression and activity. Western Blot analysis showed increased MMP2 and MMP14 expression and decreased TIMP2 expression 48 hours post-IR while zymography showed increased MMP2 gelatinase activity in A-172 and U-138 GBM cells. This IR-induced MMP2 activity was prevented by using β 1 and β 3 integrin inhibitors (Cordes et al., 2003). Others have reported IR increased the secretion of MMP2 and MMP9 by C6 glioma cells (Parthymou et al., 2004). Recent work by Adachi *et al.* (2021) indicates low dose radiation (0.5 Gy) increases the invasiveness of MDA-MB-231 breast cancer cells via the upregulation of MMP2 expression and activity, which could be suppressed using a Chk1 inhibitor (Adachi et al., 2021). Furthermore, Mao *et al.* found 2.5 Gy IR moderately increased the secretion and activation of MMP2 from U118 and U87 GBM cells (not LN18 cells), which was associated with increased ECM degradation suggestive of invadopodia activity (Mao et al., 2018). Bouchard *et al.* took an alternative approach to studying the role of MMP14 on radiation-induced metastasis by pre-irradiating the murine mammary fat pad prior to implanting D2A1 cells. It was found that pre-irradiating the mammary fat pad resulted in increased tumour growth and a greater number of lung metastases, which was abrogated by the depletion of MMP14 (Bouchard et al., 2017).

To summarize section 1.4.5, countless reports have shown that IR may induce cancer cell invasion *in vitro*. Many of these reports associate radiation-induced invasiveness with altered invadopodia signaling, namely as EGFR, integrin, Src, and MMP signaling mechanisms. However, to our knowledge, the role of radiation on invadopodia formation and function remains to be elucidated and highlights important future work.

1.5 Rationale and hypotheses.

1.5.1 Role of PTP α in breast cancer invasion.

Several findings suggest a role for PTP α in facilitating cancer cell invasion. First, PTP α protein expression is upregulated in multiple tumour types compared to normal adjacent tissue. Second, PTP α is critical for the activation of Src signaling mechanisms, as revealed by studies of embryonic fibroblasts derived from PTP α -knockout mice. Third, PTP α is an important regulator of migration and focal adhesion activity. While focal adhesions are known to facilitate cellular migration, focal adhesion structures are closely related to invadopodia suggesting a link between PTP α and cancer cell invasion. For Chapter 2, my goal is to investigate the role of PTP α in invadopodia formation and function and triple-negative breast cancer cell invasion. **I hypothesize that receptor-type protein tyrosine phosphatase alpha (PTP α) promotes Src-signaling mechanisms critical for invadopodia-mediated triple-negative breast cancer cell invasion *in vitro* and *in vivo*.**

Aim 1: Investigate the role of PTP α in facilitating invadopodia formation, matrix degradation and breast cancer cell invasion *in vitro*.

Aim 2: Investigate the role of PTP α (*i*) in Src signaling mechanisms regulating invadopodia

activity and (ii) on MMP 2, 9 and 14 expression, activity, and localization to invadopodia in breast cancer cells.

Aim 3: Investigate the role of PTP α in tumour growth and cellular invasion *in vivo* by orthotopically injecting parental and PTP α -depleted breast cancer cells into the mammary fat pad of female immunodeficient mice.

1.5.2 Role of ionizing radiation in Glioblastoma cell invasion.

The pro-migratory effects of ionizing radiation have been extensively studied by multiple groups using various tumour types. While the precise signaling mechanisms that modulate radiation-induced invasion remain to be elucidated, several findings indicate a role for IR in mediating invadopodia activity. First, IR has been found to alter the expression and activity of multiple invadopodia-associated proteins including Src and MMPs. Second, IR in combination with chemotherapy was found to increase ECM degradation of multiple GBM cell lines. Third, ROS (a byproduct of ionizing radiation) has been shown to localize to invadopodia and play a regulatory role in invadopodia activity. For the work presented in Chapters 3 and 4, **I hypothesize that ionizing radiation modulates TKS5-Src signaling mechanisms to induce invadopodia-mediated glioblastoma multiforme (GBM) cell invasion *in vitro* and *ex vivo*.**

Aim 1: Explore the role of IR in facilitating invadopodia formation, matrix degradation and GBM cell invasion *in vitro*.

Aim 2: Investigate the role of IR in TKS5-Src signaling mechanisms that regulate invadopodia activity.

Aim 3: Develop an organotypic brain slice invasion assay to explore the role of IR in facilitating invadopodia-mediated GBM cell invasion *ex vivo*.

1.5.3 Cell lines

In Chapter 2, I chose to work with MDA-MB-231 triple-negative breast cancer cells. MDA-MB-231 cells are highly invasive, express PTP α and Src, and are a widely accepted model for invadopodia research.

In Chapters 3 and 4, I chose to work with LN229 and LN18 human GBM cancer cell lines, which are highly invasive, degrade gelatin matrices, and differentially express MMP2, MMP14, Src, and TKS5 proteins. In Chapter 3, I use LN229 and LN18 cells to investigate the role of IR in facilitating invadopodia activity and *in vitro* chemotactic invasion. In Chapter 4, I investigate the role of IR in facilitating GBM cell invasion using an *ex vivo* organotypic brain slice spheroid invasion assay.

Chapter 2: Receptor-type protein tyrosine phosphatase alpha mediates

MMP14 localization and facilitates triple-negative breast cancer cell invasion.

2.1 Rationale and Hypothesis

Breast cancer is the second leading cause of death among women and accounts for 25% of new cancer diagnoses (Canadian Cancer Statistics Advisory Committee, 2019). Triple-negative breast cancer (TNBC), a subtype of breast cancer characterized by loss of progesterone receptor (PR), estrogen receptor (ER), and human epidermal growth factor receptor 2 (HER2) expression, accounts for 10-15% of all breast carcinomas (Dawson et al., 2009). Patients diagnosed with TNBC typically have a poor prognosis since TNBC is non-responsive to traditional hormone therapies and exhibits an increased likelihood to invade into the surrounding breast tissue or metastasize to lymph nodes, bone, liver or lungs (Al-Mahmood et al., 2018).

Metastasis is a complex, multi-step process during which cancer cells invade through the surrounding extracellular matrix (ECM), intravasate into the blood or lymphatic vessels, survive in circulation, and extravasate through the vessel endothelium to colonize secondary sites (Al-Mahmood et al., 2018; Scully et al., 2012). Invasion through the ECM is partially mediated by the formation of protrusive structures (Murphy and Courtneidge, 2011), including invadopodia and podosomes (collectively referred to as “invadosomes”) (Paterson and Courtneidge, 2018). These invasive structures are actin-based dynamic protrusions of the plasma membrane that form on the ventral surface of cells and represent concentrated areas of proteolytic activity (Beatty and Condeelis, 2014; Murphy and Courtneidge, 2011; Revach and Geiger, 2014). Invadopodia are characterized by the preferential enrichment of matrix metalloproteinases (MMPs), specifically MMP2, MMP9, and MT1-MMP (MMP14), with MMP function and localization to proteolytically

active structures being primarily dependent upon endocytic/exocytic trafficking (Frittoli et al., 2011; Yamaguchi et al., 2009). Invadopodia have been studied both *in vitro* and *in vivo* and are important for mediating cancer cell intravasation, extravasation and metastasis (Gligorijevic et al., 2012; Leong et al., 2014; Lohmer et al., 2014; Williams et al., 2019). A further understanding of the molecular mechanisms that regulate the formation and function of invasive plasma membrane structures, as well as mechanisms that regulate the localization of MMPs to invadopodia, is crucial for the identification of clinically relevant targets to prevent metastasis.

Receptor-type protein tyrosine phosphatase alpha (PTP α) is a widely expressed 130 KDa transmembrane PTP with a short extracellular glycosylated domain and two intracellular catalytic domains (Pallen, 2003). Other groups have shown PTP α regulates the invasiveness of colon cancer cells using an *ex vivo* chicken chorioallantoic membrane (CAM) assay (Krdija et al., 2010). Moreover, PTP α is an activator of the proto-oncogene c-Src, and other Src family kinases (SFKs), through dephosphorylation of the regulatory C-terminal tyrosine site (Tyr⁵²⁷) of c-Src *in vitro* and *in vivo* (Pallen, 2003; Ponniah et al., 1999). Fibroblasts derived from the embryos of PTP α knockout mice display enhanced Src phosphorylation at Tyr⁵²⁷ accompanied by reduced Src activity (Su et al., 1999; Ponniah et al., 1999). Moreover, these fibroblasts exhibit impaired cell spreading and migration, which is associated with a reduction in focal adhesion (FA) formation (Su et al., 1999; Von Wichert et al., 2003; L. Zeng et al., 2003). FAs and invasive structures found in cancer cells are remarkably similar structures that share several signaling mechanisms and structural components (Beaty and Condeelis, 2014; Murphy and Courtneidge, 2011; Revach and Geiger, 2014). Indeed, invadopodia formation is initiated by FAs that establish the initial cell-ECM interactions. In invasive cells, Src is released from FAs and localized to invadopodia, which

then leads to the recruitment of other key invadopodia components required for formation, maturation and function (Chan et al., 2009; Mader et al., 2011; Spinardi et al., 2004). Since (i) PTP α has been shown to regulate FA formation and cellular migration, (ii) due to the similarities between focal adhesions and invadopodia (Chen et al., 2006; Von Wichert et al., 2003; L. Zeng et al., 2003), and (iii) since the role of PTP α in cancer biology remains relatively unknown, I sought to investigate the precise role of PTP α in Src signaling mechanisms, TNBC cell invasion, and invadopodia biology.

In this chapter, I describe a novel role for PTP α in promoting triple-negative breast cancer cell invasion *in vitro* and *in vivo* and show PTP α regulates MMP14 localization to plasma membrane protrusions, suggesting a role for PTP α in intracellular trafficking of MMP14. These findings suggest a novel role for PTP α in regulating the invasion of triple-negative breast cancer cells highlighting PTP α as an attractive drug target for the treatment of TNBC.

2.2 Materials and Methods

2.2.1 Cell culture

Wild-type (+/+) and PTP α -null (-/-) mouse embryonic fibroblasts (MEFs) were derived from embryonic murine brains and spontaneously immortalized (Chen et al., 2006; L. Zeng et al., 2003). These cells were maintained in Dulbecco's modified Eagle's medium (DMEM) (Hyclone, #SH30243) and supplemented with 10% fetal bovine serum (FBS) and 1% penicillin-streptomycin (pen-strep). MDA-MB-231 cells (American Type Culture Collection, ATCC® HTB-26™) and GFP-TKS5-expressing MDA-MB-231 cells (gift from Dr. Karla Williams,

UBC) were maintained in DMEM (Hyclone, #SH30243) and supplemented with 10% FBS and 1% pen-strep (Appendix A1).

2.2.2 Transfection (siRNA and plasmids)

MDA-MB-231 cells were transfected with siRNA to transiently knockdown PTP α . Sequences for the siRNAs used to target PTP α are as follows: si α 1, 5'-GCAUUACAAUUUCACCAAA-3'; si α 2, 5'-CGGCAGAACCAGUUAAGA-3' (Thermo Scientific, J-004519-06 & J-004519-08, respectively). Control non-targeting siRNA was purchased from Dharmacon. Cells were transfected with 20 nM siRNA using Lipofectamine RNAiMAX reagent (Invitrogen) and grown for 48 h before further experimentation. The pXJ41-neo-hPTP α siRNA-resistant plasmid was co-transfected with siRNA using Lipofectamine-2000 reagent (Invitrogen) to restore wildtype PTP α expression, and cells were grown for 48 h before further experimentation. The pXJ41-neo-EGFP-PTP α and pXJ41-neo-mCherry-PTP α plasmids were generated by replacing the PacI-flanked nucleotide sequence encoding a VSVG tag (located in the extracellular domain of PTP α) in the plasmid pXJ41-neo-VSVG-PTP α (Bhandari et al., 1998) with PCR-generated PacI-flanked sequences encoding EGFP or mCherry. These plasmids were transfected into MDA-MB-231 cells with Lipofectamine-2000 reagent (Invitrogen) according to the manufacturer's instructions.

2.2.3 Lentiviral Transfection (shRNA)

For stable depletion of PTP α in MDA-MB-231 cells, shRNA constructs were transduced using lentivirus as per the manufacturer's instructions. Two shRNA expressing constructs against PTP α and control sequences were purchased from Sigma Aldrich (Cat.No. SHCLNV-NM_002836, Cat.No. SHCLNV-NM_002839 and Cat.No. shC005V, respectively). Briefly, MDA-MB-231

cells were seeded at a density of 9,000 cells per well in a 96-well plate. After 24 h, 8 µg/mL of hexadimethrine and the viral particles at a multiplicity of infection (MOI) of 1 per well were added. Transduced cells were selected using 0.5 µg/mL puromycin and maintained in puromycin-containing culture medium.

2.2.4 Antibodies and reagents

Rabbit anti-PTP α antiserum 2205 has been described previously (Chen et al., 2006; Lim et al., 1998). Primary antibodies against the following proteins were used: anti-PTP ϵ (Abcam, Cat. No. ab126788), anti-actin (Sigma, Cat.No. A2066), anti-phospho-Src (Tyr527) (Cell Signaling, Cat.No. 2105), anti-phospho-Src (Tyr416) (Cell Signaling, Cat.No. 2101), anti-Src (Calbiochem, Cat.No. OP07), anti-phosphotyrosine (BD Transduction Laboratories, Cat.No. 610000), anti-cortactin (Millipore, Cat.No. 05-180), anti-MT1-MMP (MMP14) (Millipore, Cat.No. MAB3328), anti-TKS5 (Santa Cruz, Cat.No. sc-30122), anti-EEA1 (Abcam, Cat.No. ab2900), and anti-PARP (Cell Signaling Technology, Cat.No. 9542). Secondary antibodies used were: anti-rabbit IgG peroxidase conjugate (Sigma, Cat.No. A4914), anti-mouse IgG peroxidase antibody (Sigma, Cat.No. A4416), Alexa Fluor 594-conjugated to phalloidin (ThermoFisher, Cat.No. A12381), Alexa Fluor 488-conjugated goat anti-mouse IgG (Molecular Probes, Cat. No. A11001), Alexa Fluor 647-conjugated goat anti-rabbit IgG (Life Technologies, Cat.No. A21245), Alexa Fluor 594-conjugated goat anti-mouse IgG (Life Technologies, Cat.No. A11032), and Alexa Fluor 405-conjugated goat anti-mouse IgG (Life Technologies, Cat.No. A31553). Control normal mouse (Cat.No. 12-371) and normal rabbit (Cat.No. 12-370) IgG antibodies were purchased from Millipore.

2.2.5 Matrix degradation assay

This protocol was adapted from Martin *et al.* (Martin et al., 2012). To begin, 13 mm glass coverslips were autoclaved prior to use. The coverslips were placed in wells of a sterile 24-well plate, coated with 50 µg/mL Poly-L-Lysine for 20 min at room temperature (RT), washed with PBS, incubated in 0.5% glutaraldehyde for 15 min on ice, and then washed with PBS. Each coverslip was then inverted onto a 30 µl drop of 125 µg/mL Oregon Green 488-conjugated gelatin (Invitrogen, Cat.No. G13186) for 10 min at RT. The excess gelatin was then removed, the coverslips were washed in 5 mg/mL sodium borohydride for 15 min, washed with PBS and incubated in 70% ethanol for 30 min at RT. The coverslips were washed once with sterile PBS and then serum-containing media prior to cell seeding. MDA-MB-231 (7.5×10^4) cells were added per well. After 24 h, the cells were fixed with 4% PFA and permeabilized with 0.2% Triton X-100 in PBS for immunofluorescent analysis. Approximately 90 to 120 cells were imaged (~ 15 FOVs) at 63X magnification per condition per experiment. Gelatin degradation was quantified using ImageJ. ECM degradation was analyzed by quantifying the area of gelatin degradation as a percentage of the total area per field of view and normalized to the number of cells per field.

2.2.6 Immunoblotting

MDA-MB-231 cells were lysed with RIPA buffer (50 mM Tris Cl pH 7.4, 150 mM NaCl, 1 mM EDTA, 1% Nonidet P-40, 0.5% NaDOC, 10 µg/µl Aprotinin, 10 µg/µl Leupeptin, 1mM phenylmethylsulfonyl fluoride, and 2 mM sodium orthovanadate). Total protein concentration was determined using BioRad Protein Assay Dye (Biorad, Cat.No. 5000006). The cell lysates were prepared using reducing conditions and 20 µg (PTPα, MMP14) or 30 µg (PARP) of protein was resolved by SDS-PAGE. The proteins were transferred to polyvinylidene difluoride (PVDF)

membranes, blocked in 3% BSA-PBS with 0.1% Tween-20, and immunoblotted with the indicated antibodies. The immunoblots were visualized using ECL detection methods.

2.2.7 IncuCyte chemotaxis assays

Control and shRNA expressing MDA-MB-231 cells were serum starved overnight before being resuspended in serum free medium (migration assay) or 5.0 mg/mL Matrigel (Corning, Cat.No. 356231, invasion assay) and plated into a ClearView 96-well cell migration plate (Essen Biosciences, Cat.No. 4582). Chemotactic migration and invasion were monitored using IncuCyte analysis software (Essen BioScience, Ann Arbor, MI, USA) at 2-hour intervals for 72 hours. Cellular migration and invasion were quantified as changes in cell count over time normalized to the initial cell counts (0 h).

2.2.8 MMP antibody array

A total of 1.0×10^6 shCtl and sh $\alpha 1$ MDA-MB-231 cells were plated per 6cm dish for 48 hours and starved in serum free media for an additional 24 hours. MMP antibody arrays were performed according to the manufacturer's instructions using conditioned serum free media and normalized to total cell number (Raybiotech, Cat. No. AAH-MMP-1-4).

2.2.9 ELISAs

MMP1 concentrations were assessed using a commercial ELISA kit (Abcam, Cat. No. ab100603). A total of 1.0×10^6 shCtl and sh $\alpha 1$ MDA-MB-231 cells were plated per 6cm dish for 48 hours and starved in serum free media for an additional 24 hours. Conditioned media samples were assayed in duplicate according to the manufacturer's instructions and the results were analyzed using ELISA analysis software (ElisaAnalysis.com, Leading Technology Group, Australia).

2.2.10 Flow cytometry

MDA-MB-231 cells stably expressing non-targeting (Ctl) or PTP α -specific shRNA (sh α 1 or sh α 2) were incubated with 0.1 μ g of human APC-conjugated anti-MMP-14 (R&D Systems, Cat.No. FAB9181A) or mouse IgG2B APC-conjugated control antibody (R&D Systems, Cat.No. IC0041A) in 1% BSA/PBS at 4°C for 15 min. To assess total expression, cells were fixed and permeabilized using BD Cytotfix/Cytoperm kit (BD Biosciences, Cat. No. 554714) according to manufacturer's protocol and then stained as described above. Fluorescence data were acquired on BD Accuri C6 flow cytometer (BD Biosciences) and dead cells were excluded by forward and side scatter gating. Expression of MMP-14 was quantified as geometric mean of fluorescence intensity (gMFI).

2.2.11 Immunofluorescence

Glass coverslips were coated with gelatin prior to cell seeding. Cells were fixed with 4% PFA for 15 min, washed three times in PBS, and permeabilized in 0.2% Triton X-100/PBS for 10 min, and blocked with 3% BSA in 0.2% Triton X-100/PBS for 1 h at RT. The blocking solution was removed, and the samples were incubated with primary antibodies either overnight at 4°C or at 37°C for 2h (TKS5 only) and then with secondary antibodies for 1 h at RT. Samples were incubated with phalloidin-594 for 15 minutes at RT, and then mounted with mounting medium with or without DAPI (Molecular Probes). For colocalization analysis, MDA-MB-231 cells were transfected with either mCherry-PTP α or GFP-PTP α , stained with co-markers, imaged at 100X magnification using a Leica SP5 Confocal Microscope and analyzed using ImageJ software. The percentage of colocalization was quantified across 22 – 30 PTP α -positive cells that formed

between 78-204 PTP α -positive puncta in total. To visualize MMP14 localization to plasma membrane protrusions, cells were seeded (2.5×10^4) onto 0.3 μm membranes (Costar®) in serum-free medium. The bottom chamber was filled with medium containing 10% FBS as the chemoattractant, and the plasma membrane protrusions could extend overnight at 37°C/5% CO₂. Cells were fixed onto the membrane, permeabilized, blocked, and stained as described above.

2.2.12 Orthotopic xenograft tumour model

8 to 19-week old female immunodeficient mice [NSG (NOD scid gamma) mice used for shCtl vs. sh α 1 experiments; NRG (NOD.Cg-*Rag1^{tm1Mom} Il2rg^{tm1Wjl}/SzJ*) mice used for shCtl vs. sh α 2 experiments] were bred in-house in the Animal Resource Centre at the BC Cancer Research Centre under specific pathogen-free conditions. Either shCtl, sh α 1 or sh α 2 GFP-expressing MDA-MB-231 (1.0×10^6) cells were resuspended in complete culture medium and mixed with an equal volume of high concentration Matrigel (Corning). Mice were anesthetized by 2% isoflurane inhalation, randomly divided into two groups, and the cell-Matrigel mixture was injected into the fourth mammary fat pad in a total volume of 100 μl .c Tumours and surrounding fat pads were harvested 2-weeks post implantation for further analysis. Animal experiments were performed in accordance with Institution and Canadian Council on Animal Care guidelines.

2.2.13 Immunohistochemistry

The mammary fat pads containing tumours were isolated, weighed and then fixed in 10% formalin. The samples were paraffin embedded, processed, and stained with hematoxylin/eosin (H&E) (Biocare, Cat. No. CATHE), Ki67 (Springer Bioscience, Cat.No. M3062), and/or cleaved caspase-3 (Cell Signaling, Cat. No. 9661S) by the BC Cancer Agency's Molecular and Cellular Immunology Core Facility (Victoria, Canada). Images were captured using a Zeiss Axioplan 2

microscope and Northern Eclipse software and processed using Fiji (Fiji is Just ImageJ) software. H&E staining was used to differentiate mammary fat pad from tumour cells, and the density of H&E stained nuclei was used to distinguish between the solid tumour mass and the invasive front of the tumour. The average area of invasive tumour (μm^2) was calculated as the difference between the total tumour area and the solid tumour area in 5 step sections (100 μm apart) per mouse. The expression of proliferation and apoptosis markers (Ki67 and CC3, respectively) were quantified from 3 randomly imaged FOVs (1 section per mouse) using Fiji and normalized to total tumour cell number in the section as determined by quantification of hematoxylin staining.

2.2.14 Statistical analysis

Statistical comparisons were made using unpaired, two-tailed Student's t-tests with Welch's correction. When more than two groups were analyzed, either a one-way (single time point) or two-way (time course analysis) ANOVA was performed. Significance was defined as $p < 0.05$ and all data represent at least three independent experiments. Experimental values are presented as the mean \pm standard deviation (SD).

2.3 Results

2.3.1 Depletion of PTP α does not affect PTP ϵ expression.

To examine the effects of PTP α on cancer cell motility, initial experiments focused on determining the optimal timepoint for small-interfering RNA (siRNA)-mediated knockdown of PTP α knockdown and the specificity of the siRNAs targeting PTP α . I first transfected MDA-MB-231 cells, a TNBC cell line widely used to investigate mechanisms of tumour cell migration and invasion, with either a non-targeting control siRNA (Ctl) or siRNA #1 (si α 1) targeting a specific

sequence of the PTP α gene. Protein expression of PTP α , determined by western blot analysis, was effectively depleted for at least 72 hours post-transfection (Figure 2.1A). Mouse embryonic fibroblasts (MEFs) isolated from wild-type or PTP α -null mice were used as a positive and negative control, respectively. Effective depletion of PTP α was recapitulated using siRNA #2 (si α 2) targeting another unique sequence of the PTP α gene or a pool of si α 1 and si α 2 (Figure 2.1B).

PTP α shares a high level of homology with the closely related protein tyrosine phosphatase epsilon (PTP ϵ) (Krueger et al., 1990). Notably, PTP ϵ has been found to activate Src and contribute to tumorigenesis in Neu-induced mammary tumours (Gil-Henn and Elson, 2003; Krueger et al., 1990). To confirm siRNA-mediated depletion of PTP α did not alter expression of PTP ϵ , cell lysates were collected from MDA-MB-231 cells either untransfected (P, parental) or transfected with non-targeting siRNA (NT) or siRNA #1 (si α 1) targeting PTP α and immunoblotted for PTP α , PTP ϵ , and actin. PTP α knockdown did not affect PTP ϵ expression levels, indicating siRNA specificity and lack of compensation by other related PTPs upon PTP α knockdown (Figure 2.1C). Notably, siRNA-mediated depletion of PTP α did not affect the growth of MDA-MB-231 cells *in vitro* suggesting PTP α does not alter cellular proliferation (Figure 2.1D).

2.3.2 PTP α mediates matrix degradation.

The metastatic cascade is initiated by cancer cells disseminating from the primary tumour and locally invading into the ECM and through the surrounding tissue prior to entering the vasculature. We sought to determine if PTP α plays a role in ECM degradation using a matrix degradation assay with fluorescently tagged gelatin. Both siRNAs were used together to deplete PTP α , and the introduction of siRNA-resistant wild-type PTP α into PTP α -depleted cells rescued

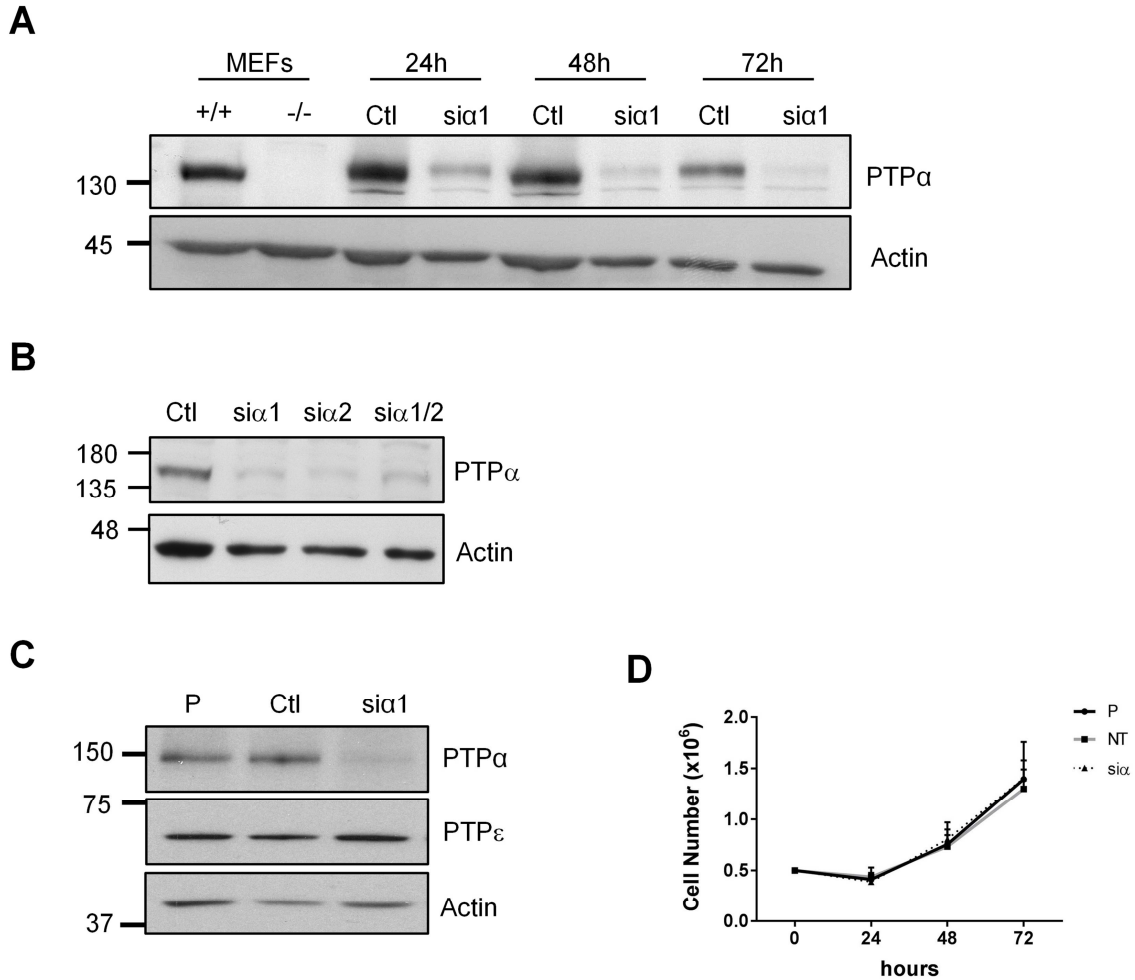


Figure 2.1. Small interfering RNA (siRNA)-mediated PTP α knockdown does not alter PTP ϵ expression or cellular proliferation *in vitro*.

(A) MDA-MB-231 cells were transfected with non-targeting siRNA (Ctl), siRNA #1 (si α 1). Cell lysates were collected 24h, 48h, and 72h post-transfection and immunoblotted for PTP α and actin (n=3). Mouse embryonic fibroblasts (MEFs) isolated from the brains of wild-type (+/+) or PTP α knockout (-/-) mice are used as positive and negative controls, respectively. (B) MDA-MB-231 cells were transfected with non-targeting siRNA (Ctl), siRNA #1 (si α 1) or siRNA #2 (si α 2) alone or together. Cell lysates were collected 48 h post-siRNA treatment and immunoblotted for PTP α and actin. (C) MDA-MB-231 cells were either untransfected (P, parental) or transfected with non-targeting siRNA (Ctl) or siRNA#1 targeting PTP α (si α 1). Cell lysates were collected 48h post-siRNA transfection and immunoblotted for PTP α , PTP ϵ , and actin (n=3). (D) Viable cell numbers of either untransfected (P, parental) or transfected with non-targeting siRNA (Ctl) or siRNA#1 targeting PTP α (si α 1) were determined 24h, 48h, and 72h post-transfection based on trypan blue staining (n=3).

the expression of PTP α (Figure 2.2A). Indeed, I observed a decrease in gelatin degradation over a 24-hour period upon PTP α knockdown, which was restored by the re-expression of PTP α (Figure 2.2B, C). These findings suggest that PTP α is important for ECM degradation and thus may play a role in the initial stages of TNBC cell invasion.

2.3.3 Expression of PTP α is important for TNBC invasion.

To further investigate the role of PTP α in cancer cell invasion, two stable MDA-MB-231 cell lines were generated in which PTP α expression was silenced using lentiviral vectors encoding short hairpin RNA (shRNA). MDA-MB-231 cells were transduced with either a non-targeting shRNA control (shCtl) or one of two shRNA-PTP α constructs (sh α 1 or sh α 2) targeting unique sequences within the three-prime untranslated (3' UTR) region or the coding region (CDS), respectively, of the human PTP α gene. Transduced cells were selected using 0.5 μ g/mL puromycin and maintained in 0.3 μ g /mL puromycin-containing cell culture media. The resulting cell lines are referred to as shCtl-231, sh α 1-231, and sh α 2-231. PTP α expression was effectively reduced in sh α 1-231 cells by $41 \pm 15\%$ ($n \geq 3$) and in sh α 2-231 cells by $38 \pm 17\%$ ($n \geq 3$) relative to shCtl-231 cells (Figure 2.3A, B).

MDA-MB-231 cell migration and invasion were quantified over time using IncuCyte chemotaxis assays. To determine the role of PTP α in TNBC motility, shCtl-231, sh α 1-231, and sh α 2-231 cells were resuspended in either serum-free medium or growth factor-reduced Matrigel to monitor migration or invasion over time, respectively. PTP α depletion resulted in a significant reduction in the ability of MDA-MB-231 cells to migrate through the transwell membrane towards the 10% FBS chemoattractant (Figure 2.4A, B). Moreover, MDA-MB-231 cells depleted of

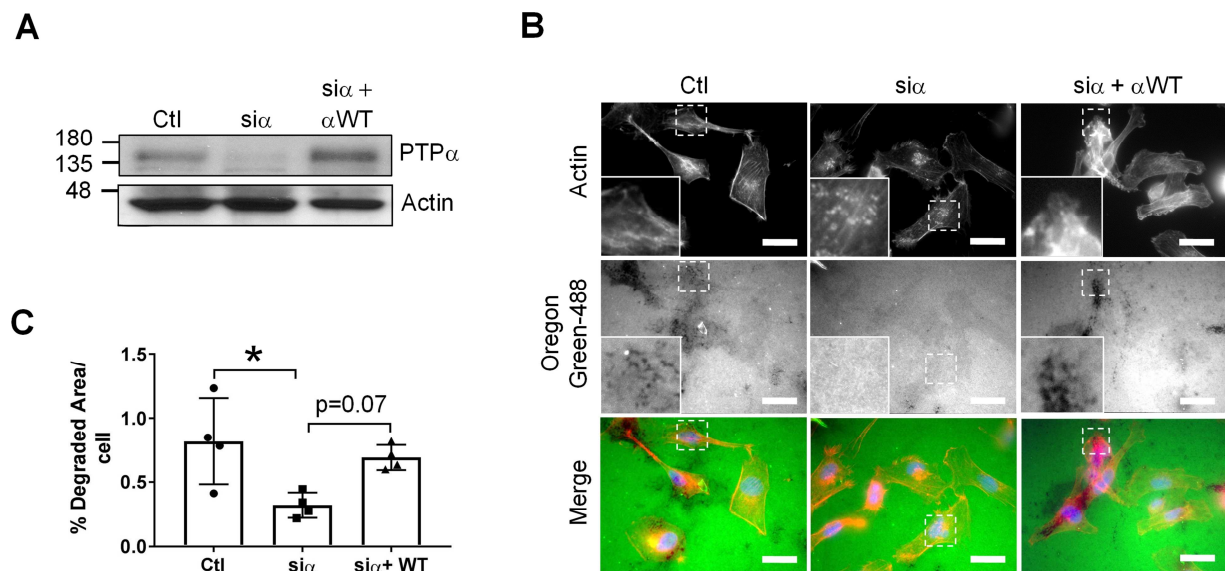


Figure 2.2. Depletion of PTP α reduces extracellular matrix (gelatin) degradation.

(A) MDA-MB-231 cells were transfected with non-targeting siRNA (Ctl) or siRNA #1 + #2 (si α) alone or together with siRNA-resistant PTP α -expressing plasmid (α WT). Cell lysates were collected 48 h post-siRNA treatment and immunoblotted for PTP α and actin. (B) Cells were plated onto Oregon Green 488-gelatin coated coverslips for 24 h and stained with DAPI and phalloidin-594 to detect actin. Scale bars = 25 μ m. The boxed regions are enlarged in the bottom left corner of each image. (C) The area of degraded matrix per cell per field of view was quantified from four independent experiments as in B, with an average of 80 cells quantified per experiment. Data are mean \pm SD (n=4, *p<0.01, one-way ANOVA with Dunnett post-hoc analysis).

PTP α showed an even greater reduction in invasion through the Matrigel (Figure 2.4C, D). These data suggest that PTP α expression is important for TNBC cell motility and particularly critical for invasion.

2.3.4 Knockdown of PTP α does not impact the secretion of soluble MMPs.

Soluble MMP2 and MMP9 proteinases are key enzymes responsible for gelatin degradation and breast cancer cell invasion (Beaty and Condeelis, 2014; Buccione et al., 2009; Eddy et al., 2017). To determine if PTP α knockdown alters the secretion of soluble MMPs, I performed an MMP antibody array as a general screen using conditioned medium collected from shCtl-231 and sh α 1-231 cells (Figure 2.5A). The MMP antibody array revealed that MMP1, TIMP1, TIMP2, and TIMP4 are the most abundantly secreted MMPs from MDA-MB-231 cells (Figure 2.5A). Furthermore, I observed no change in the expression levels of seven secreted MMPs (MMP1, MMP2, MMP3, MMP8, MMP9, MMP10, and MMP13) and three secreted TIMPs (TIMP1, TIMP2, and TIMP4) upon PTP α knockdown (Figure 2.5A). An enzyme-based immunosorbent assay (ELISA) was then used to further characterize MMP1 secretion levels, the most abundantly secreted MMP, using conditioned medium collected from shCtl-231 and sh α 1-231 cells. I found that knockdown of PTP α did not affect the secretion levels of MMP1 (Figure 2.5B). Together, these data suggest PTP α does not play a role in regulating the secretion of soluble matrix metalloproteinases. However, since I found that PTP α expression is essential for the function of gelatin-degrading invasive structures and since membrane-bound MMP14 is also a major regulator of invasion, I investigated the role of PTP α in mediating MMP14 expression and localization to protrusions resembling invadopodia.

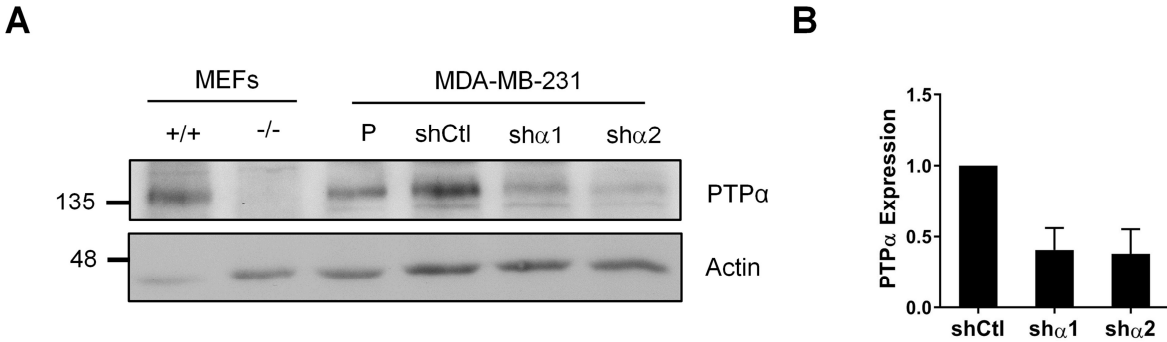


Figure 2.3. Generation of shRNA-expressing MDA-MB-231 cells stably depleted of PTP α .

(A) MDA-MB-231 cells were either untransfected (P; parental) or stably transfected with non-targeting shRNA (shCtl), shRNA-PTPa #1 (sh α 1), or shRNA-PTP α #2 (sh α 2). Cell lysates were collected 48 h post-seeding and immunoblotted for PTP α and actin. Mouse embryonic fibroblasts (MEFs) isolated from the brains of wild-type (+/+) or PTP α knockout (-/-) mice were used as positive and negative controls, respectively. (B) Densitometric quantification of PTP α expression relative to actin was performed using immunoblots of several such cell lysates and is shown in the graph as mean \pm SD ($n \geq 3$).

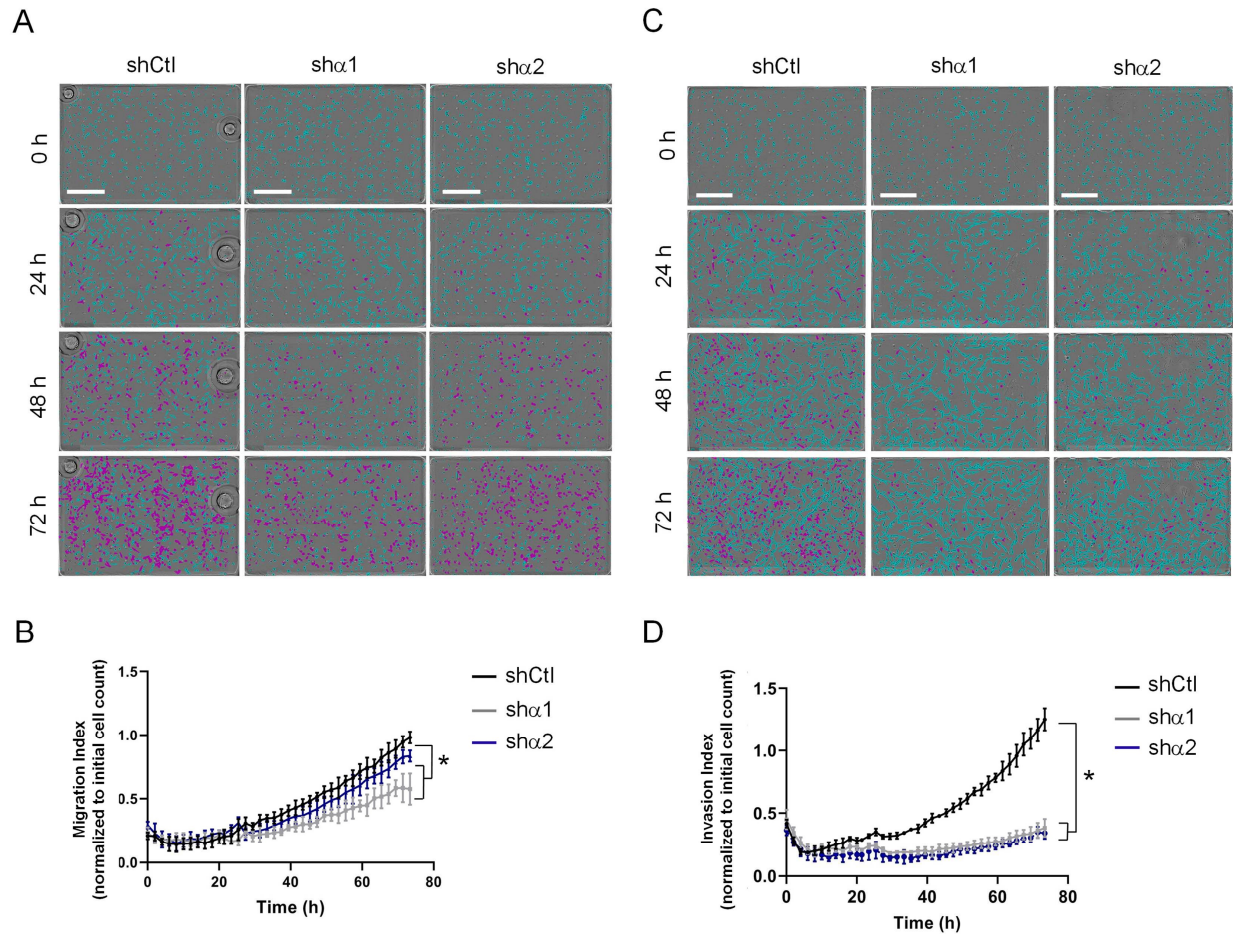


Figure 2.4. PTP α regulates migration and invasion of TNBC cells.

(A) MDA-MB-231 cells were transduced with either non-targeting shRNA control (shCtl), shRNA-PTP α #1 (sh α 1), or shRNA-PTP α #2 (sh α 2). Images of cells detected on the top (turquoise) and bottom (purple) surfaces of Transwell inserts at 0, 24, 48, and 72 h of an IncuCyte chemotaxis migration assay. Scale bars = 500 μ m. (B) Quantification of migration indices from experiments shown in (A) are displayed as cell counts normalized to initial cell number. Data are mean \pm SD (n=3, *p<0.05, two-way ANOVA with Tukey's post-hoc analysis). (C) MDA-MB-231 cells were transduced with either non-targeting shRNA control (shCtl), shRNA-PTP α #1 (sh α 1), or shRNA-PTP α #2 (sh α 2). Images of the cells detected on the top (turquoise) and bottom (purple) surfaces of Transwell Matrigel inserts at 0, 24, 48, and 72 h of an IncuCyte chemotaxis invasion assay. Scale bars = 500 μ m. (D) Quantification of invasion indices from experiments shown in (C) are displayed as relative cell counts normalized to initial cell number. Data are mean \pm SD (n=3, *p<0.05, two-way ANOVA with Tukey's post-hoc analysis).

2.3.5 PTP α mediates MMP14 localization to the membrane.

Since MDA-MB-231 cells were found to lowly express soluble MMPs, I next investigated the role of PTP α in regulating membrane-bound MMP activity, namely MMP14. More specifically, I asked if PTP α is involved in trafficking MMP14 to and/or from invadopodial structures. The localization and activity of MMP14 on the plasma membrane of cancer cells is regulated by various mechanisms, including endocytic and exocytic trafficking. Once MMP14 exits the trans-Golgi network (TGN) and reaches the cell surface, the majority of MMP14 is internalized via caveolin- or clathrin-mediated pathways and MMP14 is first shuttled to early endosomes or shuttled to lysosomes for degradation (Wang et al., 2004). A fraction of the internalized MMP14 residing in non-degradative endosomal compartments in tumour cells is then delivered to invadopodia at the plasma membrane (Gálvez et al., 2004; Jacob and Prekeris, 2015; Poincloux et al., 2009; Williams and Coppolino, 2011; Castro-Castro et al., 2016; Planchon et al., 2018). I investigated if the decrease in matrix degradation observed upon PTP α knockdown is associated with altered levels of MMP14 at the plasma membrane or in invadopodia-like membrane structures.

Total MMP14 protein levels were not found to be impacted by PTP α knockdown as determined by western blot analysis (Figure 2.6A). Thus, total versus surface expression of MMP14 was then quantified via flow cytometry using Stat3 as a positive control. I did not detect an altered level of membrane-bound MMP14 in PTP α knockdown versus control cells (Figure 2.6B). Given that MMP14 is a plasma membrane-bound protein that may be present within protrusions on the plasma membrane or elsewhere on the cell membrane, I then asked whether PTP α plays a role in the localization of MMP14 to actin and cortactin-positive plasma membrane

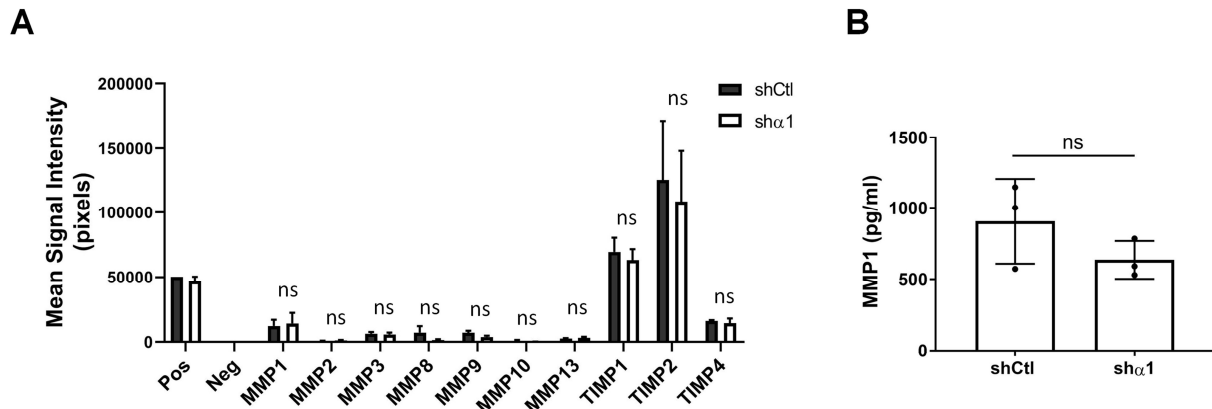


Figure 2.5. Depletion of PTP α does not alter the secretion of soluble MMPS.

(A) MMP antibody array results showing the expression of indicated MMPs and TIMPs in serum-free media (SFM) conditioned by shRNA control (shCtl) and PTP α depleted (sh α 1) MDA-MB-231 cells. MMP antibody arrays were quantified by densitometric analysis (n=3) and MMP expression is presented as mean signal intensity (pixels). Data represents the mean \pm SEM (n=3, ns = non-significant, one-way ANOVA). (B) MMP1 expression in SFM conditioned by shCtl and sh α 1 MDA-MB-231 cells were quantified by ELISA and normalized to cell number. Data are mean \pm SD (n=3, ns = non-significant, Student's t-test).

protrusions resembling invadopodia. To address this, shCtl-231, sh α 1-231, and sh α 2-231 cells were plated onto polycarbonate membranes with 0.3 μ m-diameter pores to allow the cells to form plasma membrane protrusions through the pores towards a chemoattractant. Cells were fixed, stained for cortactin/actin/MMP14 and visualized using confocal microscopy (Figure 2.6C). Z-stack images were created to visualize the plasma membrane structures extending downwards through the pores (Figure 2.6D). Consistent with results obtained via immunoblotting, I did not observe a difference in cellular MMP14 expression upon depletion of PTP α (Figure 2.6E). Importantly, the z-stack images revealed that the number of protrusions extending through the pores remained similar amongst equal numbers of control and PTP α knockdown cells (Figure 2.6F). However, the proportion of plasma membrane protrusions containing MMP14 was significantly lower in cells lacking PTP α (Figure 2.6G). Together, these results demonstrate that PTP α is important for the localization of MMP14 to plasma membrane protrusions rather than total MMP14 at the cell surface.

2.3.6 PTP α localizes to endosomes but does not localize to invadopodia.

Since PTP α was found to influence ECM degradation, cellular invasion, and MMP14 localization, I sought to determine if PTP α is a component of invadopodia by investigating its co-localization with MMP14 and TKS5, a protein considered a definitive marker of invadopodia (Abram et al., 2003; Seals et al., 2005). Firstly, I validated previously developed mCherry-tagged and GFP-tagged PTP α DNA constructs by collecting cell lysates from MDA-MB-231 cells that were either untransfected (-), transfected with mCherry or GFP alone (+) or with 0.5 μ g, 1.0 μ g, or 5.0 μ g of mCherry-tagged or GFP-tagged PTP α DNA and immunoblotting for

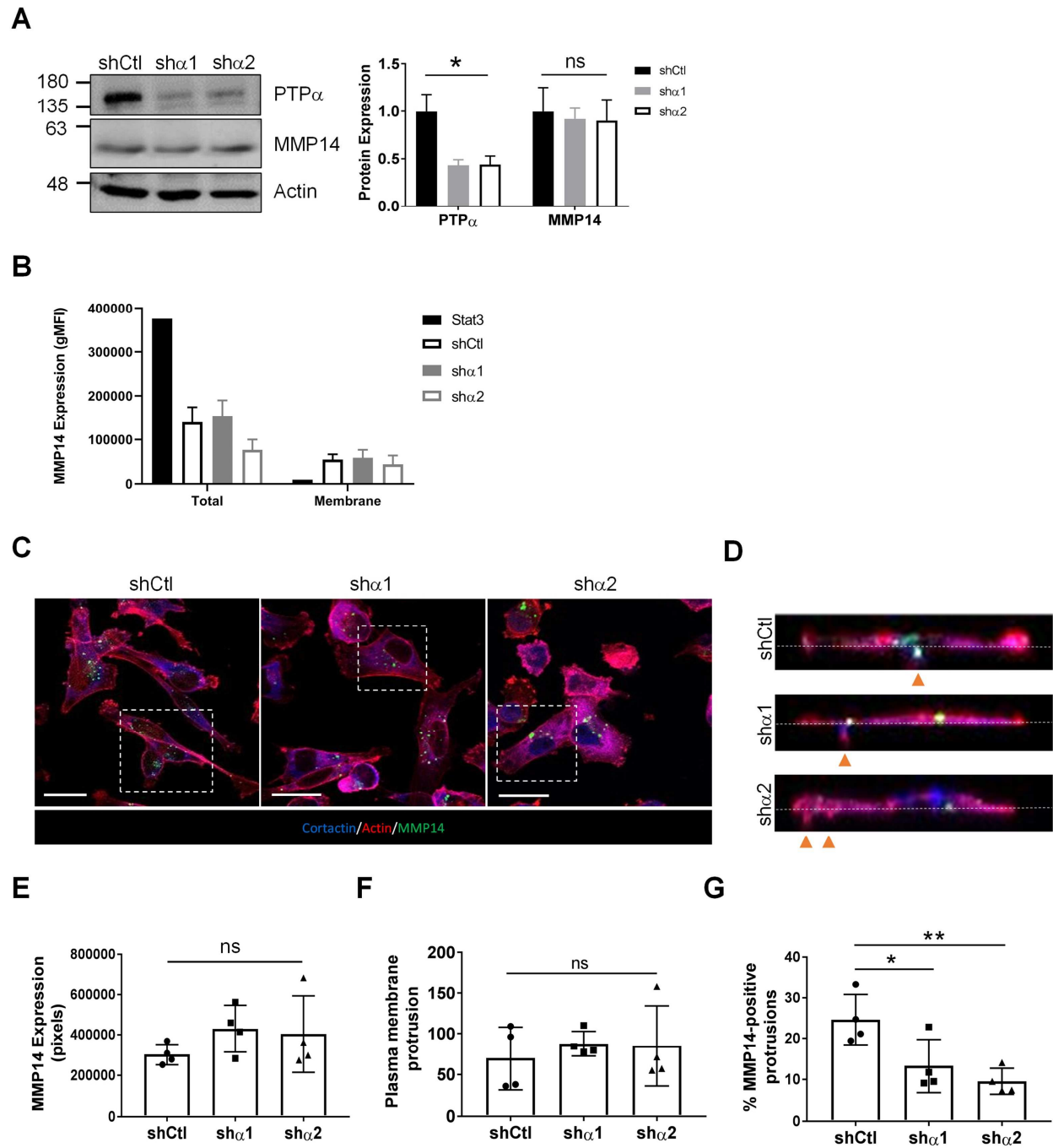


Figure 2.6. PTP α knockdown decreases MMP14 localization to plasma membrane protrusions.

Figure 2.6. PTP α knockdown decreases MMP14 localization to plasma membrane protrusions.

(A) Lysates of shCtl, sh α 1, and sh α 2 MDA-MB-231 cells were probed for PTP α , MMP14, and actin expression. Densitometric quantification of PTP α and MMP14 expression per unit actin relative to mean control samples was determined from four independent experiments. Data are mean \pm SD ($n \geq 3$, * $p < 0.05$, Student's t-test). (B) Flow cytometry analyses of total (permeabilized) and surface (non-permeabilized) MMP14 expression is presented as geometric mean fluorescence intensity (gMFI) Stat3 expression was used as a positive control ($n = 3$, ** $p < 0.01$, Student's t-test). (C) Cells were plated onto Transwell 0.3 μ m pore inserts, and immunostained for cortactin (blue), actin (red), and MMP14 (green). Scale bars = 25 μ m. (D) Representative z-stack images through the areas shown in the dotted boxes in C displaying individual plasma membrane protrusions (indicated with orange arrows). Protrusions containing actin and cortactin are pink; protrusion containing actin, cortactin and MMP14 are yellow-white, and extend through the pores below the membrane (white dotted line). (E) Total MMP14 expression in cells as shown in (C) was quantified as mean signal intensity (pixels) using ImageJ. Data are mean \pm SD. An average of 145 cells were imaged per cell type ($n = 4$, * $p < 0.05$, ** $p < 0.01$, one-way ANOVA with Tukey's post-hoc analysis). (F) Quantification of the total number of cellular protrusions. Data are mean \pm SD. An average of 145 cells were imaged per cell type ($n = 4$, * $p < 0.05$, ** $p < 0.01$, one-way ANOVA with Tukey's post-hoc analysis). (G) Quantification of the percentage of cellular protrusions containing MMP14. Data are mean \pm SD. An average of 145 cells were imaged per cell type ($n = 4$, * $p < 0.05$, ** $p < 0.01$, one-way ANOVA with Tukey's post-hoc analysis).

mCherry or GFP, PTP α , and actin. Immunoblotting for mCherry revealed a band at ~ 25 - 30 KDa in the mCherry-positive control lane and three distinct bands at ~ 130 KDa (mCherry-tagged N-glycosylated PTP α), ~ 140 KDa (mCherry-tagged N- and O- [partially] glycosylated PTP α) and ~ 160 - 170 KDa (mCherry-tagged N- and O- [fully] glycosylated PTP α) upon transfection with mCherry-PTP α (Figure 2.7A). Immunoblotting for GFP revealed a band at ~25 KDa in the GFP-only positive control lane as well as two distinct bands at ~ 130 KDa (GFP-tagged N-glycosylated PTP α), and ~ 160 KDa (GFP-tagged N- and O- glycosylated PTP α) upon transfection with GFP-PTP α (Figure 2.7B). Importantly, these bands are also visible when probing the western blots for PTP α , confirming that the fluorescent tags are conjugated to PTP α . In summary, in lysates from cells transfected with either mCherry-PTP α or GFP-PTP α , I did not observe any bands between 20 – 30 KDa that would indicate cleavage of these forms of tagged PTP α . This analysis confirms that the fluorescent proteins remain fused to PTP α and have not been cleaved.

To determine if PTP α is a component of invadopodia that contain TKS5 and/or MMP14, GFP-tagged PTP α expressing MDA-MB-231 cells were first stained for TKS5. Immunofluorescent analysis of 20 cells revealed 108 GFP-PTP α positive puncta, of which 105 (97%) of these puncta were negative for TKS5 (Figure 2.7C). I found that very few of the MDA-MB-231 cells expressing GFP-PTP α contained endogenous TKS5-positive invadopodia despite expressing cytoplasmic TKS5. To better visualize TKS5-positive invadopodia, MDA-MB-231 cells stably expressing exogenous GFP-tagged TKS5 were stained with the TSK5 antibody, confirming that this antibody was able to detect TKS5-positive invadopodial structures in TKS5 over-expressing cells and these invadopodia are identified by the GFP-TKS5 (Figure 2.7D). In

subsequent experiments, I found that when the GFP-tagged and mCherry-tagged forms of PTP α were co-expressed, the tagged forms of PTP α colocalize to the membrane and intracellular puncta validating that the cellular location of either form of exogenous PTP α was not uniquely affected by the tag or plasmid involved (Figure 2.7E). Finally, to confirm whether PTP α colocalizes with TKS5, mCherry-tagged PTP α was transfected into MDA-MB-231 cells stably expressing GFP-tagged TKS5 prior to plating the cells onto gelatin. I found that PTP α -positive puncta were distinct from TKS5-positive structures, indicating that PTP α did not co-localize with TKS5 in invadopodia (Figure 2.7F). While PTP α -positive puncta formed in close proximity to TKS5-positive invadopodia, only 7.9% (8/101) GFP-TKS5-positive invadopodia (n=16 cells) were also positive for mCherry-PTP α (Figure 2.7F). Together, these data strongly suggest that PTP α -positive structures are distinct from TKS5-positive invadopodia.

To further characterize the TKS5-negative PTP α -positive puncta shown in Figure 2.7, I investigated the co-localization of PTP α with cortactin and MMP14, noting that these proteins are present in, but not restricted to, invadopodia. MDA-MB-231 cells transfected with GFP-tagged PTP α were stained for MMP14 and cortactin (Figure 2.8A, left panel). An analysis of 30 cells revealed 204 GFP-PTP α -positive puncta, and the co-localization of PTP α with cortactin and MMP14 was then analyzed along linear tracks across individual puncta (Figure 2.8A, right panel). Of these puncta, 48.4% contained PTP α alone, 17.4% were positive for both PTP α and MMP14, 4.3% were positive for both PTP α and cortactin, and 29.5% were positive for PTP α , MMP14, and

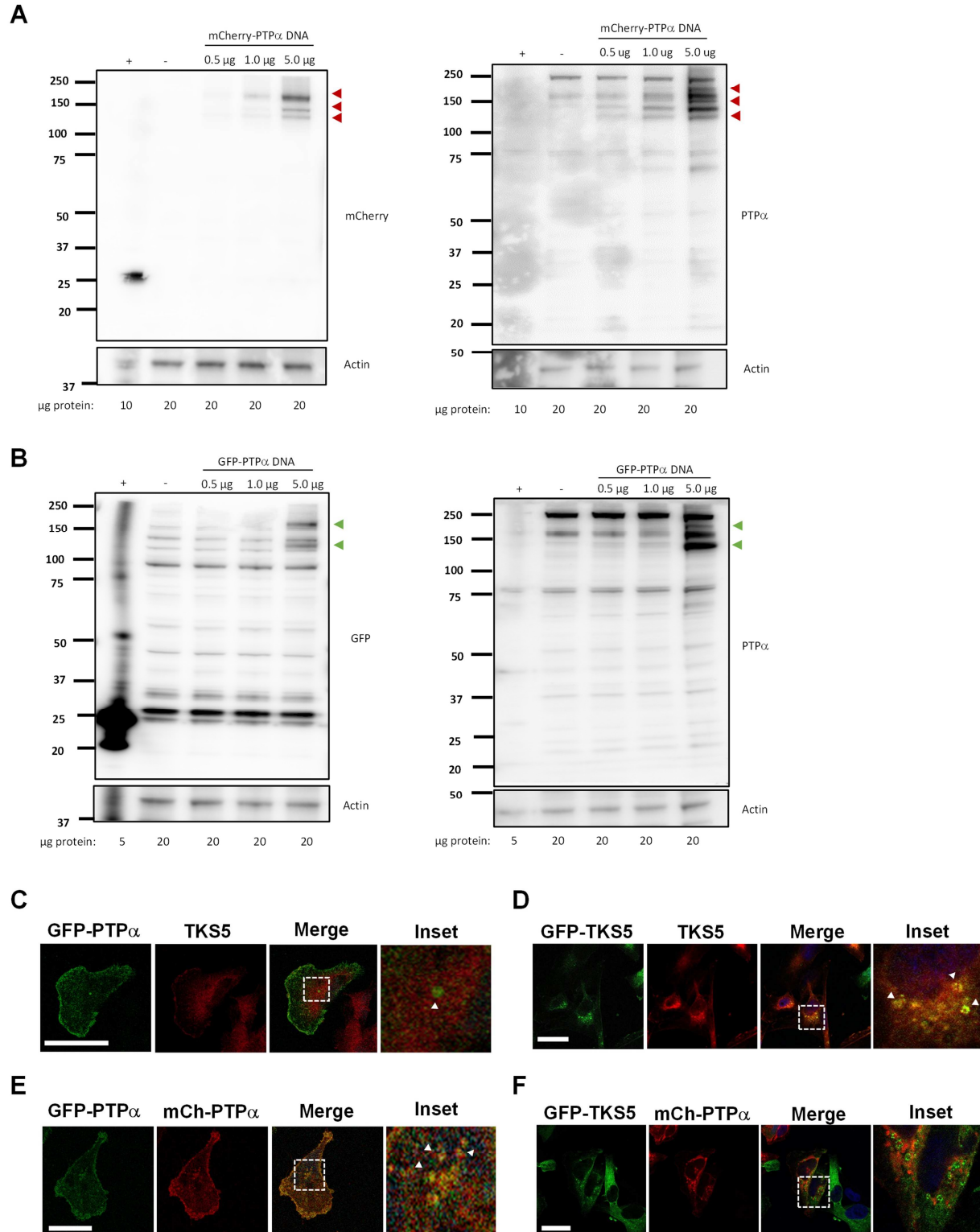


Figure 2.7. PTP α does not localize to TKS5-positive invadopodia structures.

Figure 2.7. PTP α does not localize to TKS5-positive invadopodia structures.

(A) MDA-MB-231 cells were either transfected with mCherry alone (+), untransfected (-), or with 0.5 μ g, 1.0 μ g, or 5.0 μ g of mCherry-tagged PTP α DNA. Cell lysates (5 – 20 μ g protein) were run on a NuPAGE 4-12% bis-tris gradient gel. Lysates were probed for mCherry, PTP α , or actin. Red arrows indicate PTP α tagged with mCherry. (B) MDA-MB-231 cells were either transfected with GFP alone (+), untransfected (-), or with 0.5 μ g, 1.0 μ g, or 5.0 μ g of GFP-tagged PTP α DNA. Cell lysates (5 – 20 μ g protein) were run on a NuPAGE 4-12% bis-tris gradient gel. Lysates were probed for GFP, PTP α , and actin expression. Green arrows indicate PTP α tagged with GFP. (C) Representative images of MDA-MB-231 cells expressing GFP-PTP α and stained for TKS5. Scale bars = 25 μ m. The boxed region is enlarged to the right of the merge image. (D) Representative images of MDA-MB-231 cells stably expressing GFP-TKS5 and stained for TKS5. Scale bars = 25 μ m. The boxed region is enlarged to the right of the merge image. (E) Representative images of MDA-MB-231 cells co-expressing GFP-PTP α and mCherry-PTP α . Scale bars = 25 μ m. The boxed region is enlarged to the right of the merge image. (F) Representative images of MDA-MB-231 cells stably expressing GFP-TKS5 and transiently transfected with mCherry-PTP α . Scale bars = 25 μ m. The boxed region is enlarged to the right of the merge image.

cortactin together (Figure 2.8D, left column). Together, these data indicate that PTP α is not present within TKS5-positive invadopodia, but that PTP α is found in cortactin-positive structures that are also positive for MMP14.

Caveolae are a type of lipid raft that regulate endocytic trafficking within the cell (Liu et al., 2002; Poincloux et al., 2009). Given that MMP14 localizes to caveolae (Annabi et al., 2001), that PTP α has been shown to localize to lipid rafts (Maksumova et al., 2005), and that PTP α localizes with non-invadopodial cortactin-positive MMP14-positive structures, I investigated if PTP α is present within caveolae. MDA-MB-231 cells expressing GFP-tagged PTP α were stained for MMP14 and caveolin-1 (cav-1) (Figure 2.8B), and 130 GFP-PTP α -positive puncta were detected in a population of 22 cells. It was found that 30.6% of these puncta were positive for PTP α alone, 26.2% for both PTP α and MMP14, 6.1% for both PTP α and cav-1, and 37.1% for PTP α , MMP14, and cav-1 together (Figure 2.8D, middle column).

Cav-1 also localizes to multiple intracellular compartments and vesicles including the Golgi (Fridolfsson et al., 2014), secretory vesicles, as well as exosomes and endosomes (Mundy et al., 2012; Pelkmans et al., 2004). Based on the size of the observed PTP α /MMP14/cav-1 triple-positive vesicles (>100 nm) in comparison to the known size of caveolae (<100 nm) and since cortactin is also known to co-localize to endosomes (Kaksonen et al., 2000), GFP-PTP α transfected cells were stained with a marker of early endosomes (early endosome antigen 1; EEA1). Indeed, I found that PTP α co-localized with MMP14 in EEA1-positive structures (Figure 2.8C). More specifically, a total of 78 GFP-positive puncta within 22 cells were analyzed to

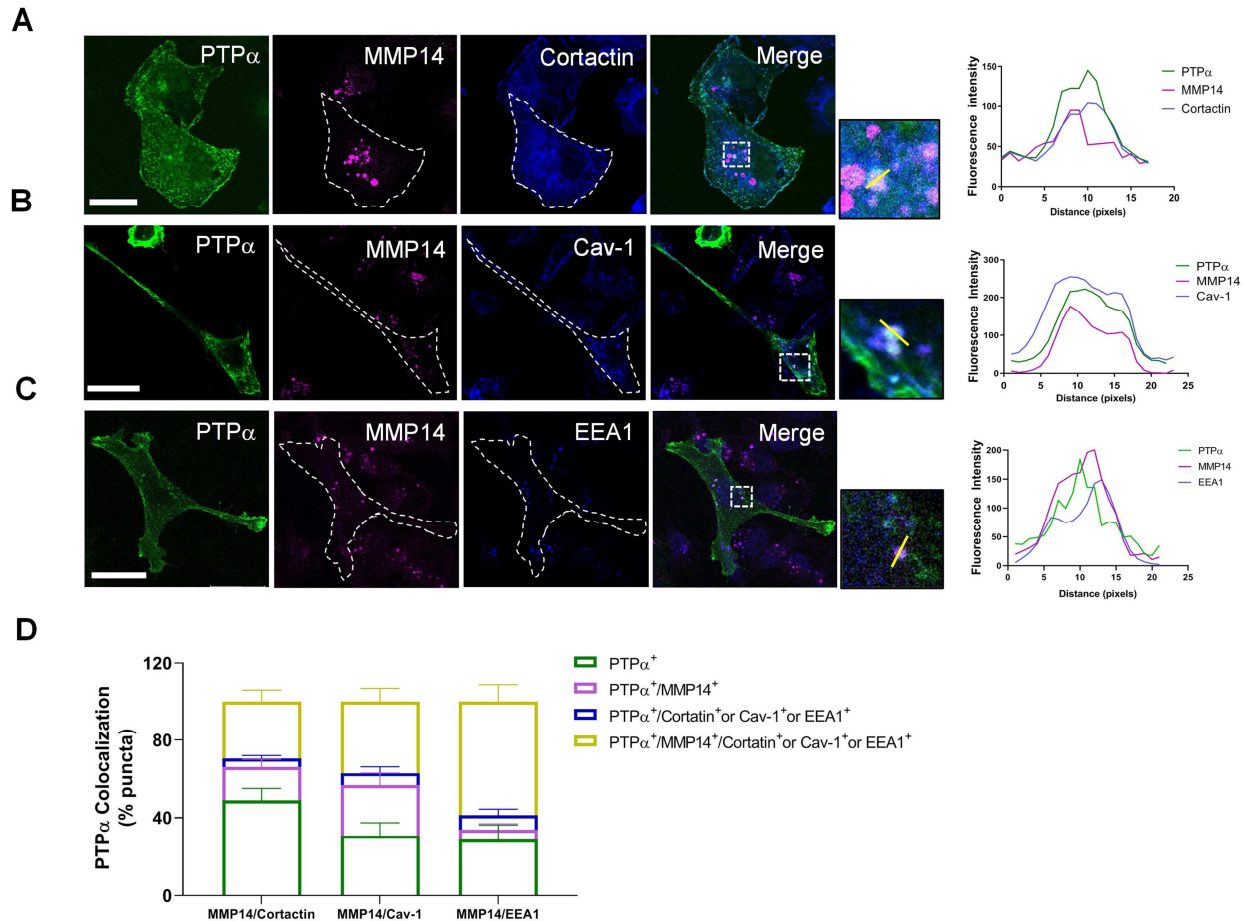


Figure 2.8. PTP α localizes to caveolin-1-positive and early endosome antigen-1-positive endosomal structures.

(A) Representative images of MDA-MB-231 cells expressing GFP-tagged PTP α and immunofluorescently stained for MMP14 and cortactin. Scale bars = 25 μ m. White dotted lines indicate cell outlines. The boxed areas with co-localized signals in the merged images are enlarged to the right. The yellow line across an individual puncta marks where fluorescence pixel intensity was quantified and is displayed in the graphs to the right. (B) Representative images of MDA-MB-231 cells expressing GFP-tagged PTP α and immunofluorescently stained for MMP14 and caveolin-1 (cav-1). (C) Representative images of MDA-MB-231 cells expressing GFP-tagged PTP α and immunofluorescently stained for MMP14 and early endosome antigen 1 (EEA1). (D) Quantification of the percentage of GFP-PTP α expressing puncta that colocalize with MMP14 alone, cortactin/cav-1/EEA1 alone, or MMP14 and either cortactin/cav-1/EEA1 (n = 22 – 30 cells).

determine the percentage of MMP14- and EEA1-positive puncta that were also positive for PTP α . It was found that 28.6% of the puncta were positive for PTP α alone, 5.2% for both PTP α and MMP14, 7.4% for both PTP α and EEA1, and 58.8% of the puncta exhibited PTP α , MMP14, and EEA1 together (Figure 2.8D, right column). These analyses indicate that PTP α preferentially localizes to puncta containing both MMP14 and EEA1. Together, these data suggest that PTP α localizes to endosomal structures within the cell.

2.3.7 Depletion of PTP α inhibits tumour growth.

Our *in vitro* data demonstrate that PTP α is an important player in the localization of MMP14, ECM degradation, and tumour cell migration and invasion. In a final set of experiments, I investigated whether PTP α regulates (i) the growth of mammary tumour xenografts, (ii) proliferation and apoptosis of breast cancer cells *in vivo*, and (iii) breast cancer cell invasion *in vivo* (Figures 2.9 – Figure 2.11).

I first transfected shCtl-231, sh α 1-231, and sh α 2-231 cells with a plasmid containing green fluorescent protein (GFP) and PTP α knockdown was confirmed via immunoblotting (Figure 2.9A). The GFP-expressing cells were then implanted into the fourth mammary fat pad of immunodeficient mice. I observed nearly a two-fold reduction in weight (mammary fat pad + tumour) upon PTP α knockdown when compared to control tumours two weeks after implantation (Figure 2.9B). The transfection of MDA-MB-231 cells with GFP will allow us to discriminate between GFP-positive tumour cells and normal cells within the mammary fat pad via IHC in future experiments (Figure 2.9C). Notably, I performed a growth experiment

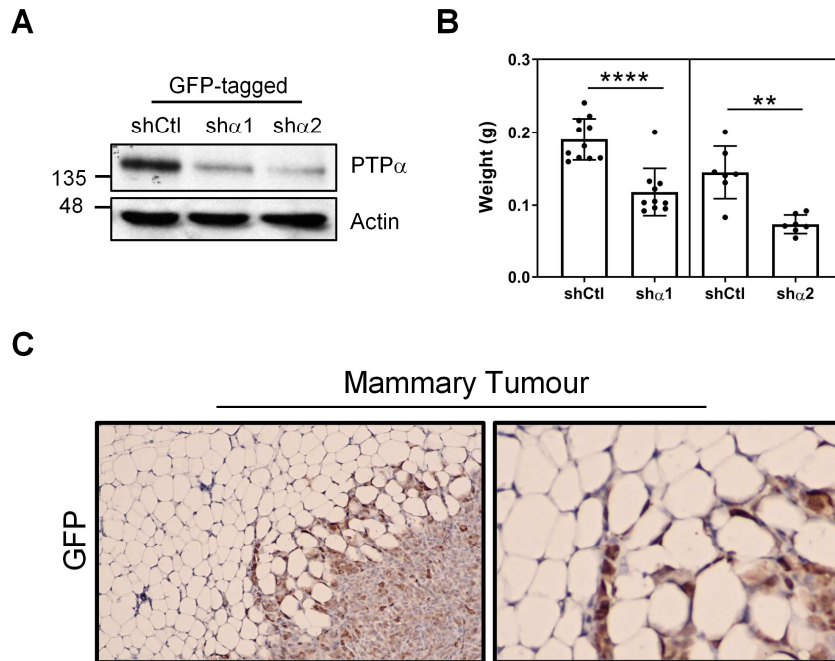


Figure 2.9. Depletion of PTP α reduces primary tumour growth of MDA-MB-231 breast xenografts.

(A) MDA-MB-231 tumour cells (1.0×10^6) were orthotopically injected into the 4th mammary fat pad of immunodeficient mice. Cell lysates of shCtl, sh α 1, and sh α 2 GFP-expressing MDA-MB-231 cells were probed for PTP α and actin expression via western blot analysis. (B) Total weight (grams) of the mammary fat pad and tumour was evaluated 14 days after implantation. (n=6-11 shCtl tumours, n=9 sh α 1 tumours, n=7 sh α 2 tumours, *p<0.05, Student's t-test). (C) Representative image of a mammary tumour stained with hematoxylin and GFP.

using non-GFP transfected shCtl (n=5 mice) and sh α 1 (n=4 mice) MDA-MB-231 cells to determine if the introduction of green fluorescent protein (GFP) had any effect on the size of the mammary tumours. GFP expression was not found to affect tumour size (data not shown).

2.3.8 PTP α knockdown upregulates *in vivo* apoptotic signaling.

I sought to determine if the decrease in tumour weight upon depletion of PTP α was due to disparities in proliferation or apoptosis *in vivo*, as determined by immunohistochemical staining of Ki67 or cleaved caspase 3 (CC3), respectively. There was no difference in the fraction of proliferative cells between mice bearing shCtl, sh α 1, and sh α 2 tumours (Figure 2.10A, B). A significant increase in the percentage of the CC3-positive area was observed in PTP α knockdown tumours compared to the control tumours (Figure 2.10A, C), indicating that reduced PTP α expression correlates with increased *in vivo* apoptotic signaling. To test the role of PTP α on apoptosis *in vitro*, lysates of MDA-MB-231 cells stably depleted of PTP α (shCtl, sh α 1, sh α 2 cells) were immunoblotted for poly (ADP-ribose) polymerase (PARP), a stress response protein that is proteolytically cleaved by caspases upon the induction of apoptosis. For a positive control, parental MDA-MB-231 cells were treated with 25 nM staurosporine (STS), an agent that inhibits cellular growth by inducing intrinsic apoptotic signaling pathways. I found that stably depleting PTP α in MDA-MB-231 cells does not induce apoptosis *in vitro* (Figure 2.10D), indicating the shRNA-expressing cells were not apoptotic before implantation and thus suggesting PTP α may be involved in protecting tumour cells from apoptosis *in vivo*.

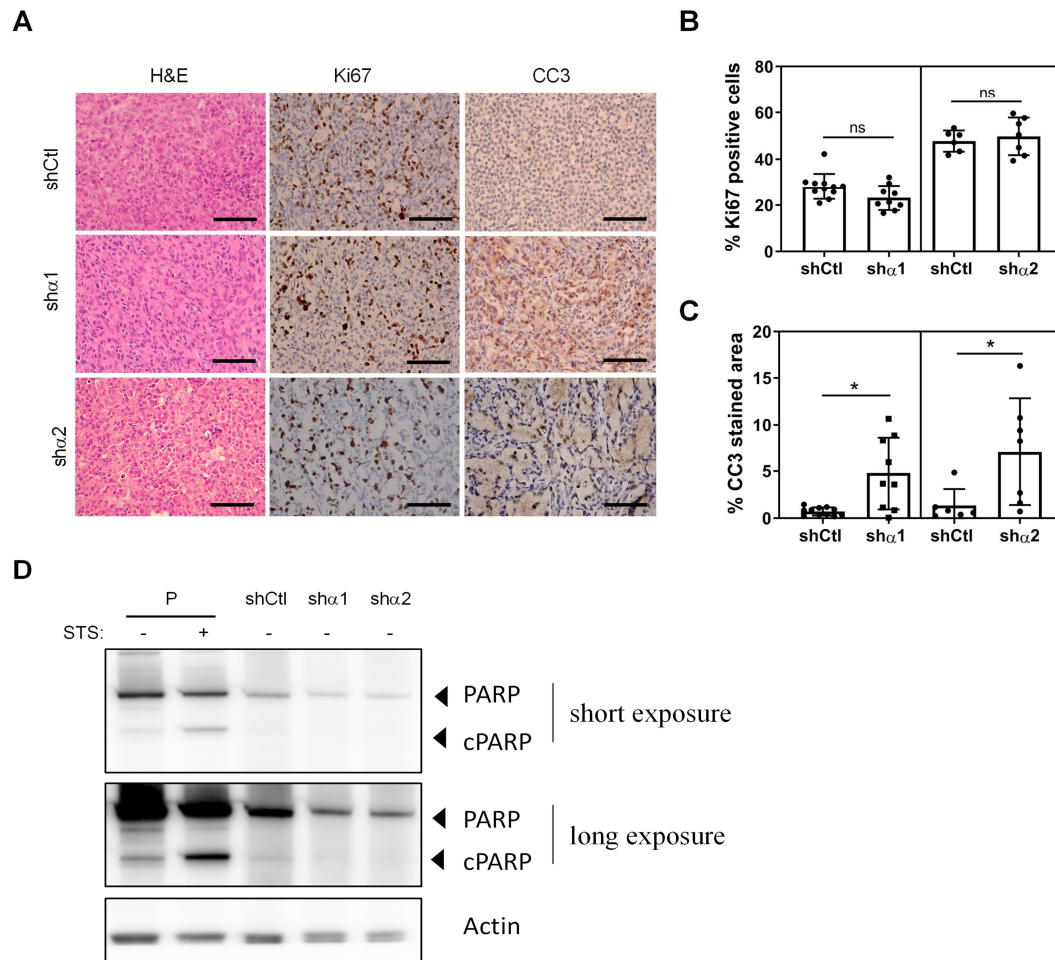


Figure 2.10. Depletion of PTP α upregulates intratumoural cleaved caspase-3 expression levels *in vivo*.

(A) MDA-MB-231 tumour cells were orthotopically injected into the mammary fat pad of female immunodeficient mice. Control (shCtl) or PTP α -knockdown (sh α 1 and sh α 2) tumours were analyzed via IHC (scale bars = 200 μ m). Tumours were stained with hematoxylin and eosin (H&E), Ki67, and cleaved caspase 3 (CC3). (B) Quantification of the percentage of Ki67-positive cells within the mammary tumours normalized to total cell number as determined by H&E staining (n=6-11 shCtl tumours, n=9 sh α 1 tumours, n=7 sh α 2 tumours, *p<0.05, Student's t-test). (C) Quantification of the percentage of the CC3-positive area within the mammary tumours normalized to total cell number as determined by H&E staining (n=6-11 shCtl tumours, n=9 sh α 1 tumours, n=7 sh α 2 tumours, *p<0.05, Student's t-test). (D) Parental MDA-MB-231 cells (P) were treated with 25 nM staurosporine (STS) as a positive control for apoptosis, and cell lysates were collected 24 h post-treatment. MDA-MB-231 cells stably transfected with non-targeting shRNA (shCtl), shRNA-PTP α #1 (sh α 1), or shRNA-PTP α #2 (sh α 2) were lysed and immunoblotted for PARP (cPARP = cleaved PARP) and actin (n=3).

2.3.9 Depletion of PTP α decreases the aggressiveness of breast tumour xenografts.

I then analyzed local invasion of shCtl-231, sh α 1-231, and sh α 2-231 cells *in vivo* and observed a striking reduction in the ability of PTP α knockdown tumour cells to invade into the surrounding mammary fat pad. It was found that control tumours often had diffuse tumour margins that extended several hundred μ m away from the primary tumour mass with invasive tracks of tumour cells extending into the fat tissue (Figure 2.11A). In contrast, the majority of tumours lacking PTP α had clearly delineated tumour margins with minimal extension into the surrounding fat pad (Figure 2.11A). The area of invasive tumour was calculated by subtracting the area of the solid tumour (black dotted line) from the total (i.e. solid and invasive) tumour area (yellow dotted line) (Figure 2.11A). I found a decrease in the total area of sh α 1 and sh α 2 MDA-MB-231 tumours compared to control tumours (Figure 2.11B), consistent with the reduced tumour weights (Figure 2.9B). Importantly, tumours grown from cells lacking PTP α displayed significantly less invasion into the surrounding mammary fat pad (Figure 2.11C). Notably, the degree of tumour cell invasion into the mammary fat pad was not associated with overall tumour size, as a wide range of solid and invasive tumour areas was observed between mice (Figure 2.11D). These data indicate that tumour cell invasion is not dependent on tumour size, and that PTP α knockdown decreases both primary tumour growth and tumour cell invasiveness *in vivo*.

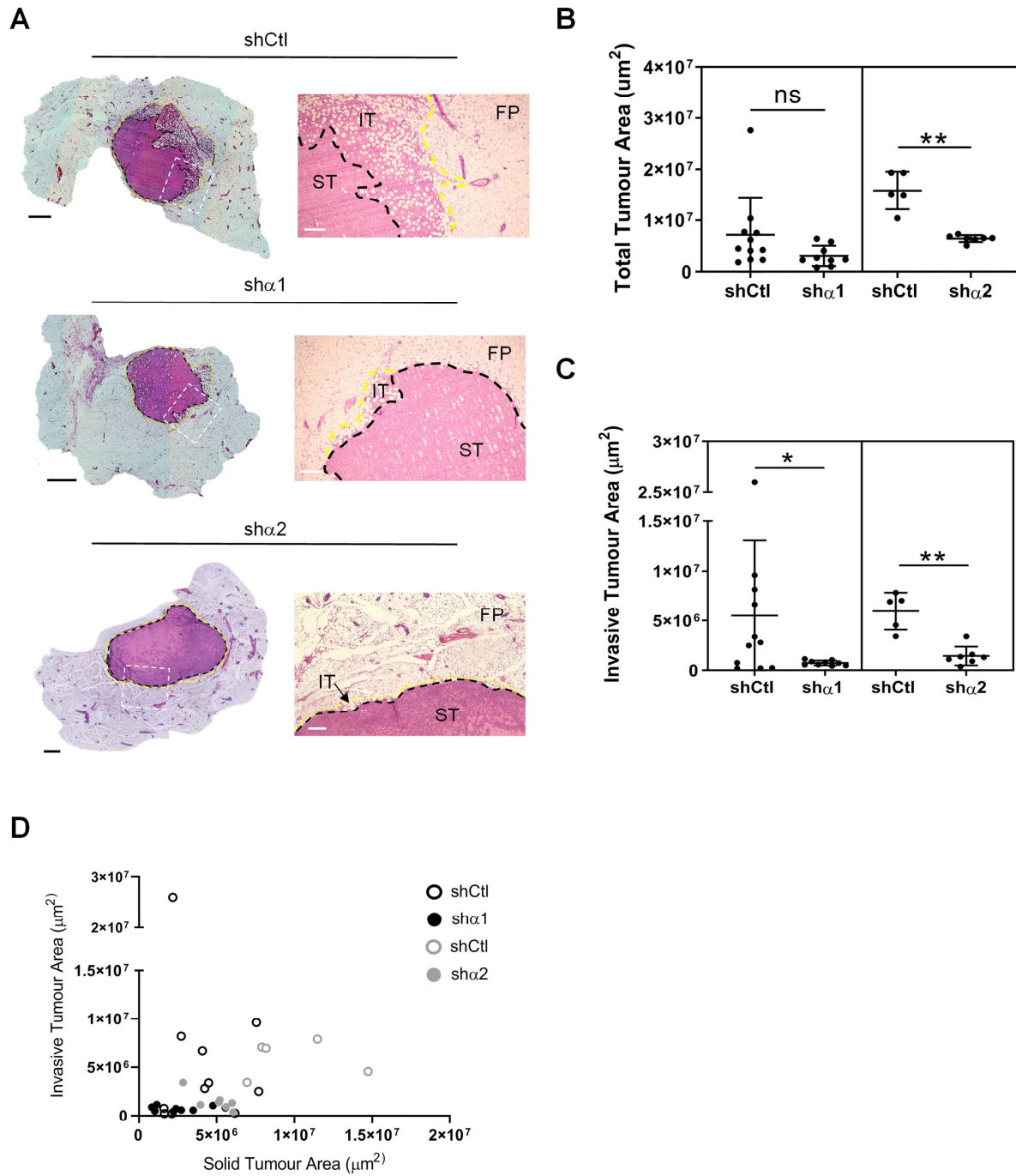


Figure 2.11. Depletion of PTP α decreases the aggressiveness of breast tumour xenografts.

(A) MDA-MB-231 tumour cells (1.0×10^6) were orthotopically injected into the 4th mammary fat pad of immunodeficient mice. Control (shCtl) or PTP α -knockdown (sh α 1 and sh α 2) mammary tumours were analyzed via immunohistochemistry. Left: Representative sections of control (shCtl) or PTP α -knockdown (sh α 1 and sh α 2) mammary tumours and fat pads stained with H&E (yellow dotted line, total tumour area; black dotted line, solid tumour area; scale bar, 500 μ m). Right: Higher magnification images of the white boxed areas (ST, solid tumour; IT, invasive tumour; FP, fat pad; black dotted line, solid tumour margin; yellow dotted line, total tumour margin; scale bars = 200 μ m). (B) Quantification of total tumour area (μ m²) in H&E sections from 5-11 shCtl, 9 sh α 1, and 7 sh α 2 tumours per group (*p<0.05, Student's t-test). (C) Quantification of invasive tumour area (μ m²) in H&E sections from 5-11 shCtl, 9 sh α 1, and 7 sh α 2 tumours per group (*p<0.05, Student's t-test). (D) Scatterplot of invasive versus solid tumour areas (μ m²) observed in control (shCtl) and PTP α -knockdown (sh α 1 or sh α 2) mammary tumours showing solid tumour area does not correlate with invasive tumour area.

2.4 Discussion

The local invasion of breast cancer cells into surrounding tissue is an important step in breast cancer metastasis that can eventually result in the formation of distant metastases. Finding new and innovative ways to stop cancer cells from infiltrating surrounding healthy tissues is key for preventing the cancer from spreading locally and throughout the rest of the body. Our overall objective was to determine if PTP α is involved in breast cancer cell invasion. In this work, I describe a novel role for PTP α in mediating ECM degradation (Figure 2.2) and MDA-MB-231 breast cancer cell invasion *in vitro* (Figure 2.4) and *in vivo* (Figure 2.11). PTP α was shown to be a component of early endosome antigen 1, caveolin-1, and MMP14-positive endosomal structures in the cell (Figure 2.8), and I determined that PTP α regulates the localization of MMP14 to plasma membrane protrusions resembling invadopodia (Figure 2.6). Importantly, I show that stable depletion of PTP α inhibits primary tumour growth and invasion of breast cancer cells into the surrounding mammary fat pad (Figure 2.9-2.11). Together, these data indicate an important role for PTP α in TNBC cell invasion and suggest that inhibition of PTP α *in vivo* may abrogate further metastasis.

Very few studies have investigated the role of PTP α in cancer progression and metastasis. Ardini *et al.* reported that PTP α expression varies greatly among tumours; however, high PTP α expression in a subset of ER-positive breast cancer correlates with low grade tumour status and reduced tumour growth and metastasis (Ardini *et al.*, 2000). Conversely, high mRNA levels of PTP α correlated with late stage colorectal carcinoma, and with increased squamous cell lung carcinoma tumours, lymph node metastasis, and depth of tumour invasion (Gu *et al.*, 2017; Tabiti *et al.*, 1995). PTP α has also been shown to regulate colon cancer cellular invasion using an *ex vivo*

chicken chorioallantoic membrane (CAM) assay (Krndija et al., 2010). Therefore, the role of PTP α in the progression of cancer appears to be tissue-specific and thus PTP α may be tumour-promoting or tumour-limiting depending on the tissue of origin. Our work and others recognize PTP α as a potential oncogene (Meyer et al., 2014; Zheng et al., 1992) and suggest that it may be an attractive drug target for the treatment of TNBC, with the added attributes that PTP α depletion is non-lethal (Ponniah et al., 1999; Su et al., 1999), it is accessible as a transmembrane receptor-type protein (Pallen, 2003), and it functions as an upstream activator of the proto-oncogene Src (Ponniah et al., 1999; Su et al., 1999; Zheng et al., 1992).

PTP α is highly homologous to PTP ϵ , which can act as an oncogene in certain contexts such as in neu-induced mammary tumour cells (Gil-Henn and Elson, 2003). Due to the structural and functional similarities between PTP α and PTP ϵ (Krueger et al., 1990), I confirmed that PTP ϵ expression is not altered in MDA-MB-231 cells depleted of PTP α ; however, this does not rule out the possibility of some, albeit incomplete, functional compensation by PTP ϵ .

It is well known that MMPs play a pivotal role in the pathogenesis of cancer and may act as tumour-promoting or tumour-limiting factors (Egeblad and Werb, 2002; Gialeli et al., 2011; Gobin et al., 2019). Normal and breast cancer cell lines express varying endogenous levels of MMPs and TIMPs (tissue inhibitors of metalloproteinases) depending on the cell type and cell culture conditions. Our data shows MDA-MB-231 cells cultured in serum-free media primarily secrete MMP1, TIMP1, TIMP2, and TIMP4, of which TIMP2 displayed the greatest protein expression levels. These results agree with previously published reports (Kousidou et al., 2004). Notably, MDA-MB-231 cells secrete low levels of MMP2 and MMP9, the major players in

invadopodia-mediated ECM degradation. However, our western blot and immunofluorescent analyses revealed MDA-MB-231 cells express high levels of MMP14. The Cancer Genome Atlas (TCGA) was recently used to screen 24 human MMPs in 15 different cancer types, which revealed MMP expression is highly heterogenous across most cancers (Gobin et al., 2019). It was found MMP1, MMP9, MMP10, MMP11, and MMP13 were most often upregulated across all tumour types while MMP3, MMP7, MMP12, and MMP14 were upregulated in certain tumour types including breast cancer (Gobin et al., 2019). These results together with our data suggests MMP14 may be a key player in facilitating MDA-MB-231 breast cancer cell invasion and ECM degradation.

The proteolytic activity of MMP14 at invadopodia is tightly regulated by endocytic/exocytic trafficking mechanisms (Beaty and Condeelis, 2014; Castro-Castro et al., 2016; Poincloux et al., 2009). PTP α was found within MMP14-positive structures that resemble endosomes (marked by EEA1 and cav-1) and MMP14 expression within plasma membrane protrusions decreased upon PTP α knockdown. However, the analysis of membrane-bound versus total MMP14 expression via flow cytometry did not reveal any changes in the expression levels of MMP14 upon PTP α knockdown. In retrospect, this was not particularly surprising as I postulate a role for PTP α in MMP14 localization specifically to plasma membrane protrusions, which may not be consistently quantifiable when analyzing MMP14 on the entire plasma membrane by flow cytometry. Together, these data raise the possibility that PTP α may be involved in endocytic signaling mechanisms. MMP14 is either expressed homogenously on the plasma membrane of cancer cells, or specifically targeted to invadopodia structures. Several studies have shown that upon MMP14 internalization via endocytosis, a fraction of MMP14 is recycled back to the plasma

membrane and distributed to invadopodia structures (Castro-Castro et al., 2016; Monteiro et al., 2013; Poincloux et al., 2009). Among other players, it has been reported that the Rho GTPases RhoA and Cdc42 are critical regulators of MMP14 delivery to invadopodia and ECM degradation (Eddy et al., 2017; Jacob and Prekeris, 2015; Sakurai-Yageta et al., 2008). Previous work from our lab has shown that PTP α regulates Cdc42 activation in a variety of signaling and cell contexts, including integrin-induced signaling in fibroblasts (Samayawardhena and Pallen, 2008; Sun et al., 2012; Wang et al., 2009, 2012). While the role of PTP α in regulating Rho GTPase signaling in cancer cells remains unknown, perhaps the depletion of PTP α in TNBC cells disrupts Cdc42 activation thus reducing the accumulation of MMP14 at invadopodia. Rab GTPases, most notably Rab5 and Rab7, are other known negative regulators of MMP14 surface expression (Linder and Scita, 2015). Recently, flotillin-induced endocytosis of plasma membrane-bound MMP14 to Rab5-positive endolysosomes was found to be critical for the subsequent targeted delivery of MMP14 to sites of ECM degradation (Planchon et al., 2018). This raises the question of whether PTP α -MMP14-EEA1-positive endosomes are also involved in flotillin-induced endocytosis of MMP14, and if depletion of PTP α downregulates flotillin expression resulting in decreased targeted delivery of MMP14 to invadopodia. Future work is also required to elucidate the precise pathways linking PTP α , caveolin-1, and EEA1 to endocytic trafficking of MMP14 in TNBC cells, and whether PTP α and MMP14 are co-trafficked to invadopodia during the later stages of invadopodia development (i.e. maturation phase).

In 2012, Wang *et al.* described a mechanism by which MMP14 is targeted to FAs by associating with a focal adhesion kinase (FAK)-p130Cas complex in pancreatic cancer cell lines (Wang and McNiven, 2012). The physical interaction between MMP14 and the FAK-p130Cas

complex required for FA-dependent ECM degradation is dependent upon Src-mediated phosphorylation of MMP14 at tyrosine residue 573 on the cytoplasmic tail of MMP14. Previous work in our lab identified a role for PTP α in Src-signaling mechanisms that regulate actin stress fiber assembly, FA dynamics, and fibroblast migration (Boivin et al., 2013; Chen et al., 2006; L. Zeng et al., 2003). Upon integrin stimulation, PTP α dephosphorylates Src at the Tyr⁵²⁷ residue to promote Src activation (Chen et al., 2006; L. Zeng et al., 2003). Active Src associates with FAK and phosphorylates FAK at various tyrosine residues. The Src-FAK complex can then phosphorylate PTP α at Tyr⁷⁸⁹, identifying PTP α as both an upstream activator and downstream effector of Src (Chen et al., 2006; L. Zeng et al., 2003). PTP α -phospho-Tyr⁷⁸⁹ was later shown to bind BCAR3 and subsequently Cas to recruit Cas to FAs where it can regulate downstream signaling (Sun et al., 2012). Due to this relationship between PTP α and the Src signaling pathway in fibroblasts, it seems plausible that PTP α could act through a similar BCAR3-Cas-Src axis to regulate MMP14 recruitment to plasma membrane structures and influence tumour cell invasion.

Importantly, using an orthotopic xenograft model, I assessed the role of PTP α in mediating TNBC tumour growth and cellular invasion *in vivo*. Tumours lacking PTP α were significantly smaller and exhibited less invasive tumour margins compared to the control MDA-MB-231 tumours, supportive of our *in vitro* data. Notably, other groups have shown that depletion of invasion-associated proteins limits tumour growth *in vivo*. Reduced expression of TKS5, an invadopodia scaffold protein, results in decreased mammary tumour growth accompanied by reduced proliferation and increased apoptosis (Blouw et al., 2015, 2008). Similarly, loss of cortactin and MMP14 profoundly reduced the growth of head and neck squamous cell carcinoma (HNSCC) and squamous cell carcinoma (SCC-1) tumours, respectively (Clark et al., 2009; Hotary

et al., 2003). In addition to decreased invasive potential, I also observed an induction of apoptosis *in vivo* upon the suppression of PTP α in TNBC tumours, which mimics the phenotype observed upon TKS5 depletion. Previous work showed depletion of PTP α had no significant effect on cellular proliferation or apoptosis, as determined by IHC staining of Her2-positive mammary tumours (Meyer et al., 2014). Interestingly, oligodendrocyte progenitor cells (OPCs) isolated from PTP α -null mouse embryonic brains and cultured *in vitro* displayed increased proliferation and decreased apoptosis compared to OPCs from WT brains (Wang et al., 2012). Other groups have reported that suppression of PTP α activity induced apoptosis in ER-negative breast cancer and colon cancer cells, but not ER-positive breast cancer cells (Zheng et al., 2008). No difference in apoptosis was observed *in vitro*, but we observed increased CC3 expression in tumours formed by PTP α -depleted TNBC cells *in vivo*, suggesting PTP α protects tumour cells from apoptosis induced within the solid tumour microenvironment.

Taken together, our data identify a novel relationship between PTP α and MMP14, with PTP α acting as an important mediator of MMP14 localization in breast cancer cells. Our findings also identify PTP α as a potential target to reduce triple-negative breast cancer invasion *in vitro* and *in vivo*.

Chapter 3: Ionizing radiation upregulates TKS5 expression in GBM cells *in vitro* independent of invadopodia activity and cellular invasion.

3.1 Rationale and Hypothesis

Gliomas are a type of brain tumour that arise from glial cells (*i.e.* astrocytes, oligodendrocytes, *etc.*) and account for nearly half of all diagnosed brain tumours. The most common glioma tumours are astrocytomas, which can be subdivided into four grades with increasing aggressiveness: pilocytic astrocytoma (Grade 1), diffuse astrocytoma (Grade 2), anaplastic astrocytoma (Grade 3), and glioblastoma multiforme (Grade 4). Glioblastoma multiforme (GBM) is considered the most aggressive form of brain cancer and accounts for 12-15% of brain tumours diagnosed within Canada. The incidence of GBM is 4 per 100,000 people and more commonly occurs in adult males than females (Mason et al., 2007). The median overall survival remains between 12-18 months despite GBM patients undergoing extensive treatment. This low survival rate can be attributed to several factors including the highly infiltrative nature of GBM, high rates of recurrence, limited treatment options due to high rates of resistance, and limited ability of many chemotherapeutic drugs to cross the blood-brain barrier.

The conventional treatment plan for newly diagnosed GBM patients includes maximal surgical resection and radiation therapy in combination with chemotherapy, typically temozolomide (TMZ), and then followed by adjuvant TMZ treatment for multiple weeks (Stupp et al., 2005). While radiation therapy is often curative since RT is effective at inducing DNA damage and tumour cell death, multiple reports indicate a subset of irradiated tumour cells may exhibit increased invasiveness (Moncharmont et al., 2014; Sundahl et al., 2018; Wank et al., 2018a, 2018b). This was first observed in 1949 when authors Kaplan and Murphy showed

irradiating mouse xenografts significantly increased the incidence of pulmonary metastases (Kaplan and Murphy, 1949). Multiple studies have since investigated the role of ionizing radiation in upregulating GBM cell invasion *in vitro* using a variety of cell lines (Kegelman et al., 2017; Wank et al., 2018a; Yoo et al., 2018; Zhang et al., 2018). Notably, work by Wild-Bode *et al.* reported increased chemotactic migration and invasion of LN229, LN18, U87-MG glioma cells as well as an upregulation of matrix metalloproteinase (MMP) expression and activity *in vitro* and *in vivo* (Wild-Bode et al., 2001). In addition to IR-induced MMP activity, multiple groups also state IR upregulates Src expression and activity (Kegelman et al., 2017; Kim et al., 2015; Park et al., 2006; Yoo et al., 2018; Zhao et al., 2016). Interestingly, many of the signaling mechanisms reported to induce IR-induced invasion are associated with invadopodia biogenesis.

Glioblastoma cells are known to be a highly infiltrative cell type and often invade into the surrounding healthy brain tissue. Specialized invasive structures termed invadopodia facilitate invasion of multiple malignant tumour types, including glioblastoma. Invadopodia are cancer-specific proteolytically active structures that remodel the surrounding microenvironment by secreting MMPs (Murphy and Courtneidge, 2011; Paterson and Courtneidge, 2018). These specialized structures were first identified in Src-transformed fibroblasts, identifying Src as a critical component for invadopodia biogenesis (Abram et al., 2003; Seals et al., 2005). Src has been shown to phosphorylate TKS5, which results in the recruitment of other critical molecular components such as Nck1/Nck2 (Stylli et al., 2009). Tyrosine kinase substrate 5 (TKS5) is a large scaffold protein that has three distinct isoforms: TKS5 α (150 KDa), TKS5 β (140 KDa), and TKS5_{short} (130 KDa) (Kudlik et al., 2020; Saini and Courtneidge, 2018). TKS5 is not found in other cellular structures and is therefore considered a definitive marker of invadopodia (Saini and Courtneidge, 2018). In addition to regulating invadopodia formation via interactions with

phosphatidylinositol-3-phosphate (PI3P) and PI(3,4)P phospholipids on the plasma membrane, TKS5 has also been found to play a role in ROS production via interactions with NOX enzyme complexes and p22^{phox}, both members of the p47 organizer family of proteins (Díaz et al., 2013; Kudlik et al., 2020). Due to the relationship between IR and ROS production well as previous reports stating IR upregulated Src expression and activity, we sought to investigate the role of IR in modulating Src-TKS5 signaling mechanisms to induce invadopodia-mediated glioblastoma cell invasion.

In this chapter, I show IR upregulates TKS5 mRNA and protein expression despite identifying focal adhesions as the primary ECM degrading structure in GBM cells, rather than invadopodia. Furthermore, IR did not alter invadopodia formation or activity, as measured using *in vitro* gelatin degradation assays. Lastly, I found IR significantly reduces *in vitro* GBM cell invasion. These findings suggest ionizing radiation regulates TKS5 expression in glioma cells in an invadopodia- and invasion-independent manner.

3.2 Materials and Methods

3.2.1 Cell culture

Human glioblastoma cell lines LN229 (Cat.No. CRL-2611), U87-MG (Cat.No. HTB-14), and LN18 (Cat.No. CRL-2610) were purchased from ATCC (www.atcc.org), while U251 and U343 cell lines were obtained from Dr. Stephen Yip's lab (BC Cancer) (Appendix A1). GBM cells were grown in Dulbecco's modified Eagle's medium (Hyclone, #SH30243) containing either 5% FBS (LN229 and LN18 cells) or 10% FBS (U87-MG, U251, and U343 cells). LN229, U87-MG, and LN18 cells were confirmed to be mycoplasma negative.

3.2.2 Antibodies and reagents

Primary antibodies against the following proteins were used: anti-TKS5 (Millipore, 09-403; Millipore, MABT336), anti-actin (Sigma, Cat.No. A2066), anti-phospho-Src (Tyr527) (Cell Signaling, Cat.No. 2105), anti-Src (Cell Signaling Technologies, Cat.No. 2110), anti-vinculin (Novus Biologicals, Cat.No. NB-600-1293), anti-phospho-FAK (Tyr397) (Cell Signaling Technologies, Cat.No. 3283), anti-FAK (Cell Signaling Technologies, Cat.No. 3285) anti-MT1-MMP (MMP14) (Millipore, Cat.No. MAB3328), and anti-MMP2 (Abcam, Cat.No. ab37150). Rabbit anti-PTP α antiserum 2205 has been described previously (Chen et al., 2006; Lim et al., 1998). Secondary antibodies used were: Alexa Fluor 594-conjugated goat anti-mouse IgG (Molecular Probes, Cat. No. A11032) and Alexa Fluor 647-conjugated goat anti-rabbit IgG (Life Technologies, Cat.No. A21245). Actin was marked using Alexa Fluor 594-conjugated to phalloidin (ThermoFisher, Cat.No. A12381). Coverslips were mounted using Prolong Gold anti-fade mounting media with DAPI (Invitrogen, Cat.No. P36941).

3.2.3 Immunoblotting

LN229 and LN18 cells were lysed with RIPA buffer containing a protease inhibitor cocktail (Thermo Scientific, Cat. No. 87787; Cat.No. 78440). Total protein concentration was determined using BioRad Protein Assay Dye (Biorad, Cat.No. 5000006). The cell lysates were prepared using reducing conditions and 20 μ g of protein was resolved by SDS-PAGE. The proteins were transferred to polyvinylidene difluoride (PVDF) membranes, blocked in 3% BSA-PBS with 0.1% Tween-20, and immunoblotted with the indicated antibodies. The immunoblots were visualized using ECL detection methods using a Bio-Rad ChemiDoc Imager. For irradiation studies, cells were irradiated as monolayers (*i.e.* adherent culture) on either plastic or gelatin-coated dishes.

3.2.4 Matrix degradation assay

Oregon Green-488 fluorescently-tagged gelatin coverslips were prepared as previously described in Section 2.2.5. In brief, LN229 and LN18 cells (5.0×10^4) were irradiated as monolayers (*i.e.* adherent culture), and then 24 hours later seeded onto the fluorescently-tagged gelatin coverslips for 4 or 24 hours (*i.e.* 28 h and 48 h post-IR) in complete cell culture media. Cells were then fixed with 4% PFA for 15 mins at RT, permeabilized with 0.2% Triton X-100 in PBS for 10 mins at RT, and stained for immunofluorescent analysis. An overall average of 40 - 66 cells per dose per experiment were imaged (12 FOV per condition) at 63X magnification. ImageJ was used to quantify (*i*) percentage of gelatin degrading cells and (*ii*) the area of degradation as a percentage of the cell area.

3.2.5 Immunofluorescence

A general immunofluorescent staining protocol has been previously described in section 2.2.11.

3.2.6 Cell Survival Assays

3.2.6.1 Clonogenic survival assay

GBM cells were irradiated as monolayers (*i.e.* adherent culture) with the indicated dose of radiation (30kV, 10mA, 5.00 Gy/min) using the Precision X-ray machine model X-RAD320 (North Branford, Connecticut, USA) and then cultured for 2 weeks at 37°C and 5% CO₂. Surviving colonies were stained with a 0.5% crystal violet and 25% methanol solution. Surviving fraction (SF), presented as a percentage, was determined using the following equations that account for plating efficiency (PE).

$$\text{SF} = \frac{\text{total colonies counted}}{\# \text{ cell plated} \times (\text{PE}/100)} \quad \text{PE} = \frac{\# \text{ of colonies (0 Gy)}}{\# \text{ cells seeded}}$$

3.2.6.2 Flow Cytometry

Cells growing as monolayers in gelatin-coated dishes were irradiated with 0 Gy or 10 Gy radiation either 7, 5, 3, 1, or 0 days before harvest using the Precision X-ray machine model X-RAD320 (North Branford, Connecticut, USA). Floating cells were collected from the media while the adherent cells were washed twice in PBS and lifted using cell dissociation buffer (Thermo Scientific, Cat.No. 13151014) for 20 mins at RT. Finally, the floating and adherent cells were pooled and resuspended in HFN buffer (Hank's balanced salt solution with 10 mM HEPES (STEMCELL Technologies), 2% FBS and 0.05% sodium azide). Cells were then stained with Propidium Iodide (0.2 µg/mL) in Annexin Binding Buffer (Abcam, Cat.No. 14085). Samples were acquired immediately on a BD LSRFortessa (FACSDiva software, BD) and analyzed with FlowJo (TreeStar). Cells fixed in 4% PFA for 15 mins at RT were used as a positive control.

3.2.7 Real time qPCR

Total RNA was extracted from cells and reverse-transcribed into cDNA using a high-capacity RNA-to-cDNA Kit (Thermo Fisher Scientific, Cat.No. 4387406). Real-time PCR was performed on the ABI StepOne System (Applied Biosystems) using TaqMan Fast Advanced Mastermix (#4444556, Applied Biosystems) and pre-designed human PrimeTime qPCR Probes (FAM reporter) MMP2 (Hs.PT.58.39114006), Tks55 (Hs.PT.58.26736427), GAPDH (Hs.PT.39a.22214836) and HPRT1 (Hs.PT.58 v.45621572). The target gene expression was normalized to the expression of house-keeping gene, GAPDH or HPRT1, and the relative changes in target gene expression were analyzed using the $2^{-\Delta\Delta C_t}$ ($2^{-\Delta\Delta C_t}$) method.

3.2.8 *In vitro* chemotaxis invasion assays

Single timepoint invasion assays were carried out using 8.0 μm Transwell polycarbonate membranes coated with Matrigel (Corning[®], Cat. No. 354480). In brief, cells were serum starved overnight, and then seeded into the upper chamber in serum-free medium (3.5×10^4 cells). The bottom chamber was filled with medium containing 10% FBS as the chemoattractant, and the cells were incubated at 37°C/5% CO₂ for 24 h. Post-incubation, inserts were removed from the 24-well plate, washed once with PBS, and the cells on the bottom surface of the membrane were fixed in 70% ethanol for 15 min. Cells were stained with 0.2% crystal violet and counted from at least four independent experiments each performed in duplicate. Time course invasion assays were performed using IncuCyte chemotaxis assays as previously described in section 2.2.7. In brief, sham and irradiated LN229 and LN18 cells were serum starved overnight before being resuspended in either 1.0 mg/mL or 5.0 mg/mL Matrigel and seeded (1.0×10^3 cells per well) into a ClearView 96-well plate (Essen Biosciences, Cat.No. 4582). The bottom chambers were filled with 20% FBS as the chemoattractant and invasion was monitored at 4-hour intervals for 72 h (LN18 cells) or 120 h (LN229 cells). Invasion was quantified as changes in cell count over time as a proportion of the initial cell counts (0 h) and then normalized to $t = 0$ h.

3.3 Results

3.3.1 TKS5 and Src expression in glioma cell lines.

To study the effects of ionizing radiation in modulating invadopodia biogenesis and GBM cell invasion, we first performed a cell line screen to identify invasive GBM cell lines suitable for future work. Five human GBM cell lines with varying mutational statuses were screened: U343 cells (p53 wild-type, PTEN mutant), LN229 cells (p53 mutant, PTEN wild-

type), U87-MG cells (p53 wild-type, PTEN null), LN18 cells (p53 mutant, PTEN wild-type), and U251 cells (p53 mutant, PTEN mutant). All five cell lines are IDH 1/2 wild-type, consistent with primary GBM tumours (Figure 3.1A). Using a standard Transwell invasion assay in which cells invade through Matrigel towards 10% FBS chemoattractant, we found U343 cells were minimally invasive while LN229, U87-MG, LN18, and U251 cells invaded through the membrane with U251 cells exhibiting the greatest level of invasiveness (Figure 3.1B). Since TKS5 and Src expression are required for invadopodia formation and function (Abram et al., 2003; Kelley et al., 2010; Mader et al., 2011; Seals et al., 2005; Sharma et al., 2013), we analyzed the expression levels of TKS5 and Src in the five human GBM cell lines. Western blot analysis revealed TKS5 and Src expression varied considerably across cell lines, with LN229 displaying the greatest expression levels and U343 exhibiting lowest expression levels (Figure 3.1C). A Pearson correlation analysis was then performed to determine the correlation between GBM cell invasion and TKS5 or Src protein expression levels. Interestingly, I found neither TKS5 nor Src protein expression levels correlated with cellular invasion (Figure 3.1E, F).

3.3.2 GBM cells primarily utilize focal adhesions to degrade ECM.

The primary role of invadopodia is the recruitment of matrix metalloproteinases to facilitate ECM remodeling (Eddy et al., 2017; Murphy and Courtneidge, 2011; Paz et al., 2014). To identify which GBM cell lines form matrix-degrading invadopodia, I next performed an *in vitro* gelatin degradation assay. This revealed only LN229 cells had the ability to degrade the gelatin by 4 hours in culture, while LN229 and LN18 cells degraded the gelatin by 18 hours (Figure 3.2 A). Interestingly, degradation occurred around the periphery of the cell rather than as

A

	LN229	U87-MG	LN18	U251	U343
TP53	Mutant	WT	Mutant	Mutant	WT
PTEN	WT	null	WT	Mutant	Mutant
IDH1/2	WT	WT	WT	WT	WT

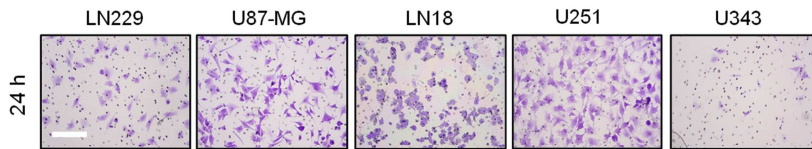
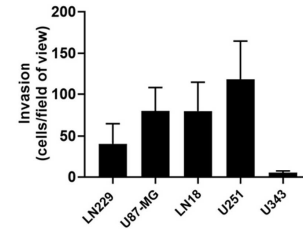
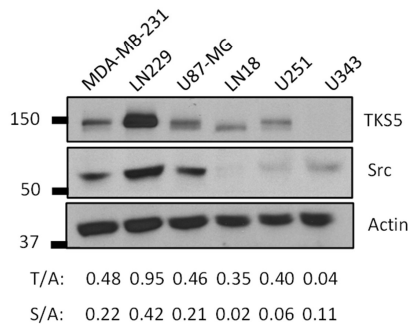
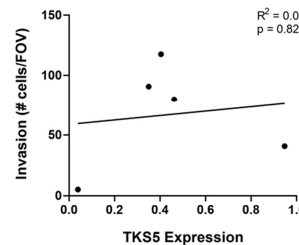
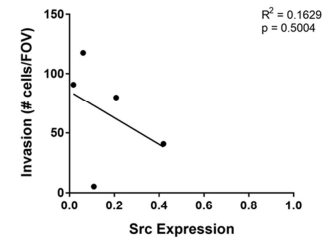
B**C****D****E****F**

Figure 3.1. TKS5 and Src protein expression levels do not predict GBM cell invasion.

(A) TP53, PTEN, and IDH1/2 mutational status of LN229, U87-MG, LN18, U251, and U343 human GBM cell lines. (B) Representative images of LN229, U87-MG, LN18, U251, and U343 cells detected on the bottom surface of Transwell Matrigel inserts after 24 h of an invasion assay. Scale bars = 200 μ m. (C) Quantification of the number of invasive cells per field of view as detected using crystal violet stain. Data represents the mean \pm SD (n=3 independent experiments). (D) LN229, U87-MG, LN18, U251, and U343 cells were immunoblotted for TKS5, Src, and Actin expression. MDA-MB-231 cells were used as a positive control. Quantification of TKS5/Actin (T/A) and Src/Actin (S/A) densitometry ratios shown under immunoblots. (E, F) The correlation between invasiveness and TKS5 (E) or Src (F) expression in LN229, U87-MG, LN18, U251, and U343 human GBM cell lines was analyzed using a two-tailed Pearson correlation test.

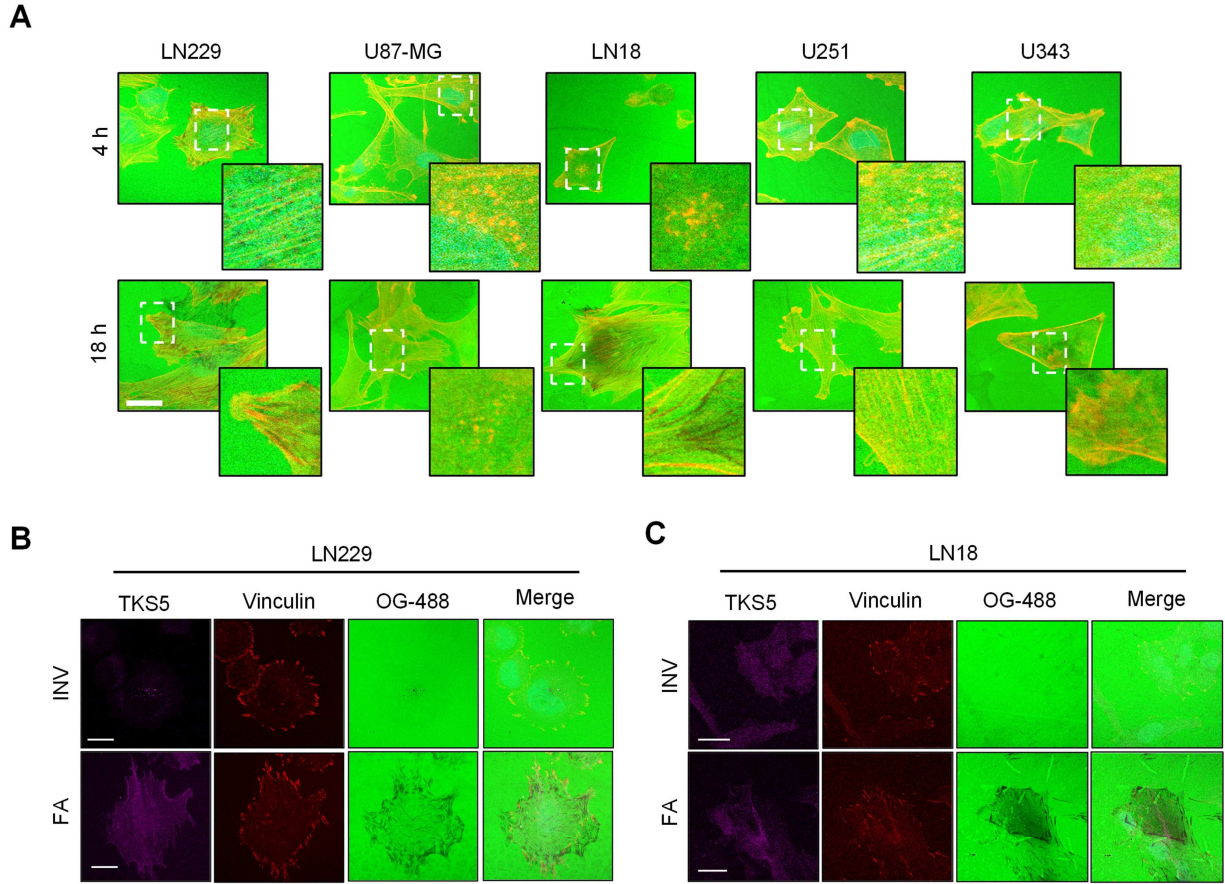


Figure 3.2. Gelatin degradation can occur at sites of invadopodia or focal adhesions in glioma cells.

(A) Representative images of LN229, U87-MG, LN18, U251, and U343 cells plated onto Oregon Green 488-gelatin coated coverslips for 4 h or 18 h and stained with DAPI and phalloidin-594 to detect actin. Scale bars = 25 μm . The boxed regions are enlarged in the bottom right corner of each image (n = 12 – 35 cells analyzed per condition). (B, C) LN229 (B) and LN18 (C) cells were plated onto Oregon Green 488-gelatin coated coverslips for 24 h and stained for TKS5 and Vinculin to distinguish between TKS5-positive puncta around the nuclei (invadopodia, INV) or vinculin-positive structures around the periphery of the cell (focal adhesions, FA) (n=3 independent experiments).

dot-like areas of degradation in close proximity to the nucleus of the cell typical of active invadopodia. To determine if the peripheral sites of degradation represent focal adhesion structures, LN229 and LN18 cells were plated onto fluorescently-tagged gelatin, fixed, and then stained for TKS5 (marker of invadopodia) and vinculin (marker of focal adhesions). This revealed LN229 cells degrade gelatin using either invadopodia or focal adhesion structures; however, invadopodia and focal adhesions were rarely observed to function in the same cell (Figure 3.2 B). Conversely, LN18 cells did not form invadopodia and only degrade gelatin using focal adhesion structures (Figure 3.2 C). Based on these observations, I have selected to work with LN229 and LN18 cells since both cell lines degrade gelatin and invade through Matrigel while differing in Src and TKS5 protein expression levels.

3.3.3 LN229 and LN18 cells respond to irradiation.

To model cellular survival following exposure to ionizing radiation, we performed a clonogenic cell survival assay. Clonogenic analysis 2 weeks following radiation exposure revealed less than 1% of cells survived following exposure to 6 – 10 Gy IR, therefore indicating LN229 and LN18 cells show similar levels of radiosensitivity (Figure 3.3 A, B). While clonogenic survival assays are the gold standard for measuring response to radiation, these assays measure tumour cell survival and proliferation into colonies 2 weeks post-IR. The majority of *in vitro* assays that will be performed to assess invadopodia formation, gelatin degradation, and cellular invasion later in Chapter 3 are completed within 3 days. It is therefore important to assess cell survival on day 0, 1, 3, 5, and 7 post-irradiation. Cell survival was analyzed by detecting the percentage of propidium iodide negative (PI-) cells as a proportion of

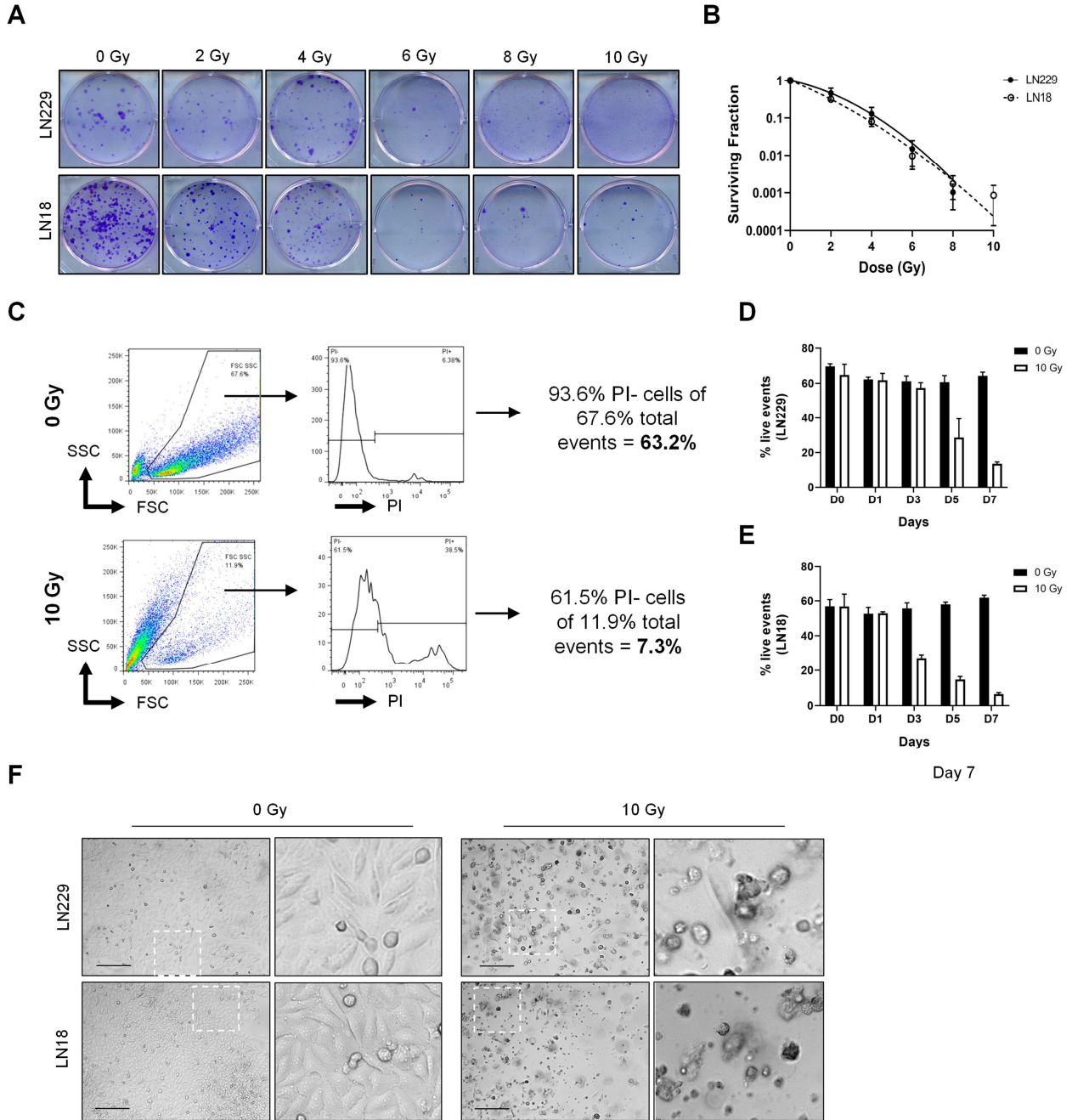


Figure 3.3. Analysis of LN229 and LN18 cell survival following exposure to ionizing radiation.

Figure 3.3. Analysis of LN229 and LN18 cell survival following exposure to ionizing radiation.

(A) LN229 and LN18 cells were exposed to single doses of ionizing radiation (0, 2, 4, 6, 8, 10 Gy) and surviving colonies were stained with crystal violet 2 weeks post-radiation. (B) Radiation survival curves for LN229 (solid line) and LN18 (dotted line) cells. Data represent mean \pm SD (n=3 independent experiments). (C) Representative flow cytometry plots displaying the gating strategy used to identify viable cells, which were discriminated based on a lack of propidium iodide (PI) staining. (D, E) Cell viability of LN229 (D) and LN18 (E) cells seeded on gelatin-coated plates was analyzed 0, 1, 3, 5, and 7 days post-irradiation. Viability is displayed as the total number of PI negative cells as a percentage of live events collected. (F) Representative images of LN229 and LN18 cells in culture 7 days post-radiation exposure. Boxed region in bottom right corner represents zoomed in perspective. Scale bar = 250 μ m.

* *Flow cytometry performed by Rachel Cederberg.*

the total events collected via flow cytometry (Figure 3.3 C). I found LN229 cells remain viable for at least 3 days following irradiation, with cell death occurring by day 5 (Figure 3.3 D). However, LN18 cells appear to die at a faster rate, with cell death occurring by 3 days post-IR (Figure 3.3 E). Moreover, a significant fraction of LN229 and LN18 cells grown on gelatin-coated plates and exposed to 10 Gy IR have died by day 7, as evidenced by cell debris floating in the plate (Figure 3.3F). Therefore, the majority of *in vitro* experiments performed herein are completed by 72 hours to limit the amount of cell death occurring.

3.3.4 Ionizing radiation upregulated TKS5 mRNA and protein expression levels.

Since LN229 and LN18 cells were found to utilize both invadopodia and focal adhesion structures to degrade gelatin matrices, this prompted an assessment of whether ionizing radiation alters signaling pathways associated with invadopodia and/or focal adhesion activity. First, we generated LN229 and LN18 cells that stably express green fluorescent protein (GFP).

Immunoblot analysis confirmed parental and GFP-positive LN229 and LN18 cells express similar levels of TKS5, PTP α , and Src (Figure 3.4 A). Next, LN229-GFP and LN18-GFP cells seeded on gelatin-coated plates were exposed to 0, 2, 4, 6, or 10 Gy IR as adherent monolayers and then probed for PTP α , TKS5, FAK-pY397, FAK, Src-pY527, Src, MMP14, MMP2, and actin 28 hours post-radiation. This revealed that IR decreased PTP α expression when exposed to 2 Gy, and that PTP α expression remained reduced when exposed to 4 – 10 Gy (Figure 3.4B).

However, IR increased TKS5 expression levels in LN229-GFP cells in a dose-dependent manner, namely the 150 KDa isoform (Figure 3.4 B). Conversely, no significant changes were observed in invadosome-associated signaling pathways in LN18-GFP cells (Figure 3.4 C).

Radiation-induced TKS5

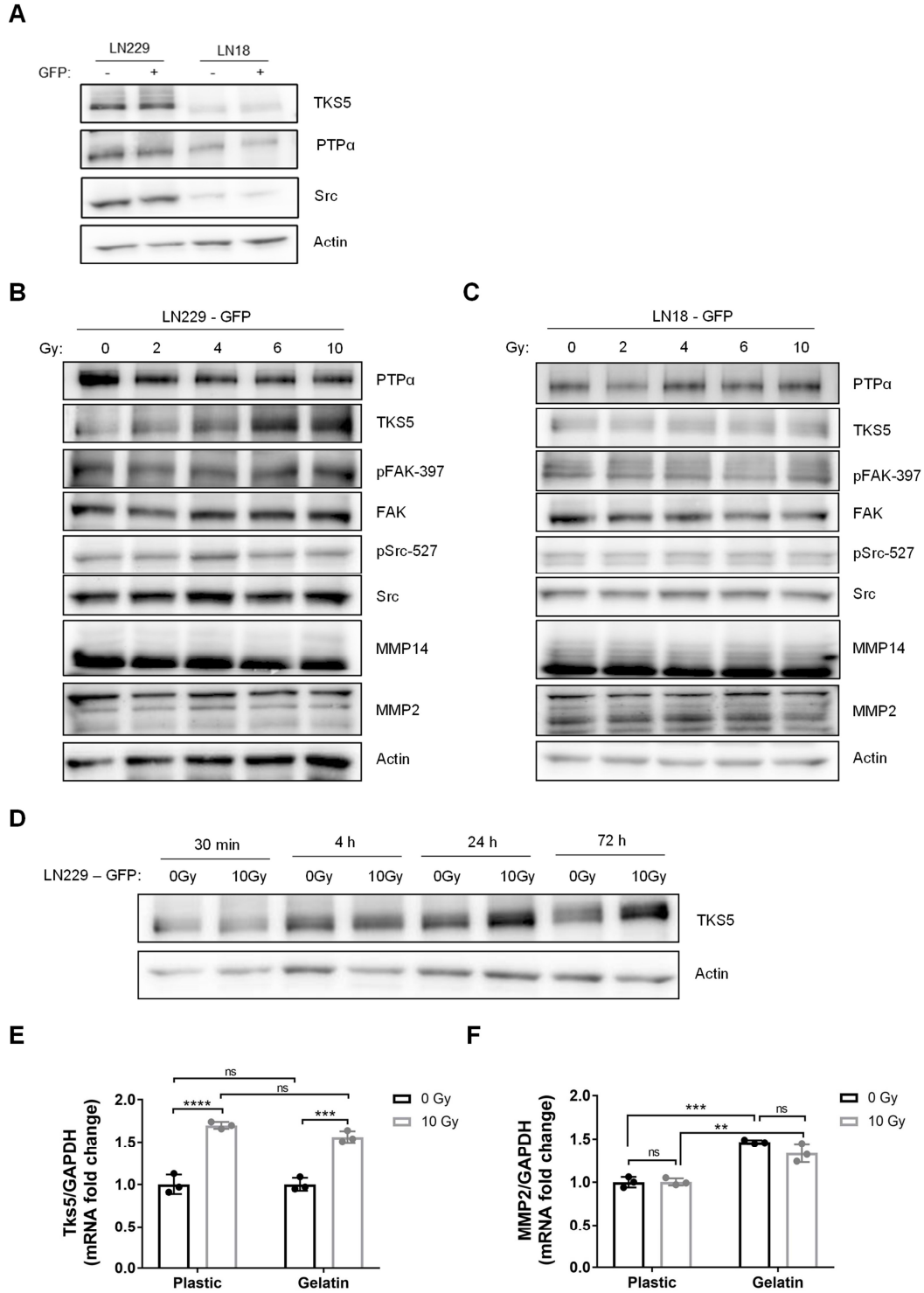


Figure 3.4. Exposure to ionizing radiation upregulates TKS5 mRNA and protein expression in LN229 cells.

Figure 3.4. Exposure to ionizing radiation upregulates TKS5 mRNA and protein expression in LN229 cells.

(A) LN229 and LN18 cells were either untransfected or stably transfected with green fluorescent protein (GFP) and immunoblotted for TKS5, PTPa, Src, and Actin. (B, C) LN229-GFP (B) and LN18-GFP (C) cells were seeded onto gelatin-coated plates, irradiated with 0, 2, 4, 6, or 10 Gy IR, and lysed 28 h post-IR. Cell lysates were probed for PTPa, TKS5, FAK-pY397, FAK, Src-pY527, Src, MMP14, MMP2, and Actin. Immunoblots are representative of at least three biological replicates. (D) LN229-GFP cells were seeded onto gelatin-coated plates, irradiated with 0 or 10 Gy IR, and lysed 30 mins, 4 h, 24 h, or 72 h post-irradiation. Cell lysates were probed for TKS5 and Actin expression. (E, F) LN229-GFP cells were seeded onto plastic or gelatin-coated plates, irradiated with 0 or 10 Gy IR, and cDNA was isolated 28 hours post-IR. Real time qPCR was used to determine the relative expression of TKS5 (E) and MMP2 (F) mRNA normalized to GAPDH (n=3 independent experiments, ns = non-significant, ***p < 0.001, ****p < 0.0001, two-way ANOVA with Sidak's multiple comparisons test).

* *Immunoblots performed by Michael Hall and Monica Hsu.*

** *Real time qPCR performed by Ling Vicky Li.*

expression was then analyzed over time by exposing LN229-GFP cells to 0 or 10 Gy IR, and then lysing cells 30 minutes, 4 hours, 24 hours, or 72 hours post-radiation. This confirmed a radiation-induced upregulation in TKS5 protein expression in a time-dependent manner (Figure 3.4 D).

While ionizing radiation has been shown to induce mRNA translation (Braunstein et al., 2009; Kabilan et al., 2020; Lü et al., 2006), alterations in gene expression has also been shown to occur at the transcriptional level by increasing RNA synthesis and stability (Narayanan et al., 2017; Pollard and Davis, 1970). Real time qPCR analysis was used to analyze TKS5 mRNA expression in LN229 cells post-irradiation. MMP2 mRNA expression was also assessed to serve as a negative control since I did not observe any changes in MMP2 protein expression via western blot analysis. Cells were first seeded onto plastic versus gelatin-coated plates to determine if IR-induced TKS5 expression was dependent on the presence of gelatin. Then, cells were irradiated with 0 versus 10 Gy IR, and cDNA was isolated 28 hours post-IR. This revealed IR significantly increased TKS5 expression independent of the presence of gelatin (Figure 3.4 E). IR did not alter MMP2 mRNA levels in LN229 cells, which aligns with the western blot results. However, cells seeded on gelatin-coated plates exhibited increased MMP2 expression irrespective of IR (Figure 3.4 F). In summary, ionizing radiation upregulates mRNA and protein expression levels of TKS5 in LN229 cells. Since TKS5 expression is critical for invadopodia activity, we next sought to determine if ionizing radiation upregulates invadopodia formation and function.

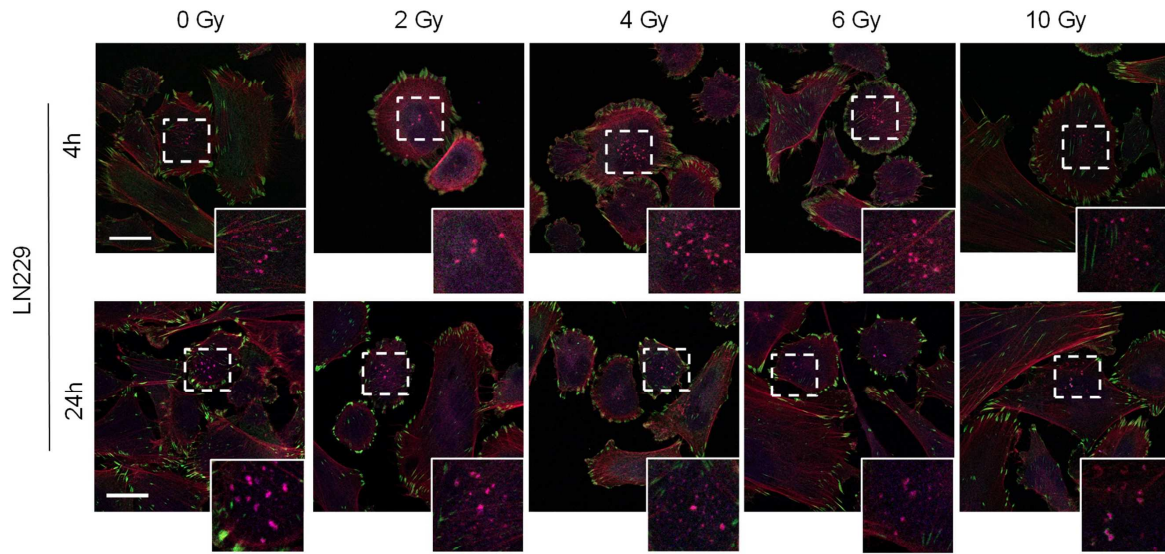
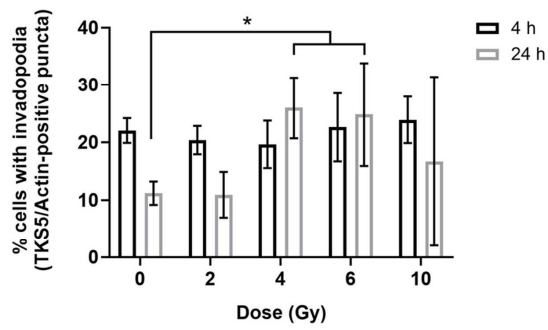
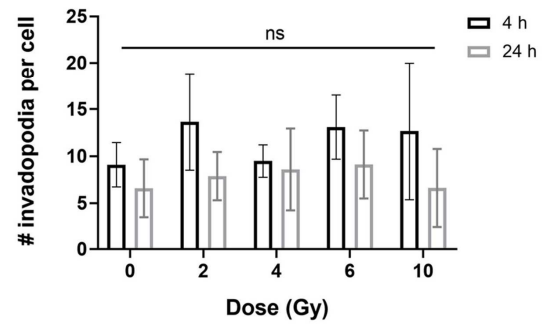
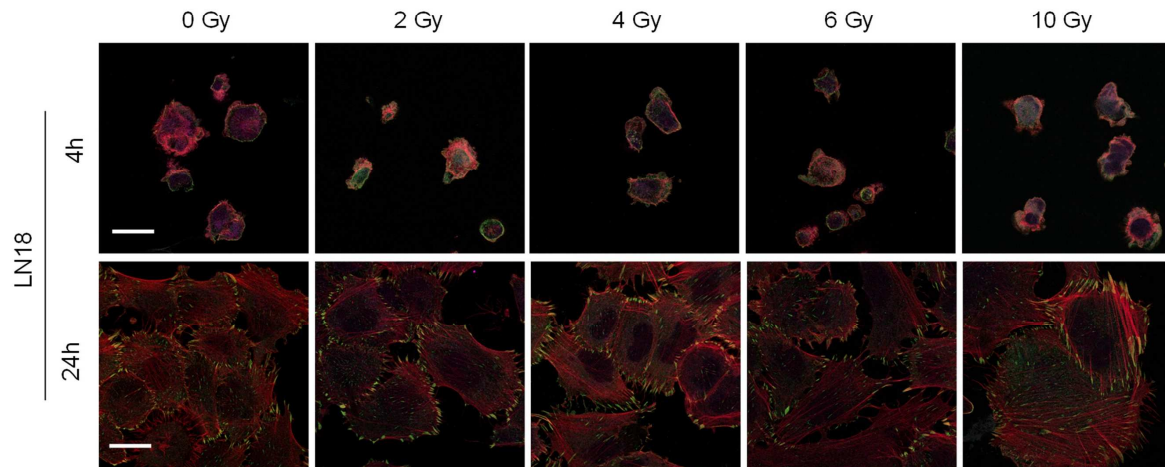
A**B****C****D**

Figure 3.5. Ionizing radiation minimally alters invadopodia formation.

Figure 3.5. Ionizing radiation minimally alters invadopodia formation.

(A) Representative images of LN229 cells irradiated with 0, 2, 4, 6, or 10 Gy and seeded onto gelatin-coated coverslips for 4 h or 24 h (28 h and 48 h post-irradiation, respectively). Cells were fixed and stained for TKS5 (pink), Vinculin (green), Actin (red), and DAPI (blue). The boxed regions are enlarged in the bottom right corner of each image. Scale bar = 20 μ m. (B, C) Quantification of the percentage of LN229 cells that form TKS5/Actin-positive invadopodia (B) and the number of invadopodia per cell in cells with more than one invadopodial structure (C). Data represents the mean \pm SD ($n \geq 3$, * $p < 0.05$, ns = non-significant, two-way ANOVA with Dunnett's multiple comparisons test). (D) Representative images of LN18 cells irradiated with 0, 2, 4, 6, or 10 Gy and seeded onto gelatin-coated coverslips for 4 h or 24 h (28 h and 48 h post-irradiation, respectively). Cells were fixed and stained for TKS5, Vinculin, Actin, and DAPI. Scale bar = 20 μ m.

3.3.5 Focal adhesion-mediated gelatin degradation is upregulated by IR.

TKS5 is thought to be a master regulator of invadopodia formation, specifically during invadopodia maturation (Sharma et al., 2013). Since our previous data indicates IR upregulates TKS5 expression levels, we next sought to investigate the role of IR in facilitating invadopodia formation. LN229 cells were irradiated with 0, 2, 4, 6, or 10 Gy IR, and then seeded onto gelatin-coated coverslips 24 hours post-IR. Cells were then fixed 4 or 24 hours post-seeding, which therefore corresponds with 28 hours and 48 hours post-IR, and stained for TKS5, vinculin, actin, and DAPI to distinguish between invadopodia and focal adhesions structures (Figure 3.5 A). No change was observed in the percentage of cells that formed invadopodia by 4 hours post-seeding; however, higher doses of radiation increased the percentage of invadopodia-forming cells by 24 hours (Figure 3.5 B). Furthermore, the number of invadopodia that form per cell remained unchanged by irradiation (Figure 3.5 C). Invadopodia formation was also assessed in LN18 cells exposed to 0, 2, 4, 6, or 10 Gy IR, which revealed LN18 cells do not form TKS5-positive invadopodia structures irrespective of radiation dose (Figure 3.5 D). I found LN18 cells did not adhere and spread out on gelatin-coated coverslips by 4 hours and therefore required a longer incubation time to analyze structure formation. Notably, we found that 100% of LN229 and LN18 cells formed focal adhesion structures (data not shown).

Since the primary function of invadopodia is to remodel surrounding matrices, we next analyzed the role of ionizing radiation in modulating invadopodia-mediated gelatin degradation. First, LN229 cells were exposed to 0, 2, 4, 6, or 10 Gy IR and then seeded onto fluorescently tagged gelatin-coated coverslips for 4 or 24 hours (Figure 3.6 A). The percentage of LN229 cells that degrade the gelatin matrix using either invadopodia (stained for TKS5) or focal adhesion

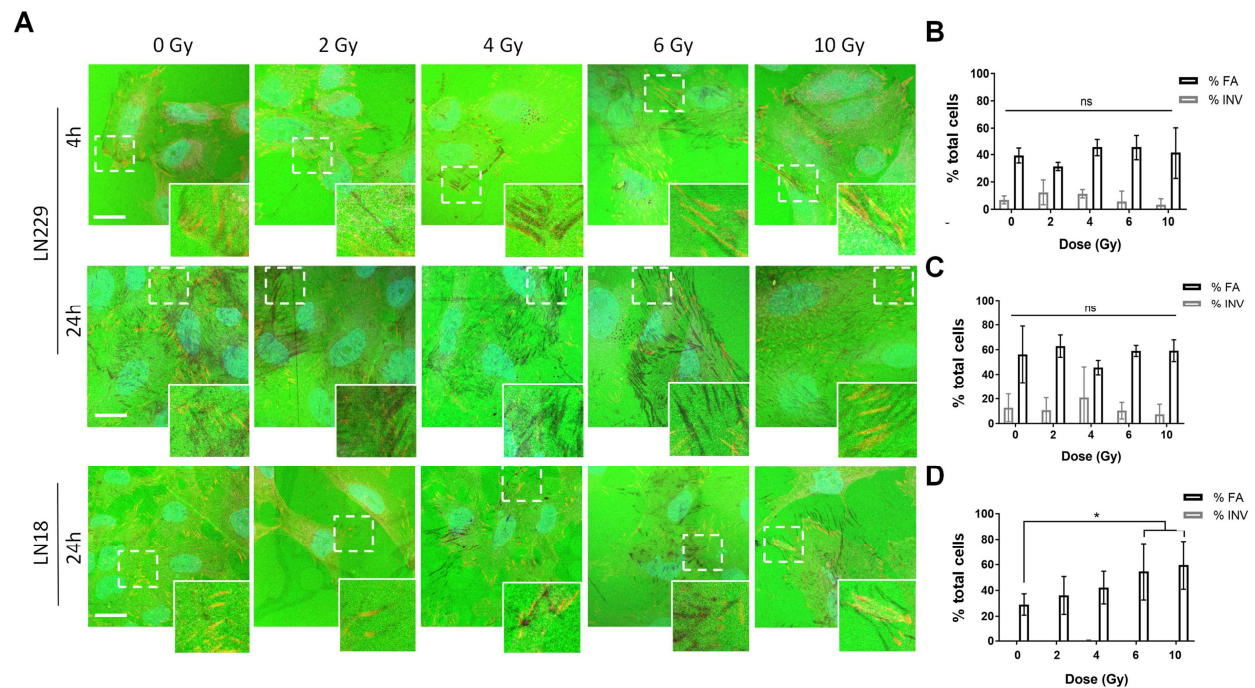


Figure 3.6. Focal adhesion-mediated ECM degradation is upregulated by ionizing radiation.

(A) Representative images of LN229 and LN18 cells irradiated with 0, 2, 4, 6, or 10 Gy ionizing radiation. At 24 h post-irradiation, cells were plated onto Oregon Green 488-gelatin coated coverslips for 4h or 24 h and stained with TKS5, Vinculin, and DAPI. The boxed regions are enlarged in the bottom right corner of each image. Scale bars = 20 μ m. (B, C, D) Quantification of the percentage of invadopodia-mediated (INV) or focal adhesion-mediated (FA) gelatin degrading cells as a proportion of the total cells. LN229 cells were quantified 4 h (B) or 24 h (C) post-seeding, while LN18 cells were quantified at 24 h (D) post-seeding onto Oregon Green 488-gelatin coated coverslips. Data represent the mean \pm SD (n = 3, *p < 0.05, ns = non-significant, two-way ANOVA with Dunnett's multiple comparisons test).

(stained for vinculin) structures was quantified, which revealed LN229 cells primarily utilize focal adhesion to degrade gelatin and the activity of either structure remained unaffected by exposure to radiation (Figure 3.6 B, C). Conversely, LN18 cells exposed to 6 or 10 Gy IR exhibited an increase in focal adhesion-mediated gelatin degradation, while invadopodia activity remained null and unaffected (Figure 3.6 D). In summary, I found IR does not greatly alter the percentage of cells that form focal adhesion or invadopodia structures; however, higher doses of IR were found to increase focal adhesion-mediated gelatin degradation in LN18 cells, specifically. Due to the important role of invadosomes in regulating cellular motility, we next sought to investigate the role of ionizing radiation in controlling GBM cell invasion.

3.3.6 Ionizing radiation decreases *in vitro* GBM cell invasion.

To investigate the role of ionizing radiation in facilitating GBM motility, cellular invasion was analyzed over time using an IncuCyte chemotaxis assay. LN229-GFP and LN18-GFP cells were irradiated with 0, 4, or 10 Gy IR 24 hours in advance of the chemotaxis assays, and then resuspended in 1.0 mg/mL or 5.0 mg/mL growth factor-reduced Matrigel. Chemotaxis was assessed towards chemoattractant fetal bovine serum (FBS) every 4 hours for 72-120 hours total (Figure 3.7 A, B). Importantly, LN229 cell invasion was monitored for 120 hours while LN18 invasion was limited to 72 hours since these cells are more sensitive to the effects of radiation and begin to die by 3 days in culture (Figure 3.3 D, E). Despite our previous results showing IR upregulates TKS5 expression in LN229 cells and FA-mediated gelatin degradation in LN18 cells, I did not observe increased GBM cell invasion. In fact, I found both LN229-GFP and LN18-GFP cells exposed to 4 Gy or 10 Gy irradiation showed significantly less invasion through both soft (1.0 mg/mL) and stiff (5.0 g/mL) Matrigel barriers (Figure 3.7 C, D). Together,

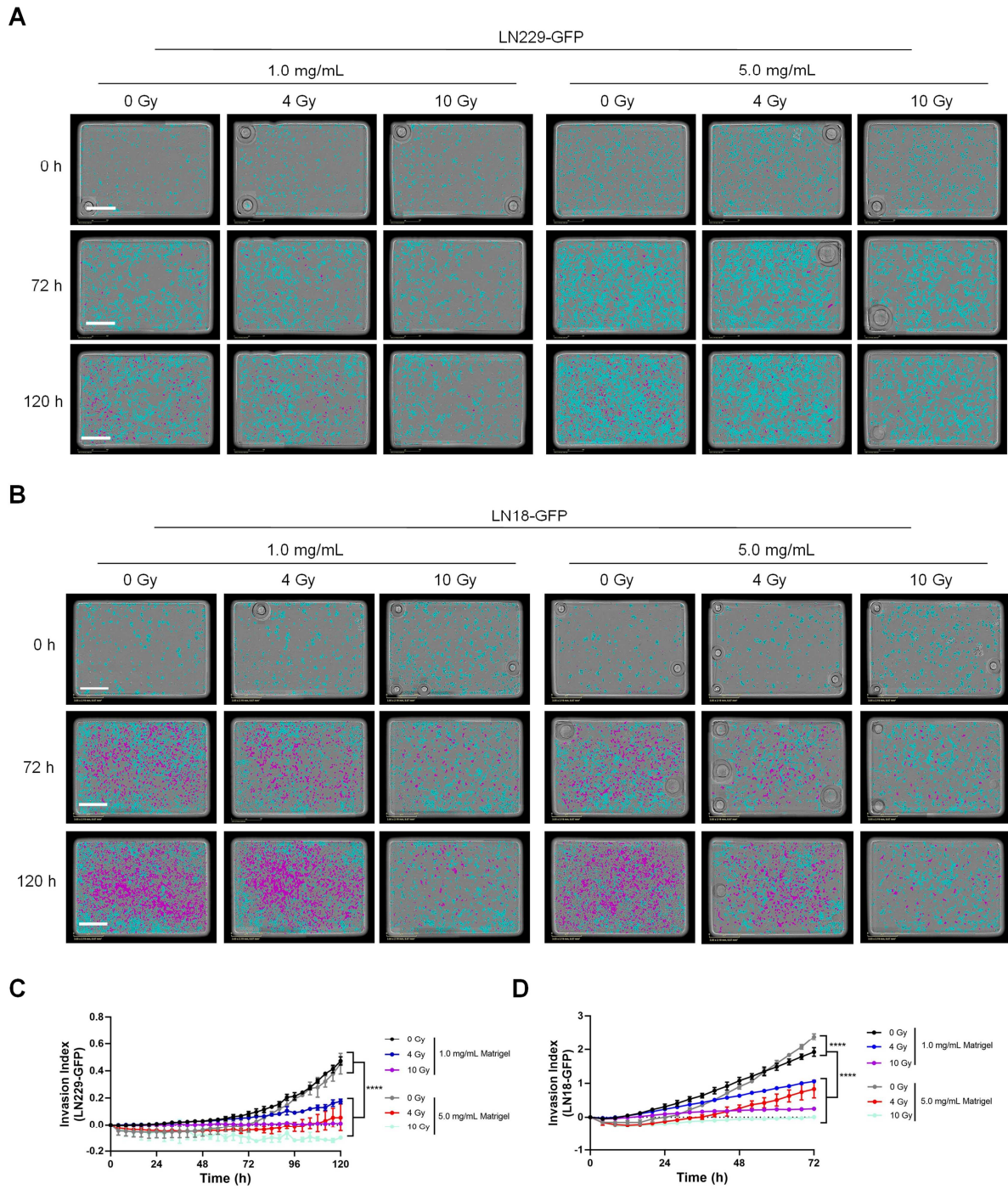


Figure 3.7. Ionizing radiation reduces *in vitro* GBM cell invasion through Matrigel.

Figure 3.7. Ionizing radiation reduces *in vitro* GBM cell invasion through Matrigel.

(**A, B**) Representative images of LN229-GFP (A) and LN18-GFP (B) cells detected on the top (turquoise) and bottom (purple) surfaces of Transwell inserts at 0, 72, and 120 h of an IncuCyte chemotaxis invasion assay. Scale bars = 600 μm . (**C**) Quantification of invasion indices from experiments shown in (A) are displayed as cell counts normalized to initial cell number and then normalized to $t = 0$ h. Data are mean \pm SD ($n=2$ independent experiments, **** $p < 0.0001$, two-way ANOVA with Tukey's multiple comparison test). (**D**) Quantification of invasion indices from experiments shown in (B) are displayed as relative cell counts normalized to initial cell number and then normalized to $t = 0$ h. Data are mean \pm SD ($n=3$ independent experiments, **** $p < 0.0001$, two-way ANOVA with Tukey's multiple comparison test).

these data suggest that despite radiation upregulating TKS5 expression, these alterations do not result in increased invasiveness *in vitro*.

3.4 Discussion

Radiation therapy (RT) is a common therapeutic modality that delivers ionizing radiation (IR) to sites of malignant disease. While RT is among the most common and effective treatment options for cancer patients, it has also been shown that RT can paradoxically increase the aggressiveness of cancer cells. Our overall objective was to identify the precise mechanisms that facilitate IR-induced glioblastoma multiforme (GBM) cell invasion *in vitro*. Here, I show IR upregulates TKS5 mRNA and protein expression in LN229 cells (Figure 3.4). I also found LN229 and LN18 cells primarily utilize focal adhesion (FA) structures, rather than invadopodia, to facilitate local degradation of gelatin substrates (Figure 3.2). Moreover, despite the observed increase in TKS5 expression after radiation, I did not detect significant changes in invadopodia formation or activity (Figures 3.5 and 3.6). Rather, I found IR upregulated FA-mediated gelatin degradation in LN18 cells (Figure 3.6). Finally, exposure to IR did not upregulate GBM cell invasion *in vitro* (Figure 3.7) as previously described by others. These data suggest GBM cells preferentially utilize focal adhesions as invasive structures, and IR upregulates TKS5 expression without increasing invadopodia activity and cellular invasion. Together, this indicates an alternative role for TKS5 in glioma biology.

Invadopodia, which are proteolytically active protrusions that form at the plasma membrane of cancer cells, have been shown to facilitate several stages of the metastatic process including local invasion, intravasation, and extravasation (Buccione et al., 2009; Eddy et al., 2017; Gligorijevic et al., 2012; Murphy and Courtneidge, 2011; Paterson and Courtneidge, 2018;

Paz et al., 2014; Williams et al., 2019). Invadopodia are molecularly similar to focal adhesion structures, which primarily facilitate cellular migration and act as adhesive sites between the cell and the surrounding extracellular matrix (Burrige, 2017). Thus, invadopodia are typically thought to regulate invasion while focal adhesions regulate adhesion and migration. Recently, MMP14 has been found to localize to gelatin-degrading focal adhesion structures suggesting focal adhesions may also facilitate cancer cell invasion of various pancreatic adenocarcinoma and fibrosarcoma cell lines (Hsu et al., 2019; Wang and McNiven, 2012). Here, we show for the first time that two glioblastoma cell lines, LN229 and LN18 cells, primarily utilize focal adhesions to degrade gelatin matrices. While most cancer types will enter the vasculature or lymphatic systems via intravasation and travel to distant organs (Karaman and Detmar, 2014; van Zijl et al., 2011), it is well known that GBM cells seldom metastasize out of the brain tissue (Choucair et al., 1986; Esmaeili et al., 2018). In fact, it has been found that GBM cells more often invade along pre-existing structures such as blood vessels, white matter tracts, or astrocytes, rather than intravasating into the vasculature (Cuddapah et al., 2014; Esmaeili et al., 2018; Liu et al., 2019; Mair et al., 2018). Given our data showing GBM cells seldom use invadopodia to degrade gelatin and IR upregulated FA-mediated gelatin degradation, perhaps this suggests invadopodia are irrelevant in brain tissue and that focal adhesions are the primary invasive structure. Future work is required to investigate the role of IR in facilitating FA-mediated GBM cell invasion along brain-specific structures using biologically relevant *ex vivo* or *in vivo* models of glioma.

Despite invadopodia and focal adhesions being molecularly similar structures, the relative contribution of each structure to the invasive process remains relatively unclear. Others have reported that FAK regulates whether tyrosine phosphorylation occurs at focal adhesions or invadopodia, and that loss of FAK impairs cellular invasion (Chan et al., 2009). This suggests a

balance between active focal adhesion and invadopodia structures is required for invasion, rather than the two structures existing in competition. Here, I report IR decreases *in vitro* cellular invasion. Although I found IR does not alter the total expression of phosphorylated Src or FAK, perhaps IR disrupts the localization of phosphorylated proteins to focal adhesions versus invadopodia resulting in decreased invasion. Further investigations are required to determine how IR plays a role in mediating FA-mediated versus invadopodia-mediated ECM degradation.

It is well known that TKS5 is a master regulator of invadopodia formation and function (Abram et al., 2003; Eckert et al., 2011; Seals et al., 2005; Sharma et al., 2013; Stylli et al., 2009). Here, we found IR upregulated TKS5 mRNA and protein expression, which did not correlate with increased invadopodia formation, ECM degradation, or invasion. While TKS5 primarily regulates cellular motility, TKS5 has also been found to play a role in proliferation, cell cycle progression, survival, and ROS production (Blouw et al., 2015; Diaz et al., 2009; Moodley et al., 2015; Weaver, 2009). ROS has been shown to localize to invadopodia structures (Caires-dos-Santos et al., 2020) and regulate invadopodia formation and function (Weaver, 2009). Previous reports have also shown that inhibiting ROS production decreases ECM degradation (Diaz et al., 2009; Gianni et al., 2010, 2009). Depleting TKS5 has been shown to decrease ROS generated by NADPH oxidases (NOX) (Diaz et al., 2009). However, it is known that IR increases ROS production via the radiolysis of water molecules independent of NOX (Desouky et al., 2015; Kim et al., 2019). It therefore seems unlikely for TKS5 to play a role in ROS production post-irradiation. Alternatively, TKS5 has also been described to regulate cellular proliferation and cell cycle progression (Blouw et al., 2015; Moodley et al., 2015). More specifically, the downregulation of TKS5 resulted in reduced cellular proliferation and the accumulation of cells in the G1 phase of the cell cycle (Moodley et al., 2015). Since we observed

an IR-mediated increase in TKS5 expression, then perhaps the surviving population of cells requires TKS5 to repopulate post-IR. Of course, future work is required to determine the invasion-independent role for IR-induced TKS5 expression in glioma, if any.

TKS5 is a scaffold protein with many binding partners, one being ADAMs or sheddases. ADAMs are a family of disintegrins and metalloproteinases that cleave various growth factors, cytokines (*i.e.* EGF, TNF α , etc.), and adhesion molecules (Seals and Courtneidge, 2003). TKS5 has been shown to associate with several ADAMs (12,15,19) with ADAM12 specifically co-localizing to podosomes in Src-transformed cells (Abram et al., 2003). Furthermore, knockdown of TKS5 does not affect the secretion or activity of MMP2/MMP9 (Seals et al., 2005), which agrees with my data showing IR-induced increase in TKS5 expression does not alter MMP2 expression. Despite ADAMs also playing a role in ECM degradation and migration (Seals and Courtneidge, 2003), perhaps GBM cells rely on MMPs (2, 9, 14) rather than ADAMs to facilitate invasion. Nevertheless, future investigations are required to determine why increased TKS5 expression alone is insufficient for upregulating GBM cell invasion. Perhaps increased TKS5 expression is accompanied by compensatory mechanisms that facilitate invasion and therefore performing a proteomic screen of untreated versus irradiated GBM cells would reveal other proteins involved in invadopodia/focal adhesion function and cellular motility post-radiation.

I found ionizing radiation decreased LN229 and LN18 glioblastoma cell invasion through Matrigel using an IncuCyte chemotaxis assay (Figure 3.7). These data contradict previously published results stating IR increases LN229 and LN18 chemotactic invasion (Whitehead et al., 2018; Wild-Bode et al., 2001). GBM tumours are highly heterogeneous, which may account for the observed differences between commonly used cell lines (Inda et al., 2014). Many of the previously published reports stating IR increased *in vitro* GBM cell invasion performed standard

Transwell invasion assays. Since single-time point Transwell assays also come with a host of issues, such as being highly dependent on the initial cell seeding density per well, I performed a time course invasion assay using the IncuCyte Matrigel invasion assay. Since brain tissue is uniquely soft compared to other organs (Axpe et al., 2020), I chose to analyze cellular invasion through two different Matrigel concentrations (1.0 mg/mL versus 5.0 mg/mL) to model invasion through a soft versus stiff ECM, respectively. For these reasons, my results more comprehensively and definitively show radiation does not induce *in vitro* GBM cell invasion through Matrigel, but rather decreases invasion (Figure 3.7). To fully maximize the physiological relevance of irradiation experiments, we decided to develop an *ex vivo* brain slice invasion assay to supplement *in vitro* invasion assays (Chapter 4).

Taken together, the data presented in Chapter 3 shows ionizing radiation upregulates TKS5 expression in LN229 glioma cells without increasing invadopodia activity and *in vitro* invasion. Interestingly, it was found that IR increased FA-mediated gelatin degradation, which was insufficient to induce LN18 cell invasion. Future work is required to identify the alternate role of TKS5 in glioma biology and determine if *in vitro* assays are suitable for studying glioblastoma invasion.

Chapter 4: Development and validation of an advanced *ex vivo* brain slice invasion assay to model glioblastoma cell invasion into the complex brain microenvironment.

4.1 Rationale and Hypothesis

Glioblastoma multiforme (GBM), classified as a late-stage astrocytoma brain tumour, is highly aggressive and associated with poor survival rates. GBM tumour cells are highly infiltrative and often invade into the surrounding brain tissue. In Canada, only 4-7% of patients diagnosed with GBM will live more than 5-years (Smith T et al., 2019; Yuan et al., 2016). Despite decades of research, few advancements have been made to improve survival outcomes for GBM patients. This can be partially attributed to a lack of appropriate model systems that accurately recapitulate the complex brain environment. For instance, many pre-clinical models of invasion lack the brain structures (*i.e.* vasculature, white matter tracts, etc.) and unique ECM constituents that are necessary to accurately model GBM cell invasion. The development of more advanced model systems is required to better understand the complex mechanisms of GBM cell invasion and ultimately improve patient outcome.

Brain tissue is a unique environment that contains high levels of astrocytes, proteoglycans/glycoproteins and hyaluronic acid (HA), while consisting of low levels of fibrous proteins (laminin, fibronectin, gelatin). The majority of fibrous proteins are restricted to the basement membrane surrounding the vasculature (Cha and Kim, 2017; Lau et al., 2013). Thus, brain tissue is softer than other organs. Typical *in vitro* models of cancer cell invasion use a cocktail of synthetic ECM proteins including laminin and collagen (*i.e.* Matrigel, gelatin, etc.), lack other brain specific components and do not represent a suitable model for brain cancer

research. Another unique feature of GBM invasion is that GBM cells seldom intravasate into the vasculature. As early as 1938, researcher Hans Joachim Scherer found glioma cells migrate along brain structures later termed “Scherer’s structures” (Scherer, 1938). It is now well understood that brain tumour cells preferentially grow and invade along pre-existing structures including myelinated axons, blood vessels, white matter tracts in the parenchyma or through the fluid-filled perivascular space surrounding the vasculature (Cuddapah et al., 2014; Esmaeili et al., 2018; Liu et al., 2019; Mair et al., 2018).

To more accurately model GBM cell invasion, an organotypic brain slice invasion assay was first developed by Ohnishi and colleagues in 1998 (Ohnishi et al., 1998). The organotypic *ex vivo* brain slice invasion assay is a model in which brain slices are harvested from mice, for instance, and cultured on semi-permeable membranes to be used as a scaffold to monitor cellular invasion. This assay offers many benefits compared to other *in vitro* or *in vivo* models of invasion, including a three-dimensional model system with intact tissue-specific architecture (astrocytes, microglia, vasculature, white matter tracts etc.), biologically relevant substrate stiffness, the ability to easily manipulate the microenvironment (*i.e.*, nutrients, oxygen, *etc.*), high-throughput capabilities for drug studies, and as well as being cost effective compared to long-term *in vivo* models. Furthermore, typical *in vitro* invasion assays including the Boyden chamber assay model invasion in two dimensions towards a chemoattractant (FBS), which may not be present in physiological environments. Combining the organotypic brain slice invasion assay with 3D tumour spheroids would more accurately model cell-cell interactions as well as cell-stroma interactions and thus better recapitulate the complex brain tumour microenvironment.

Over the years, many groups have published a version of the *ex vivo* brain slice model using various methods for implanting tumour cells and imaging cellular motility. For instance,

some groups use the technique of seeding tumour spheroids on top of brain sections (Gritsenko et al., 2017; Jung et al., 2002; Neve et al., 2017), implanting tumour spheroids within the slice using a blunt-edge needle (Eisemann et al., 2018), or simply seeding tumour cells on top of the brain slice in a small droplet of media (Grabiec et al., 2017). Other groups use alternative approaches such as cutting the brain slices in half and seeding tumour cells onto the membrane to create a “cell field” between the two hemispheres (Pencheva et al., 2017) or mixing tumour cells with ECM (i.e. Matrigel) and seeding the mixture into a cell spacer directly adjacent to the edge of the brain slice (Chuang et al., 2013). Imaging strategies are also varied, which range from taking a single image of the brain slice-spheroid interface to taking z-stack images through the brain slice on a confocal microscope. Importantly, many of these previous reports do not distinguish between migration along the top of the slice and invasion of cells into the slice. Here, our goal is to develop a universal technique for implanting tumour spheroids onto *ex vivo* brain slices without the use of Matrigel or other exogenous matrices not present in the brain environment and outline an improved imaging strategy for visualizing cellular invasion into the brain slice.

Investigating the precise mechanisms of GBM invasion has been limited by a lack of physiologically relevant model systems. Here, I describe an optimized method for assessing *ex vivo* GBM cell invasion into the brain slice using tumour spheroids and highlight the phenotypic differences observed using *in vitro* and *ex vivo* models of invasion. Furthermore, I utilize our version of the *ex vivo* brain slice invasion assay to further explore the link between irradiation and GBM cell invasion and measure the agreement between *in vitro* and *ex vivo* models of invasion. The refinement of biologically relevant models of GBM invasion will undoubtedly lead

to the advancement of therapeutic options available to GBM patients and improve patient outcomes.

4.2 Materials and Methods

4.2.1 Cell culture

GBM cells were maintained as described in section 3.2.1 (Appendix A1). LN229 and LN18 GFP-expressing cells were grown in 8 $\mu\text{g}/\text{mL}$ blasticidin-containing media for 3 days to select for blasticidin-resistant cells. The GFP-expressing cell population were exposed to blasticidin-containing media for 3 days approximately every 3 months to maintain GFP expression.

4.2.2 Detection of spheroid hypoxia

Spheroids were generated by first coating a U-bottom 96-well plate with a thin layer of 1% agar. Cells (1.0×10^4 cells) resuspended in 100 μL of complete cell culture media were seeded per well, centrifuged at 800 rpm for 3 minutes, and then incubated at $37^\circ\text{C}/5\% \text{CO}_2$ for 3 days. To detect levels of hypoxia, spheroids were incubated in cell culture media containing 200 μM pimonidazole for 3 h at 21% O_2 , 37°C , and 5% CO_2 . For a positive control, spheroids were incubated at 1% O_2 overnight (16 h) prior to the addition of pimonidazole. Spheroids were then fixed in 4% PFA for 1 h at RT, washed in PBS, dehydrated in 30% sucrose overnight at 4°C , and then embedded in OCT compound (TissueTek, Cat.No. 4583). Cryosections (10 μm each) were cut and placed onto microscope slides, permeabilized and blocked using 3% FBS, 3% BSA, 0.2% PBS-Tx for 1 h at RT, and then stained with FITC-conjugated anti-pimonidazole for 2 h at RT (Hypoxyprobe, Cat.No. HP6-100) followed by DAPI (2 $\mu\text{g}/\text{mL}$) for 5 mins at RT.

4.2.3 *In vitro* spheroid invasion assay

Spheroids were generated as described in section 4.2.2. In brief, spheroids were irradiated (0, 2, 4, 6, 10 Gy) in suspension and then transferred to a new U-bottom 96-well plate coated with 1% agar and grown in complete media (control) or embedded in 5.0 mg/mL Matrigel (Corning, Cat.No. 356231) for 1 h at 37°C. Post-polymerization, an additional 100 µl of 10% FBS-containing DMEM was added to each well. Bright field microscopy was used to image spheroid invasion at 4X magnification for 5 days. The invasive area was determined by measuring the total area of the spheroid embedded in Matrigel and subtracting the area of the spheroid grown in complete media.

4.2.4 Generation of organotypic brain slices

The generation of organotypic brain slices (shown in Figure 4.3) was based on previously described protocols (Eisemann et al., 2018; Gritsenko et al., 2017; Pencheva et al., 2017). In brief, healthy brains were harvested from 6-week-old male C57BL/6J mice. The cerebellum and olfactory bulb were removed using a razor blade, and the cerebral cortex was glued directly to the stage of the vibratome beside a block of 5% agar. The tissue was then submerged in cold slicing media: 1X HBSS (ThermoScientific, Cat.No, 14025134) with the addition of 1% pen-strep, 4 mM magnesium chloride (MgCl₂-6H₂O), and 5 mM D-glucose (dextrose). The slicing media is then exposed to carbogen gas (95% O₂, 5% CO₂) for 30 minutes at RT (resultant pH = 7.2). A Leica Vibratome (VT1000S; speed: 0.15 mm/s; frequency: 80 Hz) was used to generate 300 µm brain slices, which were then transferred to a 6-well dish containing permeable membranes with 0.4 µm pores (Millipore, Cat.No. PICM03050) and 1.25 mL of DMEM-F12 media supplemented with 25% FBS and 1% pen-strep per well (250 µL top of insert, 1 mL

bottom of insert) allowing the top of the brain slice to be exposed to air. A maximum of 3 slices were cultured per 6-well insert.

4.2.5 Alamar blue metabolic assay

Brain slice viability was measured using an alamar blue metabolic assay. Slices were cultured in serum free DMEM-F12 media (SFM), SFM with 1X B27 neuronal supplement, DMEM-F12 containing 5% or 25% FBS, or DMEM-F12 containing 5% or 25% heat inactivated horse serum (HI-HS) for 0, 2, 4, 7, and 14 days *in vitro* (DIV). All media was supplemented with 1% pen-strep. At each indicated timepoint, the slices were transferred into 10% alamar blue solution diluted in SFM, SFM with 1X B27 neuronal supplement, DMEM-F12 containing 5% or 25% FBS, or DMEM-F12 containing 5% or 25% HI-HS and cultured for an additional 24 hours at 37°C/5% CO₂. The fluorescence intensity (560/590 nm) of alamar blue was measured using a Biotek Cytation3 plate reader.

4.2.6 *Ex vivo* brain slice spheroid invasion assay

GFP-expressing GBM cells (1.0×10^4 cells) were seeded into U-bottom 96-well plates coated with 1% agar to allow for spheroid formation as described in section 4.2.2. The organotypic brain slices were generated a day prior to the invasion assay and were maintained in 25% FBS/1% pen-strep containing DMEM-F12 media as described in section 4.2.4. GBM spheroids were irradiated (0, 2, 4, 6, 10 Gy) in suspension. The brain slice media was refreshed and the GBM spheroids were then placed on top of brain slices using a p200 pipette tip. For irradiation experiments, spheroids were irradiated with the indicated dose of radiation (30kV, 10mA, 5.00 Gy/min) using the Precision X-ray machine model X-RAD320 (North Branford, Connecticut, USA) and then immediately implanted onto corresponding brain slices. The invasion assay was

allowed to proceed for 3 days (irradiation experiments) or 8 days (time course experiments), after which the slices were fixed in 4% PFA for 2h at RT.

4.2.7 Antibodies

Primary antibodies are listed as follows: anti-GFAP (Abcam, Cat.No. ab7260), anti-MBP (Abcam, Cat.No. ab40390), and anti- α -SMA (Abcam, Cat.No. ab7817). Alexa Fluor 594-conjugated goat anti-mouse IgG (Molecular Probes, Cat. No. A11032), and Alexa Fluor 647-conjugated goat anti-rabbit IgG (Life Technologies, Cat.No. A21245) were used as secondary antibodies.

4.2.8 Immunofluorescence

A general immunofluorescent staining protocol has been previously described in section 2.2.11, which has been adapted to stain brain slices *ex vivo*. Brain slices were fixed in 4% PFA for 2h at RT, then washed three times with PBS. One slice was placed into each well of a 24-well plate, and permeabilized with 0.5% Triton-X-100 in PBS for 30 minutes at RT. Slices were then blocked in 3% FBS, 3% BSA, 0.2% Triton-X-100 PBS blocking solution for 2 h at RT, washed with PBS, and stained for anti-GFAP (1:200 in blocking solution) for 2 days at 4°C. Secondary antibodies (1:200 in PBS) were applied overnight at 4°C, and then brain slices were washed in PBS and counter-stained with DAPI (2 μ g/ μ l) for 30 mins at RT. Stained brain slices were then embedded in 4% agar blocks, re-sectioned in the z-direction using the vibratome, and the 200 μ m z-sections were finally imaged using high resolution confocal microscopy. The “InvBrainZ” ImageJ macro was used to quantify spheroid invasion into the brain slices:

<https://github.com/ldecotret/InvBrainZ.git>

4.3 Results

4.3.1 Ionizing radiation decreases GBM spheroid invasion *in vitro*.

I previously found irradiating LN229 and LN18 GBM cells with 4 or 10 Gy IR resulted in reduced chemotactic invasion towards a chemoattract (FBS). Next, I was interested in determining whether tumour cell invasion from 3-dimensional spheroids would respond differently to ionizing radiation *in vitro*. Since tumour spheroids have the potential of developing a hypoxic core and due to the known link between hypoxia and radioresistance (Brown, 1999; Gray et al., 1953), I analyzed the levels of hypoxia present in GBM tumour spheroids prior to delivering IR. First, LN229-GFP and LN18-GFP spheroids were initiated by seeding 10,000 cells per well of a non-adherent U-bottom 96-well plate and allowing cells to aggregate. By 3 days in culture, LN229-GFP and LN18-GFP spheroids had an average diameter of $413.1 \mu\text{m} \pm 32.33 \text{ SD}$ and $452.9 \mu\text{m} \pm 33.03 \text{ SD}$, respectively (Figure 4.1A). LN229 and LN18 spheroid cultures and incubated in 1% or 21% oxygen overnight and then pimonidazole, a 2-nitromidazole that is reduced within hypoxic environments, was added to the spheroid culture for 3 hours. The spheroids were then fixed, cryosectioned, and stained for anti-pimonidazole, which revealed the LN229 and LN18 spheroids were not intrinsically hypoxic (Figure 4.1B). Notably, the positive control spheroids exposed to 1% oxygen stained positively for pimonidazole (Figure 4.1B). The fluorescence intensity of pimonidazole was quantified by measuring the pixel intensity through the center of each spheroid, confirming spheroids grown at 21% oxygen were not hypoxic suggesting the cells in the interior of the spheroid will not be radioresistant due to low oxygen (Figure 4.1C, D).

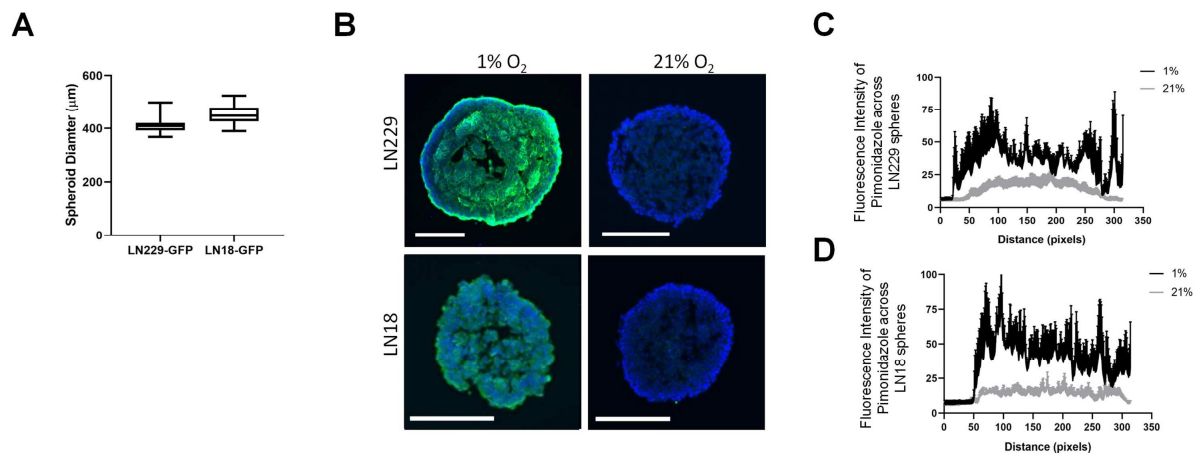


Figure 4.1. Assessment of spheroid size and levels of hypoxia prior to irradiation.

(A) LN229-GFP and LN18-GFP (1.0×10^4) cells were seeded per well of a U-bottom 96-well dish for 3 days to initiate spheroid formation. Data represents mean spheroid diameter (μm) on day $3 \pm \text{SD}$ ($n = 12\text{-}40$ spheroids per group). (B) Representative images of LN229 and LN18 spheroids exposed to 1% or 21% oxygen (O_2) for 16 hours and then stained for pimonidazole (green) for 3 hours followed by DAPI (blue). Scale bar represents $200 \mu\text{m}$. (C, D) Pimonidazole fluorescence pixel intensity across the center of LN229 (C) and LN18 (D) spheroids exposed to either 1% or 21% O_2 ($n = 5 - 9$ spheroids per condition).

Due to the many disadvantages of two-dimensional (2D) *in vitro* chemotaxis assays, I sought to further investigate the role of IR in facilitating GBM cell invasion using a three-dimensional (3D) spheroid invasion assay. Firstly, LN229 and LN18 spheroids did not invade into gelatin, suggesting gelatin alone is not an effective scaffold for modelling GBM cell invasion (data not shown). LN229 and LN18 spheroids were therefore embedded in 0, 0.25, 1.0, or 5.0 mg/mL Matrigel and invasion was monitored for 5 days. The lower concentrations of Matrigel (0.25 or 1.0 mg/mL) increased spheroid size; however, GBM cells did not invade into these softer matrices. In contrast, LN229 and LN18 cells effectively invaded into the stiffer matrix (5.0 mg/mL Matrigel) (Figure 4.2A). To analyze the role of IR on facilitating GBM spheroid invasion, LN229-GFP and LN18-GFP spheroids were exposed to 0, 2, 4, 6, or 10 Gy IR and embedded in 5.0 mg/mL Matrigel (Figure 4.2B). Spheroid invasion was imaged every 24 hours for 5 days and the invasive area was determined by quantifying the area of cells outside of the spheroid core, as determined by the area of spheroids grown in complete media without Matrigel subtracted from the total area of spheroids embedded within Matrigel. This revealed that higher doses of IR significantly reduced invasion (Figure 4.2C, D). Furthermore, LN229-GFP and LN18-GFP spheroids exposed to 0 or 10 Gy IR were embedded in 5.0 mg/mL Matrigel and stained for propidium iodide (PI), a marker of cell death, 5 days post-invasion (Figure 4.2E). These data suggest that the majority of GBM cells invading into the surrounding Matrigel represent the surviving fraction of cells. In summary, both the 2D chemotaxis assay (Figure 3.7) and 3D spheroid invasion assay (Figure 4.2) show radiation decreases LN229 and LN18 cell invasion in a dose-dependent manner. Interestingly, both *in vitro* models show single cell invasion into stiffer synthetic matrices rather than collective strands of invasion. However, brain tissue is considered one of the softest organs in the body and GBM cells invade into brain tissue

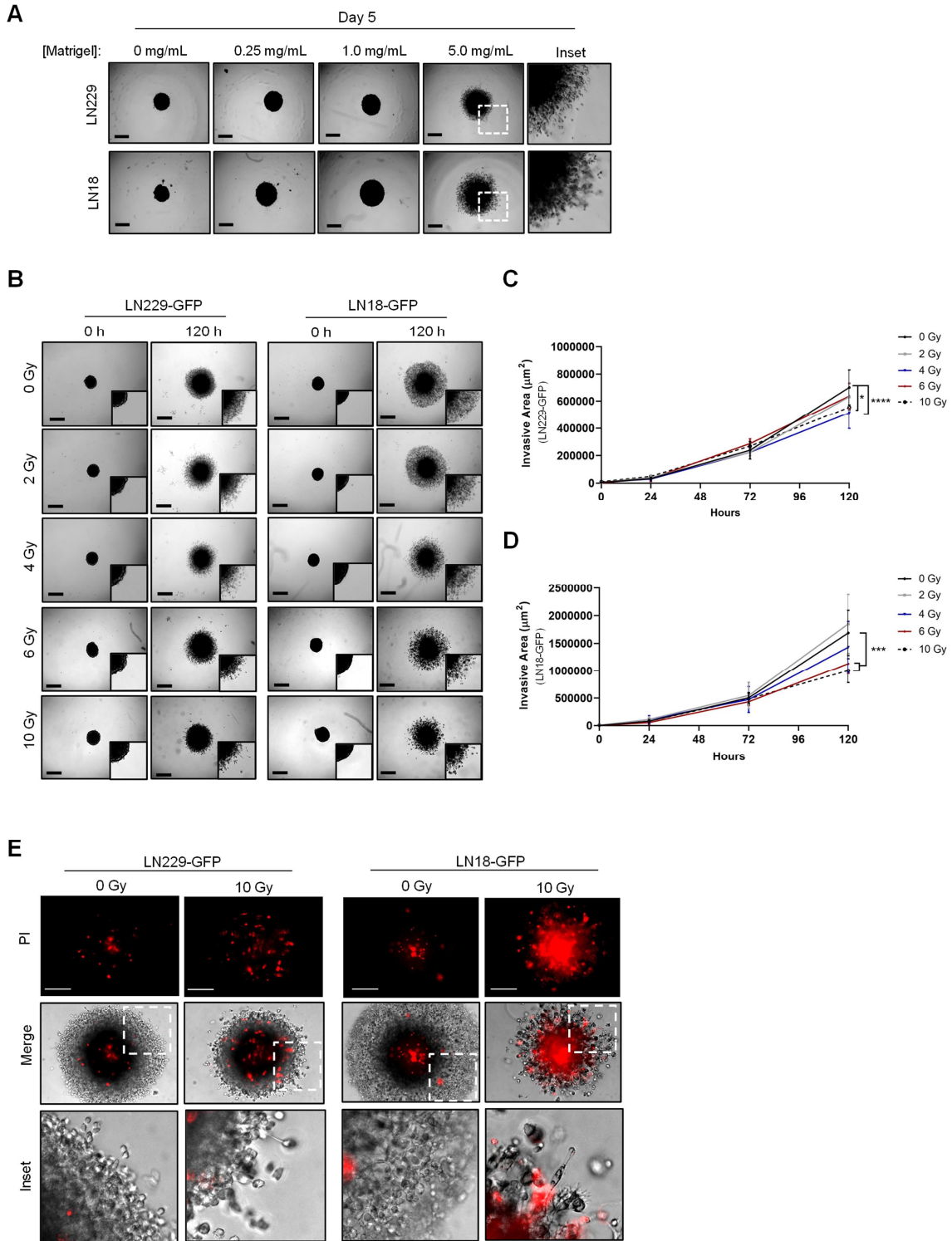


Figure 4.2. Ionizing radiation inhibits GBM spheroid invasion in a dose-dependent manner.

Figure 4.2. Ionizing radiation inhibits GBM spheroid invasion in a dose-dependent manner.

(A) LN229-GFP and LN18-GFP spheroids were embedded in 0, 0.25, 1.0, or 5.0 mg/mL Matrigel for 5 days. The boxed areas are enlarged to the right. Scale bar = 500 μm . (B) Representative images of LN229-GFP and LN18-GFP spheroids exposed to 0, 2, 4, 6 or 10 Gy ionizing radiation and embedded in 5.0 mg/mL Matrigel. Spheroid invasion was imaged every 24 hours for 5 days. Scale bar = 500 μm . (C, D) The invasive area (μm^2) of LN229-GFP spheroids (C) and LN18-GFP spheroids (D) exposed to 0, 2, 4, 6, or 10 Gy ionizing radiation was quantified at 24 h, 72 h, and 120 h. Data represents mean \pm SD ($n \geq 3$ independent experiments, * $p < 0.05$, *** $p < 0.001$, **** $p < 0.0001$, two-way ANOVA with Dunnett post-hoc analysis). (E) Representative images of LN229-GFP and LN18-GFP spheroids that have invaded into the Matrigel for 5 days, and then stained with 10 ng/mL propidium iodide (PI) for 1 hour at 37°C. The boxed areas are enlarged below. Scale bar = 250 μm .

as single cells and collective strands of cells. We therefore developed an *ex vivo* brain slice invasion assay as a more biologically relevant model of GBM cell motility.

4.3.2 Development of an advanced *ex vivo* brain slice invasion assay.

Organotypic slice cultures are a well-established tool in neuroscience research, including electrophysiology studies, modeling neurodegeneration, and cancer research. To generate organotypic brain slice cultures in our lab, we adapted protocols from multiple publications (Eisemann et al., 2018; Gritsenko et al., 2017; Gritsenko and Friedl, 2018; Pencheva et al., 2017; Shih et al., 2017). An overview of our methodology is provided in Figure 4.3. First, whole brains were harvested from male C57BL/6J mice (*i*) and the cerebral cortex was isolated by removing the occipital lobe and cerebellum using a razor blade (*ii*). A 5% agar block was then glued directly to the vibratome stage (*iii*) and the cerebral cortex was glued to the stage next to the agar block with the forebrain facing upward (*iv*). The vibratome stage was then submerged in ice-cold slicing solution (Hanks' Balanced Salt Solution (HBSS) supplemented with 1% pen/strep, 5 mM glucose, and 4 mM MgCl₂) and the vibratome was used to generate 300 µm slices (*v*, *vi*). As slices are collected, they are transferred to a beaker containing slicing solution (*vii*) and then transferred to a permeable cell culture membrane (*viii*). To model GBM cell invasion, GFP-expressing GBM spheroids (400-500 µm in diameter) were generated (*ix*) and implanted on top of the brain slices (*x*). In terms of experimental timeline (Figure 4.3B), tumour spheroids were generated two days in advance of harvesting brain tissue and generating brain slices. The following day, tumour spheroids were implanted on top of the brain slices and incubated in culture for a length of time that requires optimization depending on the cell line. At

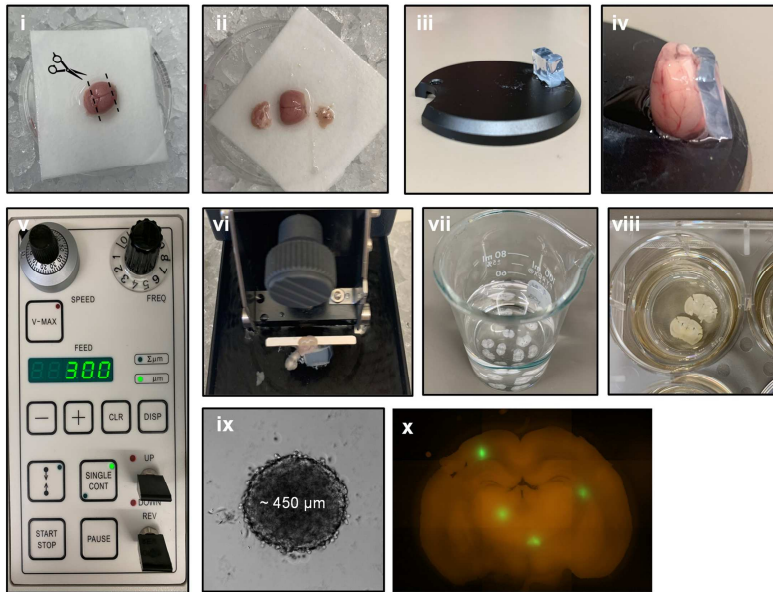
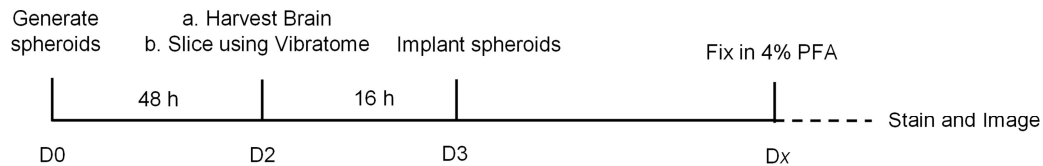
A**B**

Figure 4.3. *Ex vivo* brain slice spheroid invasion assay workflow.

(A) Experimental steps required to perform the *ex vivo* brain slice invasion assay: (i) Whole brains were harvested from 6-week-old male C57BL/6J mice and (ii) the olfactory bulb and cerebellum were removed. (iii) A block of solidified 5% agar was glued to the edge of the vibratome disc directly opposite the disc indentation. (iv) The isolated cerebral cortex was then glued directly to the vibratome disc such that it is leaning against the agar block with the forebrain facing upwards. (v) A Leica vibratome (VT100S) was used to generate brain slices (speed: 0.15 mm/s; frequency: 80 Hz). (vi) The vibratome disc containing the brain was submerged in ice-cold carbogenated slicing solution and (vii) 300 μ m brain slices were collected into a beaker containing the cold slicing solution. (viii) Once all brain slices are collected, 2-3 brain slices were transferred onto permeable cell culture inserts submerged in 25% FBS-containing DMEM/F12 media. (ix) GBM spheroids were generated and (x) implanted onto the brain slices *ex vivo*. (B) Summary of the *ex vivo* brain slice invasion assay experimental timeline.

the experimental end point, the slices can then be fixed in 4% PFA for 2 hours at RT, then stained and imaged to visualize cellular invasion into the brain slice.

4.3.3 Optimization of deep tissue imaging strategies.

Many previously published reports that implant tumour spheroids onto brain slices *ex vivo* tend to model migration along the brain slice rather than tumour cell invasion into the slice. To further advance the previously established *ex vivo* brain slice invasion assays, I sought to improve deep tissue imaging strategies such that visualizing cellular invasion into the brain slice is possible. First, I used the z-stack function on the confocal microscope to image GBM invasion into the brain slices. Brain slices containing GFP-positive GBM spheroids was placed onto a microscope slide, secured with a coverslip (Figure 4.4 Ai-ii), and then 20 μm sections were imaged using confocal microscopy. Imaging in the X/Y direction revealed many GFP-positive projections extending across the top of the brain slice (Figure 4.4B). However, despite imaging the brain slices on an inverted microscope slide such that confocal laser only passes through the 0.17 mm coverslip, the maximum depth of imaging I achieved was approximately 250 μm . This method of confocal imaging was insufficient for visualizing any projections that may occur below the spheroid and for accurately determining the depth of the projections (Figure 4.4B). To optimize imaging depth, I then embedded the brain slice containing GFP-positive GBM spheroids in a block of 4% agar (Figure 4.4Ci-ii). The brain slices were stained for GFAP to mark astrocytes prior to this process. The agar block was then glued directly to the vibratome stage using quick dry superglue, and the orientation of the brain slice was marked (Figure 4.4Cii). Next, I used the Vibratome to generate 200 μm z-sections and each section was placed

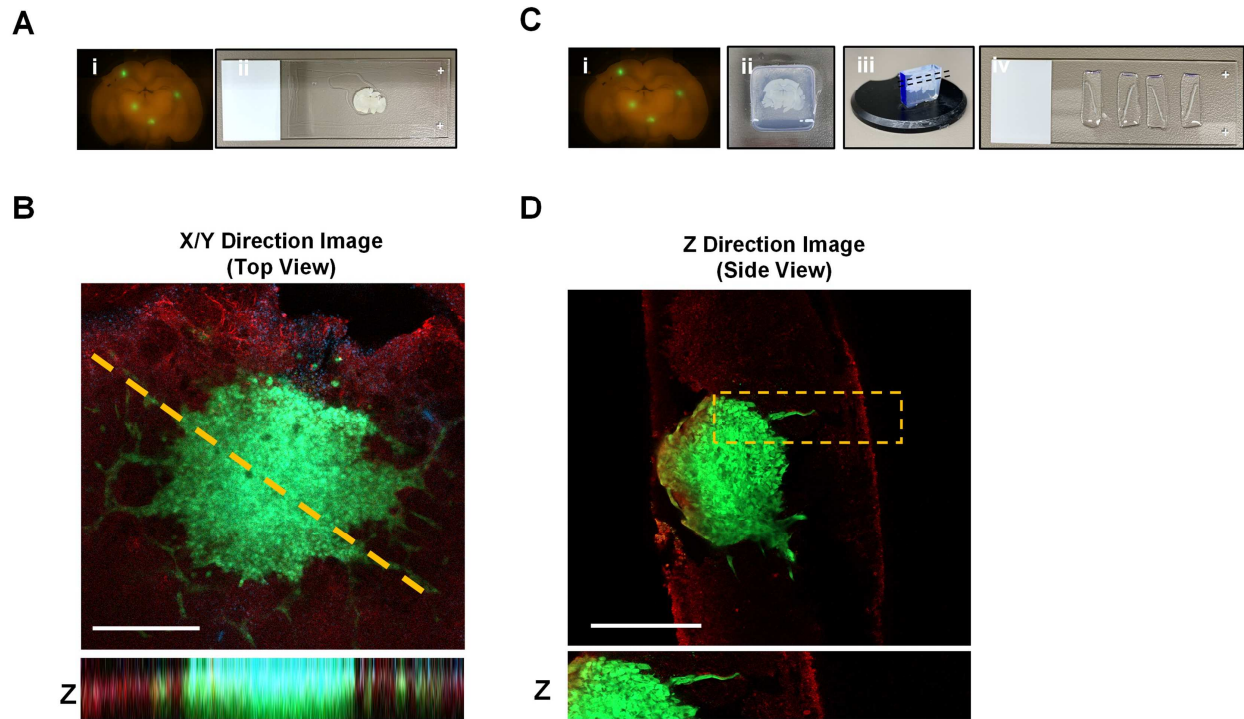


Figure 4.4. Confocal imaging techniques to improve depth of imaging.

(A) Experimental steps required to image whole brain slices using confocal microscopy. (i) A brain slice containing GFP-positive GBM spheroids is (ii) transferred to a microscope slide and secured in place with a glass coverslip. (B) Representative image displaying a LN18-GFP tagged spheroid invading into a brain slice stained for GFAP (red) and imaged in the X/Y direction. The microscope slide is inverted, and 20 μm section z-stack images (100 μm max) were achieved on the confocal microscope. Scale bar = 500 μm . (C) Experimental steps required to generate brain slice z-sections. (i) A brain slice containing GFP-positive GBM spheroids (ii) is transferred to a plastic cryomold and embedded in 4% agar. (iii) Once the agar is solidified, the agar block is removed from the cryomold, the orientation is marked with a sharpie marker, and the agar block is glued to the vibratome disc. (iv) The vibratome was used to generate 200 μm z-sections. Each z-section was collected and mounted onto microscope slides for imaging. (D) Representative image displaying a LN18-GFP tagged spheroid invading into a brain slice stained for GFAP and imaged in the Z-direction. The microscope slide was inverted and a single image was achieved using confocal microscopy. Scale bar = 250 μm .

in sequential order onto a microscope slide (Figure 4.4Civ). The z-sections were then imaged using confocal microscopy, which revealed projections below the spheroid (Figure 4.4D) that were not visible with the other imaging method. Notably, the GFAP stain was maintained through the sectioning process. In summary, I show that imaging brain slices in the X/Y direction models migration of cells across the brain slice while re-sectioning the brain slices and imaging in the Z direction more accurately models GBM cell invasion into the brain slice.

4.3.4 GBM cells exhibit different patterns of invasion *in vitro* versus *ex vivo*.

To directly compare between *in vitro* and *ex vivo* models of GBM invasion, I evaluated the invasiveness of GBM cells when invading into Matrigel versus *ex vivo* brain slices (Figure 4.5). First, LN229-GFP and LN18-GFP spheroids were either embedded in Matrigel or seeded on top of a thin layer of Matrigel. This revealed both LN229 and LN18 cells invade into the Matrigel or migrate along the top of the Matrigel as diffuse single cells (Figure 4.5 A, B). Next, LN229-GFP and LN18-GFP spheroids were seeded on top of 300 μm thick organotypic brain slices and cultured *ex vivo*. The brain slices were then imaged using confocal microscopy as described in section 4.3.3. In brief, brain slices were imaged in the X/Y direction to achieve a top view of the spheroid invading along the top of the brain slice or sectioned and imaged in the Z direction to achieve a side view of the spheroid invading into the brain slice. These imaging techniques revealed GBM spheroids tend to invade as collective strands along the top of the brain slice or a combination of single cells and collective strands when invading into the brain slice (Figure 4.5 A, B).

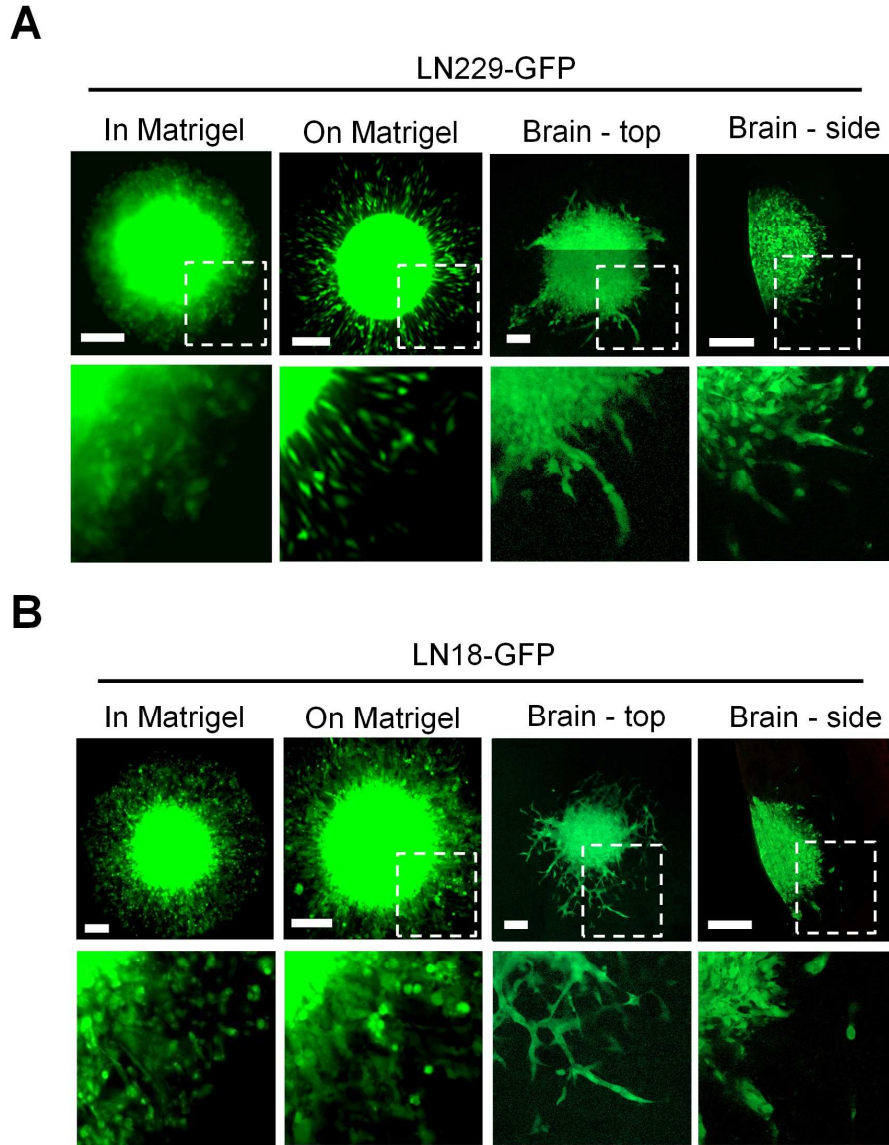


Figure 4.5. Different invasive phenotypes of GBM cells when embedded into Matrigel versus murine brain tissue.

(A, B) Representative images of LN229-GFP (A) and LN18-GFP (B) spheroids either embedded within 5.0 mg/mL Matrigel *in vitro* (in Matrigel), seeded on top of a thin layer of Matrigel *in vitro* (on Matrigel), seeded on top of *ex vivo* brain slice and imaged in the X/Y direction (Brain – top), or seeded on top of an *ex vivo* brain slice and imaged in the Z direction (Brain – side) on Day 5. The boxed regions are enlarged below each image. Scale bars = 200 μ m.

4.3.5 Quantifying tumour cell invasion into brain slices.

To quantify *ex vivo* tumour cell invasion into the brain slices, we first implanted untreated GFP-expressing LN229 spheroids onto brain slices for 5 days *in vitro* (DIV). These spheroids were used to develop a semi-automated ImageJ macro to quantify the invasive area (*i.e.* total cell area outside of the edge of the spheroid) and the distance of each cell from the edge of the spheroid (Figure 4.6A). In brief, the GFP-only channel was separated from the raw image, converted to an 8-bit image, and a mask was created using ImageJ. The semi-automated macro applies an ellipse to the mask image and the user can then position the ellipse over the spheroid core being careful to avoid the invasive edge. The ellipse is subtracted to remove the spheroid core and then a watershed transformation is applied to the image. The ImageJ program then quantifies the following parameters for pixels outside of the ellipse: (1) the number of particles detected (defined by greater than 10 pixels² in size), (2) the area of each particle, and (3) the distance of each particle to the nearest edge of the ellipse based on the gradient map (Figure 4.6A). With this information, we can calculate the sum invasive area and the average distance the tumour cells have travelled into the brain slice to determine the overall level of invasiveness of each spheroid.

To demonstrate that our *ex vivo* brain slice invasion assay models GBM cell invasion, I first performed a time course analysis by sequentially implanting GFP-expressing LN229 and LN18 spheroids onto murine brain slices between 0 and 8 days prior to imaging (Figure 4.7A). Notably, all spheroids are implanted onto the same slice to reduce slice-to-slice variability. The time course analysis revealed that approximately 25% of the volume of each LN229-GFP and LN18-GFP spheroid are within the brain slice on day 0, while nearly 100% of the volume of

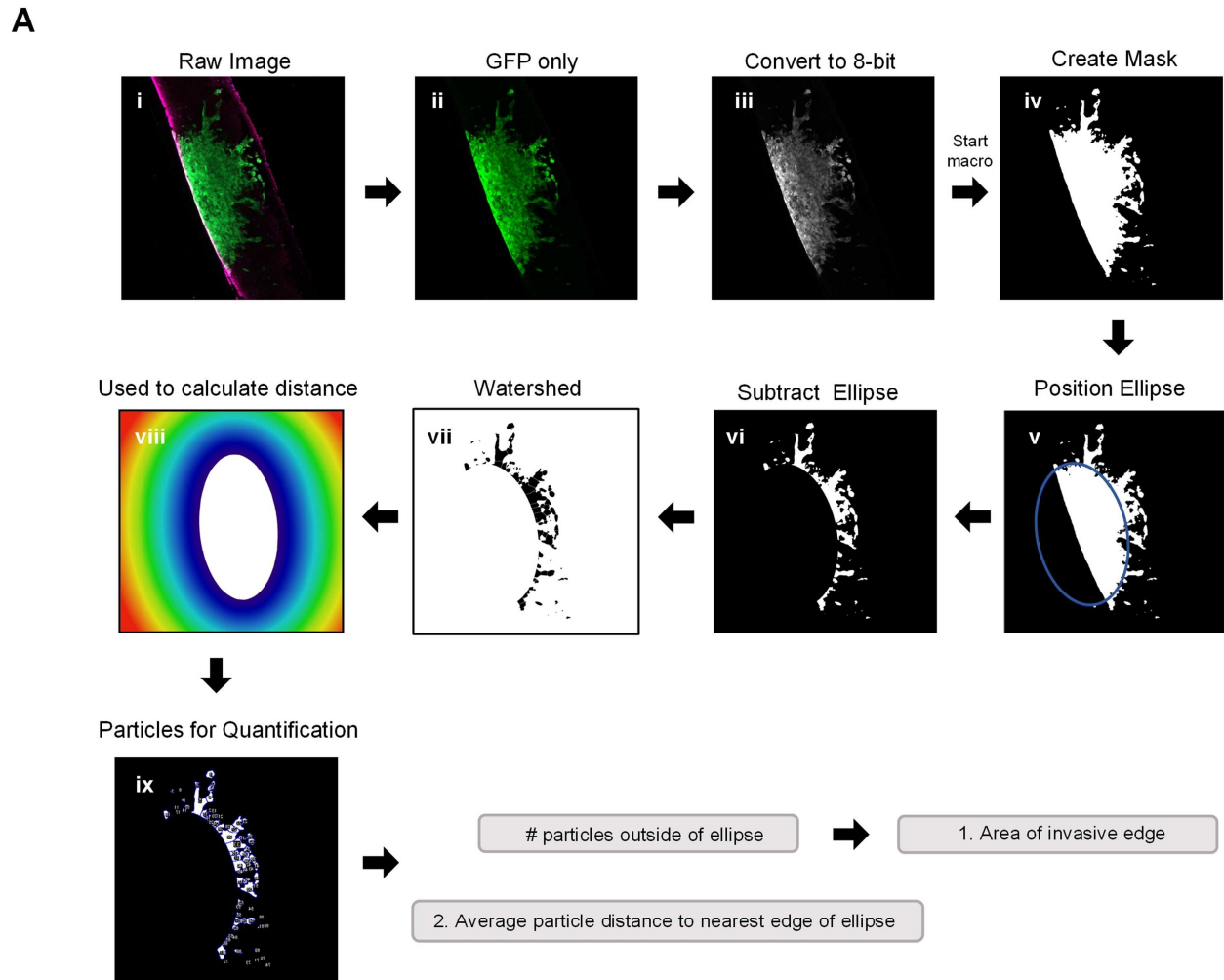


Figure 4.6. Workflow of a semi-automated ImageJ macro used to quantify invasion into *ex vivo* brain slice cultures.

(A) This ImageJ macro consists of 9 semi-automated steps for analyzing the number of particles, area of each particle, and distance of each particle to the nearest edge of the ellipse. (i) A raw image is split into individual channels and (ii) the GFP only channel is converted to an 8-bit image (iii). The ImageJ macro then starts by creating a mask of the binary image (iv) and the software places an ellipse (blue circle) over the core of the spheroid, which can be adjusted if necessary (v). The ellipse is subtracted from the image (vi) and the particles detected in the invasive edge are watershed (vii). Finally, a colour map (viii) is used by the software to calculate the distance of each particle from the nearest edge of the ellipse (ix) as well as the area of invasive edge.

* ImageJ macro developed by Rocky Shi.

each spheroid was within the brain slice by days 3 and 5, respectively (Figure 4.7B, C). The ImageJ macro (Figure 4.6) was used to quantify the invasive area, which revealed that LN229-GFP spheroids increase in overall invasiveness overtime, while the invasiveness of LN18-GFP spheroids plateaued by 3 days in vitro (DIV) (Figure 4.7D). Moreover, I found LN229-GFP spheroids remained spherical up to 3 DIV, after which the edge of the spheroid was difficult to differentiate from the invasive edge (Figure 4.7B). LN18-GFP spheroids seemed to maintain their shape making it easier to determine the invasive edge up to 8 DIV (Figure 4.7B). Finally, the average invasive distance was determined by measuring the distance of each particle to the nearest edge of ellipse, which revealed the average distance of the invasive cells increased at 1 DIV and then plateaued up to 8 DIV indicating the invasive front progresses at a steady rate (Figure 4.7E).

4.3.6 Organotypic brain slices from adult C57BL/6J mice exhibit increased viability in serum-containing media.

We next sought to identify a cell culture media for maintaining murine brain slices in culture for 4 days with sufficient viability. Brain slice viability was analyzed using an Alamar blue metabolic assay (Figure 4.8 A-D). First, I cultured brain slices harvested from 6-week-old male C57BL/6J mice in serum-free DMEM-F12 media (SFM), SFM supplemented with 1X B27 (a serum-free neuronal cell supplement), DMEM-F12 media containing 5% or 25% FBS, and finally DMEM-F12 media containing 5% or 25% heat-inactivated horse serum (HI-HS). This analysis revealed slices maintained in 25% FBS or 25% HI-HS were significantly more viable than slices in serum-free DMEM-F12 media or serum-free media containing 1X B27 (Figure 4.8A). In addition to low viability, I also observed that brain slices cultured in SFM or SFM

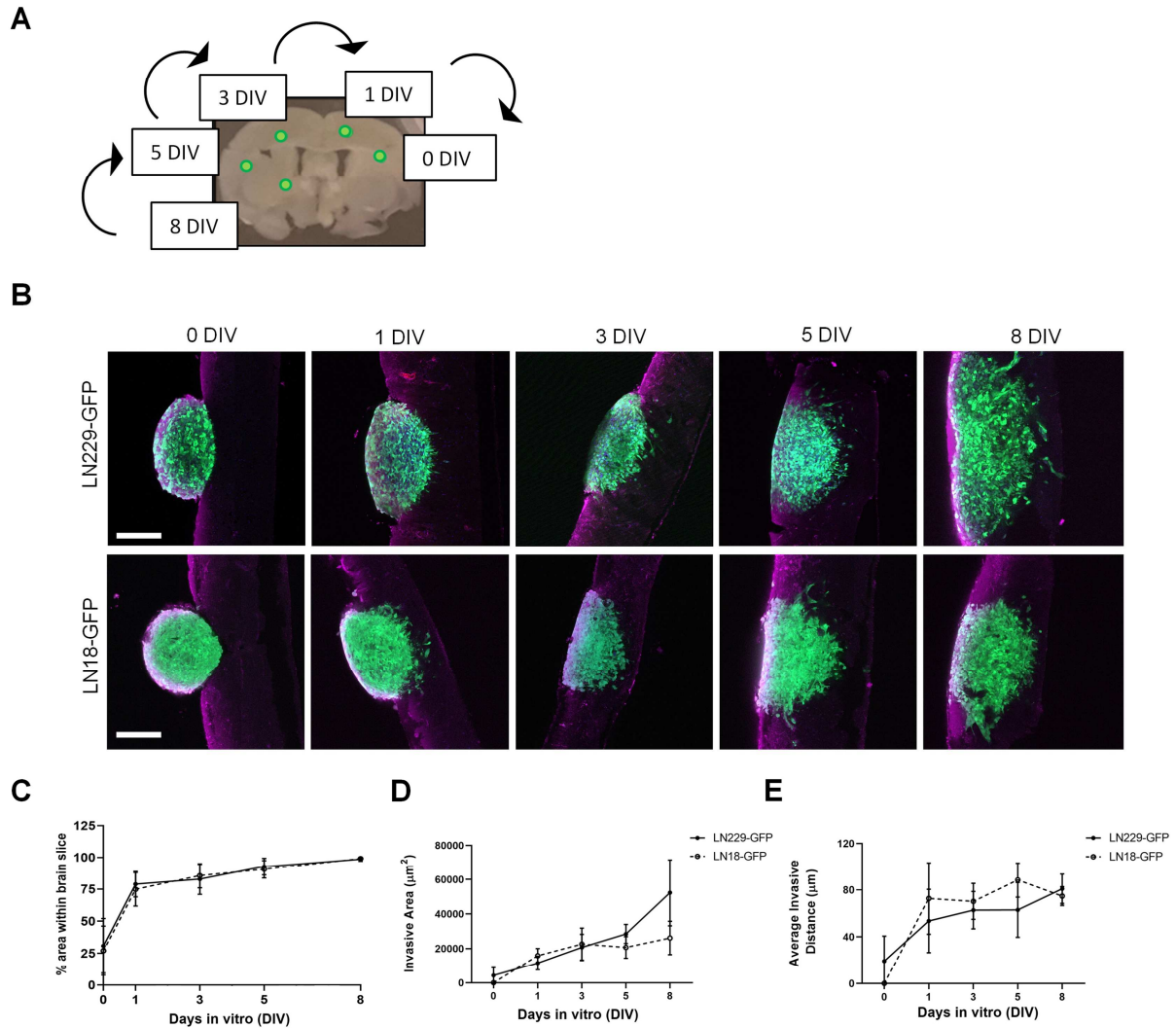


Figure 4.7. Time course of LN229 and LN18 GFP-tagged GBM spheroids invading into brain tissue *ex vivo*.

(A) A schematic displaying the typical location of GFP-expressing spheroids sequentially implanted onto brain slices and cultured *ex vivo* for the indicated amount of time. (B) Representative images of LN229-GFP and LN18-GFP tagged GBM spheroids invading into brain slices *ex vivo* for 0, 1, 3, 5, and 8 days *in vitro* (DIV). Brain slices were co-stained for GFAP (astrocytes) and DAPI (nuclei). Scale bar = 200 μm . (C, D, E) Quantification of the (C) % spheroid area within the brain slice, (D) the invasive area (μm^2), and (E) the average particle distance from the nearest edge of the ellipse ($n = 4 - 8$ spheroids per condition implanted on slices collected from ≥ 4 mice; 3 independent experiments).

containing 1X B27 swelled to twice the original size and lost slice integrity. Thus, brain slices collected from adult C57BL/6J mice maintain structure and exhibit improved cellular viability when cultured in high serum-containing media. Since media containing 25% HI-HS did not significantly increase brain slice viability compared to 25% FBS, and since all *in vitro* studies were performed using FBS, I decided to move forward with DMEM-F12 media containing 25% FBS.

Next, I harvested brain slices from 6-week-old male C57BL/6J mice and cultured the slices in 25% FBS DMEM-F12 media for 14 DIV. Brain slice viability was analyzed overtime, which revealed that brain slices maintain greater than 50% cell viability by 4 DIV, as compared to 0 DIV brain slices (Figure 4.8B). I then collected brain slices from 6-week-old, 8-week-old, and 22-week-old male C57BL/6J mice to determine the role of age on slice viability. Here, I show slices harvested from 6-week-old mice are significantly more viable at 0 DIV compared to the older mice (Figure 4.8C). Notably, we limited the mouse age to a minimum of 6-weeks old to ensure the brains are large enough to collect at least 6 slices per brain. Lastly, the viability of each slice collected from 8-week-old mice was analyzed to determine if time spent in the slicing solution impacts brain slice viability. This revealed no difference in slice viability when comparing the first slice (Slice 1) to the last slice collected (Slice 18), which represent the slices closest to the occipital lobe and cerebellum, respectively (Figure 4.8D). Nevertheless, I typically use slices 6 to 12 for the *ex vivo* brain slice invasion assay since these slices are similar in size, viability, and architecture (Figure 4.8E).

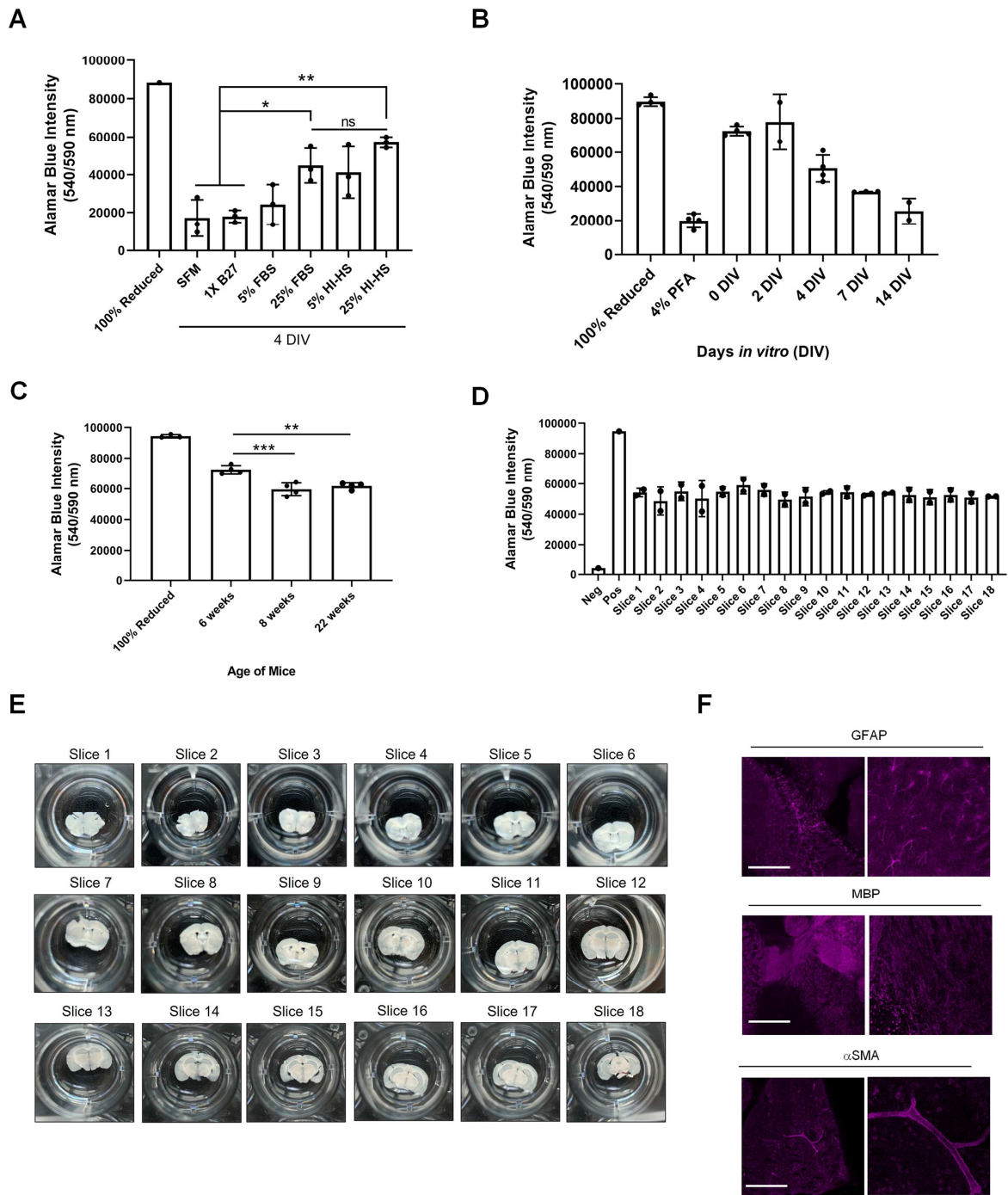


Figure 4.8. Assessment of brain slice viability in culture.

Figure 4.8. Assessment of brain slice viability in culture.

(A) Brain slices were collected in duplicate from 6-week old male mice and cultured in serum-free media (SFM), media containing 1X B27 supplement, DMEM containing 5% or 25% fetal bovine serum (FBS), or DMEM containing 5% or 25% heat-inactivated horse serum (HI-HS) for 4 days *in vitro* (DIV). Cell viability was assessed by incubating brain slices in 10% alamar blue for 24 hours. Autoclaved alamar blue solution (100% reduced) is used as the positive control and 10% alamar blue solution with no brain slice represents the negative control. Data represent the mean \pm SD (n=3 mice, *p < 0.05, **p < 0.01, one-way ANOVA with Tukey's multiple comparison test). (B) Brain slices collected from 6-week old mice were incubated in DMEM containing 5% FBS for 0, 2, 4, 7, and 14 days *in vitro* (DIV) and brain slice viability was assessed via alamar blue intensity. Data represent the mean \pm SD (n \geq 2 mice). (C) Data represent the mean \pm SD (n=4 mice, **p < 0.01, ***p < 0.001, one-way ANOVA with Tukey's multiple comparison test). (D) Brain slice viability of each slice collected from 8-week old mice was determined via alamar blue fluorescent intensity at 0 DIV (n=2 mice). (E) Representative images of brain slice sections collected from one 8-week old murine brain. Slice 1 represents the first slice collected starting at the base of the olfactory bulb while slice 18 represents the base of the cerebral cortex. (F) Representative images of brain slices culture for 5 DIV stained for glial fibrillary acidic protein (GFAP), myelin basic protein (MBP), and alpha smooth muscle actin (α SMA). Scale bar = 500 μ m.

Importantly, the *ex vivo* brain slices were found to express GFAP-positive astrocytes, MBP-positive white matter tracts, and alpha smooth muscle actin (α SMA)-positive vasculature in culture (Figure 4.7F). Together, these data indicate that brain slices collected from 6-week-old male C57BL/6J mice maintained in 25% FBS-DMEM/F12 cell culture media for 4 days confers sufficient cellular viability, as defined as greater than 50% of the original slice viability.

Coronal murine brain slices are organized into several distinct regions, including the cortex region, corpus collosum, striatum region, and the ventricles (Allen Reference Atlas – Mouse Brain). To determine if certain regions of the brain are more permissive to GBM cell invasion, multiple untreated LN229-GFP and LN18-GFP spheroids were randomly implanted onto brain slices for 3 days *in vitro* (DIV) (Figure 4.9A). Each brain slice was divided into 6 quadrants (top left, top middle, top right, bottom left, bottom middle, and bottom right) to analyze the invasive area of LN229-GFP and LN18-GFP cells within each quadrant, which revealed that spheroid location does not significantly impact invasiveness (Figure 4.9B). Comparing the invasive area of all LN229-GFP and LN18-GFP spheroids from each slice revealed certain brain slices impact GBM more than other slices (Figure 4.9C). These results indicate certain brain slices may result in a global increase in invasiveness suggesting the need to implant all irradiation doses onto one slice, rather than each slice being dedicated to a single dose of irradiation. This suggests that the *ex vivo* brain environment is equally receptive to GBM cell invasion and that perhaps invasiveness is driven by the intrinsic properties of tumour cells rather than the surrounding *ex vivo* brain environment.

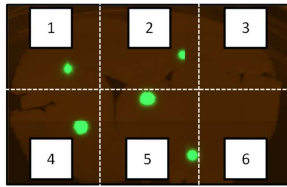
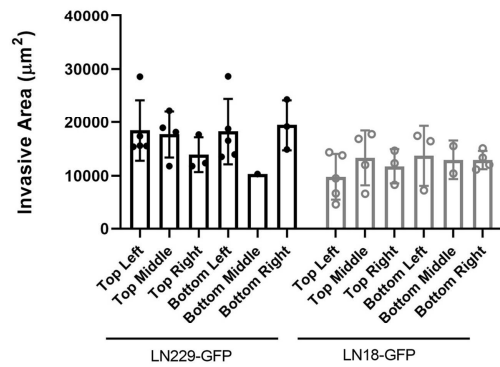
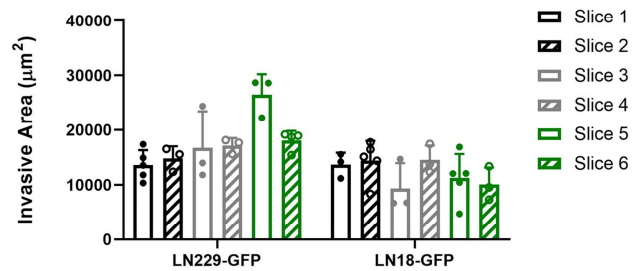
A**B****C**

Figure 4.9. Spheroid placement does not impact invasiveness.

(A) A representative image of a brain slice containing 6 randomly implanted GFP-expressing spheroid divided into 6 quadrants (1 = top left, 2 = top middle, 3 = top right, 4 = bottom left, 5 = bottom middle, 6 = bottom right). (B, C) Quantification of the invasive area (μm^2) of untreated LN229-GFP and LN18-GFP spheroids implanted onto brain slices and cultured *ex vivo* for 3 days. Data are plotted based on (B) spheroid location or (C) individual brain slices ($n = 21$ spheroids total implanted randomly onto 6 brain slices collected from 4-5 mice (represents slices 6 – 10); two independent experiments).

4.3.7 Ionizing radiation alters GBM cell invasion into *ex vivo* brain slices.

My previous data revealed IR significantly reduced *in vitro* chemotactic cell invasion (Figure 3.7) and *in vitro* invasion of cells invading away from spheroids (Figure 4.2). To explore the influence of the brain microenvironment on the invasiveness of irradiated and non-irradiated GBM cells *ex vivo*, I performed our advanced *ex vivo* brain slice invasion assay. In brief, I generated LN229-GFP and LN18-GFP spheroids (Day 0), harvested brain slices from 6-week-old male C57BL/6J mice using the vibratome (Day 2), spheroids were irradiated with 0, 2, 4, 6, or 10 Gy IR and implanted onto the brain slices (Day 3), and then fixed the slices 72 hours post-spheroid implantation (Day 6). Finally, each brain slice was stained, re-sectioned and imaged on the confocal microscope to visualize GBM cell invasion (Figure 4.10A). Notably, spheroids exposed to various doses of irradiation were implanted onto one brain slice to reduce slice-slice variability (Figure 4.10B). These data revealed that irradiating LN229-GFP spheroids does not change invasiveness by 3 DIV (Figure 4.10C, D). However, I observed a trend towards increased invasion from LN18-GFP spheroids irradiated with 4 Gy or 6 Gy IR (Figure 4.10C). More specifically, four out of eleven (4/11) spheroids exposed to 2 Gy, three out of nine (3/9) spheroids exposed to 4 Gy, two out of eight (2/8) spheroids exposed to 6 Gy, and four out of nine (4/9) exposed to 10 Gy exhibited increased invasiveness compared to non-irradiated LN18-GFP controls (Figure 4.10D). This radiation-induced increase, although insignificant, was not observed using *in vitro* models therefore suggesting an important role for the brain microenvironment in facilitating radiation-induced invasion of GBM tumour cells.

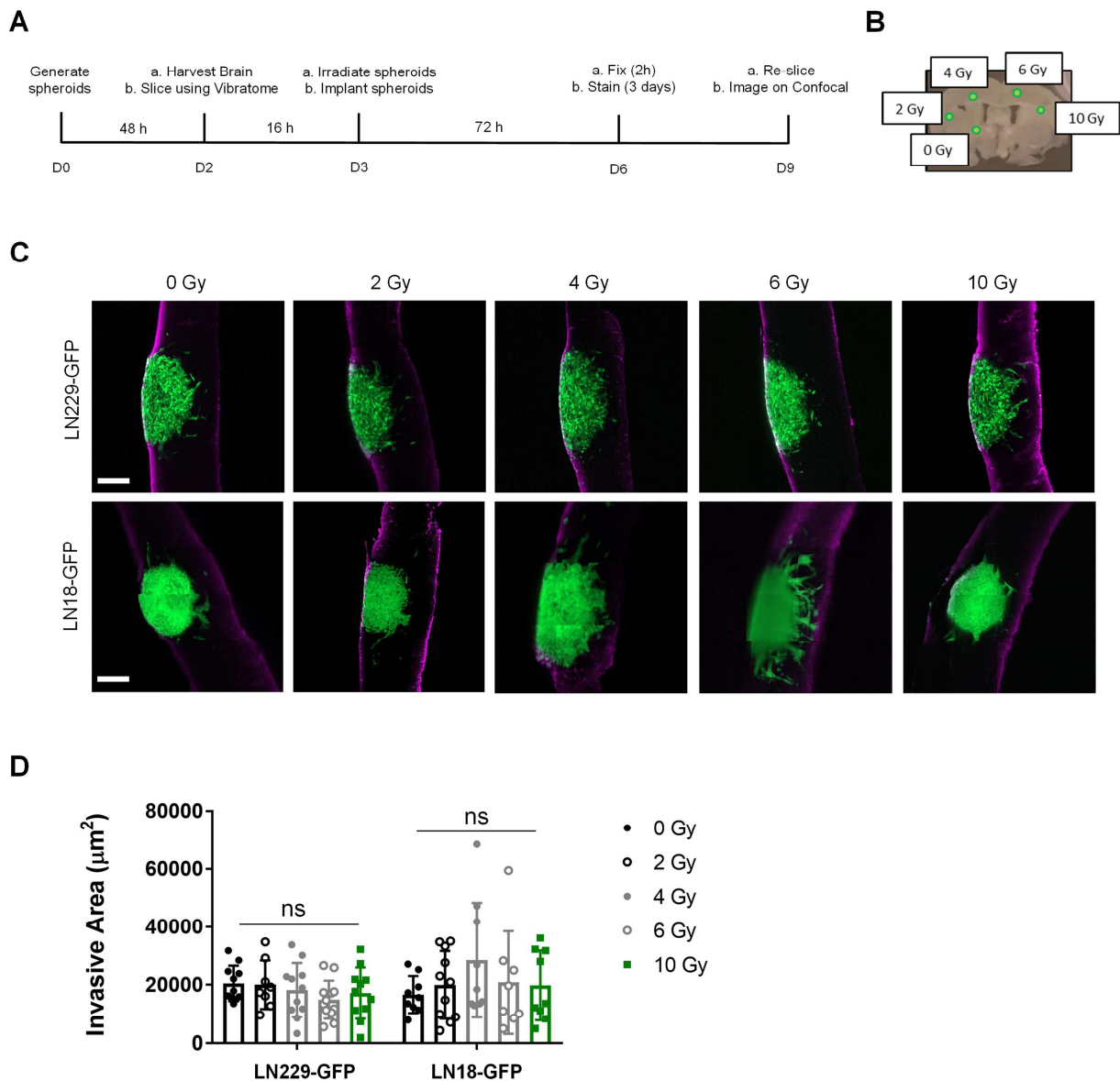


Figure 4.10. Ionizing radiation minimally impacts GBM spheroids invasion into brain tissue *ex vivo*.

(A) Experimental timeline showing time of spheroid irradiation prior to implantation onto *ex vivo* brain slices. (B) A schematic displaying the approximate location of where irradiated spheroids were implanted onto each brain slices. (C) Representative images of LN229-GFP and LN18-GFP spheroids exposed to 0, 2, 4, 6, or 10 Gy IR and cultured on *ex vivo* brain slices for 3 days *in vitro* (3 DIV). Slices were stained for GFAP. Scale bar = 200 μm . (D) Quantification of the invasive area (μm^2) of each spheroid ($n = 8 - 12$ spheroids per condition, ns = non-significant, one-way ANOVA with Dunnett multiple comparison test).

4.4 Discussion

For decades, GBM cell invasion has typically been modeled in two dimensions using chemotactic assays and synthetic basement membranes. These traditional assays lack environmental influences specific to the central nervous system and may not accurately model the precise mechanisms of GBM cell invasion. Thus, there is a great need to transition from overly simplistic *in vitro* assays to utilizing more physiologically relevant model systems to study GBM invasion, which will undoubtedly improve the development of more effective therapeutics for GBM patients. Here, I developed an advanced *ex vivo* brain slice invasion assay to more accurately model brain cancer invasion. A troubleshooting guide highlighting any issues that may arise and possible solutions has been prepared to allow for reproducibility of this model system (Appendix A2).

Our version of the *ex vivo* brain slice invasion assay greatly improves upon the imaging techniques used to visualize invasion into the brain slice. Here, I present a novel technique that involves staining brain slices, embedding the stained slices in agar, and then re-sectioning the brain slice in the Z direction to allow for visualization of the spheroid-brain slice interface. While this technique improves the imaging depth of a confocal microscope, another option is to use a two-photon microscope. Two-photon microscopy is an alternative to confocal microscopy that offers increased resolution when imaging thick tissue sections and images at depths unachievable using a confocal microscope (Benninger and Piston, 2013). However, two-photon microscopes are highly specialized and expensive machines inaccessible to many labs. Alternatively, fixed tissue can be cleared using a variety of treatment methods. Tissue clearing methods results in transparent tissue allowing for increased imaging depth such that light from the confocal microscope can penetrate into much thicker samples (Hama et al., 2015, 2011; Ke et al., 2013).

Major disadvantages of tissue clearing include the use of harsh organic solvents, which may result in loss of lipids over time and tissue shrinkage, as well as fluorescent quenching (Ariel, 2017; Gómez-Gaviro et al., 2020). Furthermore, tissue clearing processing can take weeks to complete. Our novel imaging method offers a more accessible way to image brain slices while offering advantages over other imaging techniques (*i.e.*, two-photon microscopy or tissue clearing procedures) by improving staining quality and tissue architecture.

The donor age for organotypic brain slices plays an important role in determining the long-term survival of brain slices in culture (Humpel, 2015). For electrophysiology and neurodegeneration studies, organotypic brain slices are typically collected from embryonic or postnatal donors due to increased viability in culture compared to adult donors (Croft et al., 2019; Semple et al., 2013). In terms of brain development and maturation, many differences exist between embryonic, postnatal, and adult brain tissue. For instance, the process of myelination commences postnatally and continues into adulthood suggesting increased myelination of white matter tracts in adult brain tissue (Menassa and Gomez-Nicola, 2018). Due to the important role of white matter tracts in facilitating brain cell motility, it therefore seems plausible that GBM cells would invade differently into brain tissue collected from pre- and postnatal versus adult donors. While GBM may occur at any age, GBM is primarily diagnosed in older patients with the median age at diagnosis being 65 years old (Chen et al., 2021). However, limited studies exist showing brain tissue from adult donors can survive in culture for extended periods of time. We have developed a brain slicing solution and identified specific culture conditions that allow for brain slices harvested from 6-week-old male C57BL/6J mice to remain sufficiently viable in culture for 4-7 days. Nonetheless, there is a great need to further improve the viability of adult organotypic brain slices such that long-term culture is possible.

Organotypic models of invasion offer many advantages over *in vitro* and *in vivo* assays. Embedding tumour cells onto brain slices *ex vivo* requires far less technical expertise than performing intracranial implants to establish brain tumours in mice. Furthermore, less mice are required to perform *ex vivo* versus *in vivo* experiments highlighting *ex vivo* models as a more cost-effective and ethical option (Vollmann-Zwerenz et al., 2020). Lastly, organotypic slice cultures offer a 3D scaffold that contains tissue-specific ECM as well as stromal and immune cells populations that are often not present within *in vitro* models. Notably, others have shown that organotypic slices collected from fresh pancreatic ductal adenocarcinoma tumours could be cultured *ex vivo* for one week while maintaining macrophages and T cells immune cell populations (Jiang et al., 2019). While there are many benefits to using organotypic models of invasion, limitations still exist. For instance, while brain slices maintain vascular architecture *ex vivo*, the vessels are non-functional and thus do not facilitate immune cell infiltration nor tumour cell extravasation. Other limitations of *ex vivo* slice cultures include viability-dependent time constraints as well as the need to purchase specialized equipment (*i.e.*, vibratome). Despite these limitations, *ex vivo* brain slice invasion assays offer many advantages over traditional two-dimensional chemotactic invasion assays and represent an important step forward for GBM research.

Glioblastoma tumours are highly invasive and typically invade within 1-2 cm from the primary tumour margins while rarely metastasizing to distant organs (Choucair et al., 1986; Esmaeili et al., 2018). Notably, GBM cells tend to invade into brain tissue as single cells, or along pre-existing brain structures in collective strands (Alieva et al., 2019; Claes et al., 2007; Haeger et al., 2014; Scherer, 1938). To determine the best method for modelling these distinct mechanisms of GBM cell invasion, I compared the invasive patterns of GBM cells when using

an *in vitro* spheroid invasion assay and an *ex vivo* brain slice invasion assay. Interestingly, this revealed that LN229 and LN18 GFP-expressing GBM spheroids typically invade as diffuse single cells when either seeded on top of a thin layer of Matrigel or embedded within the Matrigel *in vitro*. Conversely, when the same GBM spheroids were implanted on top of murine brain slices *ex vivo*, I observed GBM cells migrate along the top of the slice as collective invasive strands while invading into the brain slice as both single cells and in strands. These data therefore suggest *in vitro* models of invasion are lacking critical structures necessary to facilitate collective invasion and that modeling GBM invasion using *ex vivo* brain slices better mimics the modes of invasion observed in human GBM tumours.

When investigating the role of ionizing radiation in facilitating GBM cell invasion, I noted differences in the results collected using *in vitro* versus *ex vivo* models. Chemotactic invasion assays revealed higher doses of radiation (4 and 10 Gy) significantly reduced LN229 and LN18 cell invasion through Matrigel (Figure 3.7), with *in vitro* spheroid invasion assays showing similar results (Figure 4.2). Since Matrigel is a cocktail of synthetic ECM proteins that lacks many of the necessary components unique to the brain microenvironment, we further investigated the role of IR on GBM cell invasion using an *ex vivo* brain slice invasion assay. We found IR increased the invasion of a subset of LN18-GFP spheroids while LN229-GFP spheroids remained unchanged (Figure 4.10). These data highlight clear differences in the results collected using *in vitro* and *ex vivo* models of invasion. However, the modes of invasion observed using our *ex vivo* brain slice invasion assay more accurately depict what is observed in human tumours indicating *ex vivo* models should be used when investigating GBM invasion.

Taken together, I propose using my advanced version of the *ex vivo* brain slice invasion assay and novel imaging technique to more accurately model invasion into brain tissue. Our data

highlights the importance of transitioning from *in vitro* models to organ-specific *ex vivo* models of invasion to better recapitulate features of the innate tumour microenvironment. This will undoubtedly result in an improved understanding of the precise mechanisms that drive GBM cell invasion and lead the advancement of therapeutic options available to brain cancer patients.

Chapter 5: Conclusions and Future Directions

5.1 Summary

Metastasis is the leading cause of cancer related mortality. The metastatic cascade is a complex process that includes migration and invasion of cancer cells into neighboring tissue. Mechanisms of migration and invasion require the coordination of many signaling pathways, which can be triggered by both intrinsic and extrinsic signals. A further understanding of the intrinsic and extrinsic mechanisms of cancer cell invasion is critical for identifying suitable targets to limit or prevent the spread of cancer.

In **Chapter 2**, I report a novel role of PTP α in mediating triple-negative breast cancer cell invasion *in vitro* and *in vivo*. Mechanistically, I show depletion of PTP α results in decreased ECM degradation *in vitro* and reduced localization of MMP14 to plasma membrane protrusions resembling invadopodia, suggesting a role for PTP α in intracellular trafficking of MMP14. Overall, these findings indicate a novel role for PTP α as an intrinsic regulator of triple-negative breast cancer cell invasion and highlight PTP α as an attractive drug target for the treatment of TNBC.

In **Chapter 3**, I investigated the role of ionizing radiation in facilitating invadopodia-mediated GBM cell invasion *in vitro*. Initial studies revealed LN229 and LN18 GBM cells primarily use focal adhesions rather than invadopodia to degrade ECM *in vitro*. Interestingly, I found ionizing radiation increased TKS5 mRNA and protein expression levels; however, this increase in TKS5 expression did not correlate with an increase in invadopodia-mediated ECM degradation or GBM cell invasion. Together, these findings suggest that, in our hands, ionizing radiation does not extrinsically regulate GBM cell invasion *in vitro* despite contradictory

previously published reports. Lastly, my findings suggest the need to further investigate a potential invadopodia-independent role for TKS5 in brain cancer biology.

In **Chapter 4**, I focused on developing an advanced version of an organotypic brain slice invasion assay to further investigate the role of ionizing radiation on facilitating GBM cell invasion into murine brain tissue. Here, I state the optimal conditions for harvesting murine brain slices and maintaining these slices in culture for 4-7 days. I also outline an optimized method for implanting tumour spheroids onto brain slices and describe a novel technique for imaging cellular invasion into the slices. Lastly, I used the *ex vivo* brain slice spheroid invasion assay to further investigate the effects of ionizing radiation in facilitating GBM cell invasion.

In summary, I used multiple model systems to investigate mechanisms of cancer cell invasion *in vitro*, *in vivo*, and *ex vivo*, resulting in a better understanding of the complexities of the metastatic cascade. My most important contributions to the field include reporting a novel role of PTP α in facilitating triple negative breast cancer cell invasion and developing an advanced method to more accurately model *ex vivo* GBM cell invasion.

5.2 Future Directions

In this section, I will highlight key findings from each data chapter and propose future experiments to address important outstanding questions.

In **Chapter 2**, I observed that depletion of receptor-type protein tyrosine phosphatase alpha (PTP α) inhibits the invasion of MDA-MB-231 triple-negative breast cancer cells *in vitro* and *in vivo*. In this study, I also show PTP α localizes to early endosome antigen 1, caveolin-1, and MMP14-positive endosomal structures in the cell and facilitates the localization of MMP14

to invasive protrusions on the plasma membrane. Therefore, I suggest MMP14 localization to the plasma membrane as a key player in MDA-MB-231 cellular invasion. Future experiments are required to determine how PTP α regulates the trafficking of MMP14 to invadopodia structures. The use of time-lapse microscopy would be valuable for visualizing the localization of MMP14 to invadopodia structures and how PTP α is involved in this process. Since I found PTP α does not localize to invadopodia, perhaps PTP α is involved in co-trafficking of MMP14 to invadopodia but remains bound to the membrane of the endosomes. Of course, future work is required to determine the precise signaling mechanisms involved in facilitating this process.

To further investigate the role of PTP α in membrane dynamics and trafficking, I have conducted preliminary experiments focused on immunoblotting shCtl-231, sh α 1-231, and sh α 2-231 cell lysates for PTP α , Cav-1-pY14, total Cav-1, and actin. I found a decrease in the levels of Cav-1-pY14 upon PTP α knockdown, which was also accompanied by an increase in phosphorylation of an unknown protein (Figure 5.1A). Since phosphatases function by dephosphorylating tyrosine residues and since PTP α depletion resulted in less Cav-1 phosphorylation, it seems more likely that PTP α acts through other molecular players to dephosphorylate Cav-1 at tyrosine residue 14. One group found PTP1B, a non-transmembrane PTP, dephosphorylated Cav-1-Y14 resulting in reduced migration, invasion, and metastasis (Martínez-Meza et al., 2019). While PTP α knockdown did not impact the expression levels of similarly related PTP ϵ , we cannot exclude the possibility that the expression levels of other PTPs within the PTP superfamily are not altered to compensate for the loss of PTP α . To determine the relative expression of PTPs, particularly PTP1B, upon the depletion of PTP α in MDA-MB-231

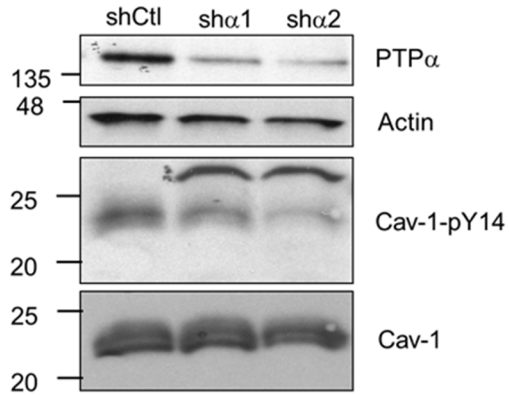


Figure 5.1. Preliminary data shows PTP α knockdown decreases caveolin-1 phosphorylation at tyrosine position 14 (cav-1-pY14).

Control (shCtl) and PTP α depleted (sha1 and sha2) MDA-MB-231 cells were lysed and immunoblotted for PTP α , actin, caveolin-1-phosphotyrosine position 14 (cav-1-pY14), and total caveolin-1 (n=1 independent replicate).

cells, it would be useful to perform a proteomic screen. Perhaps PTP α knockdown increases PTP1B expression resulting in the dephosphorylation of Cav-1. Since kinases act as phosphorylating agents, another possibility is that PTP α knockdown results in reduced kinase activity. Although the role of PTP α in Src signaling mechanisms has not been investigated in MDA-MB-231 cells specifically, PTP α has been shown to be an activator of Src kinases in mouse embryonic fibroblasts (MEFs) (Pallen, 2003; Ponniah et al., 1999). Furthermore, others have shown Cav-1-pY14 is the primary phosphorylation site for Src (Li et al., 1996; Sverdlov et al., 2007; Zimnicka et al., 2016). Future work is required to determine if PTP α acts through Src to phosphorylate Cav-1 at tyrosine residue 14, and if this phosphorylating event affects the migration and invasion of MDA-MB-231 cells.

Immunohistochemical analysis of mammary fat pads containing either control or PTP α -depleted tumours revealed PTP α knockdown correlated with increased CC3 expression, suggesting a role for PTP α in apoptotic signaling mechanisms. Further examination of PTP α and CC3 expression levels in human tumour samples via IHC staining of patient biopsies would be necessary for validating these findings. Due to the important role of hypoxia in facilitating tumour progression, perhaps staining the tumour tissue for markers of hypoxia (carbonic anhydrase IX; CAIX, hypoxia inducible factor 1 subunit alpha; HIF-1 α , etc.) would be useful for determining why tumours lacking PTP α exhibit higher CC3 expression and reduced outward growth. Whether not the effects I observed on tumour growth are due to the lack of MMP14 localization to the plasma membrane or another function of PTP α independent of cancer cell invasion remains to be elucidated.

Furthermore, my work focused on the role of PTP α in facilitating the local invasion of breast cancer cells within the mammary fat pad. It would be interesting to further this work by investigating the role of PTP α in mediating the dissemination of tumour cells to distant organs. This question could be addressed by orthotopically implanting control versus PTP α -knockdown MDA-MB-231 cells into the mammary fat pads of female NSG mice and monitoring the levels of lung metastasis and colonization via immunohistochemistry. Since PTP α is highly expressed in brain tissue, further investigating the role of PTP α in facilitating (i) the metastasis of breast cancer cells to the brain and (ii) the local invasion of brain cancer cells within the surrounding brain tissue would be interesting follow-up studies. Notably, MDA-MB-231 cells do not metastasize to the brain. Therefore, using MDA-MB-231 BR cells, a cell line derived from a spontaneous brain metastasis lesion (Yoneda et al., 2001), would be useful to address the role of PTP α in facilitating the metastasis of TNBC to the brain.

PTP α has low tissue specificity and is expressed in many different cell types. Some groups have shown PTP α expression increases in tumour cells compared to normal adjacent tissue (Ardini et al., 2000; Gu et al., 2017; Lin et al., 2020; Wu et al., 2006). Nevertheless, a major limitation of this work would be to develop a therapeutic drug against PTP α such that only cancer cells are targeted. Especially because PTP α plays a role in many important physiological processes including embryogenesis and wound healing. Perhaps performing comparative proteomic analysis via mass spectrometry to compare PTP α protein expressed in normal versus tumour tissue would be helpful to identify a unique sequence or mutation only present in cancerous tissue.

In **Chapter 3**, I investigated the role of ionizing radiation in facilitating *in vitro* GBM cell invasion. TKS5, a member of the tyrosine kinase substrate (TKS) adaptor protein family, plays a role as a scaffold protein critical for invadopodia formation and function (Iizuka et al., 2016; Saini and Courtneidge, 2018; Seals et al., 2005). I found higher doses of ionizing radiation increased TKS5 mRNA and protein expression. The increase in TKS5 expression did not correlate with increased invadopodia function or GBM cell invasion suggesting a potential alternate role for TKS5 in GBM biology. Other groups have shown an invasion-independent role for TKS5 in mediating proliferation and tumour growth (Blouw et al., 2015). Furthermore, it has been shown that TKS5 knockdown results in reduced cellular proliferation, cell cycle arrest and an accumulation of cells in the G1 phase, as well increased apoptosis (Moodley et al., 2015). Therefore, future experiments would require stably depleting TKS5 in LN229 cells and monitoring *in vitro* cell invasion through Matrigel. Furthermore, TKS5 knockdown cells would be useful for investigating if TKS5 plays a role in DNA damage repair and radiation response.

In Chapter 3, I also report focal adhesions as matrix-degrading structures in glioblastoma cells. Of the five human GBM cell lines screened (LN229, LN18, U87-MG, U251, and U343 cells), LN229 and LN18 cells were found to primarily use focal adhesions to degrade gelatin. These data support previous limited reports showing focal adhesion-mediated ECM degradation (Hsu et al., 2019; McNiven, 2013; Wang and McNiven, 2012). To date, matrix degrading focal adhesions have been identified in various human pancreatic adenocarcinoma cell lines (PANC-1, BxPC3, PANC-4.03), fibrosarcoma cells (HT1080), rat fibroblasts, and retinal pigment epithelial cells (APRE19) (Hsu et al., 2019; McNiven, 2013; Wang and McNiven, 2012). Given the limited publications reporting the invasive properties of focal adhesions, it would be important to determine why some cells use invadopodia while others use focal adhesions to degrade the

surrounding ECM. Interestingly, the majority of the cell lines listed above display an epithelial-like phenotype, particularly LN18, HT1080, PANC-1, and BxPC-3 cells. Due to the known role of epithelial-to-mesenchymal transition (EMT) in facilitating invadopodia formation and function (Eckert et al., 2011) and the previous reports suggesting focal adhesions are precursor structures to invadopodia (McNiven, 2013), perhaps epithelial-like cells preferentially use focal adhesions while mesenchymal-like cells use invadopodia structures to facilitate ECM degradation and invasion. Future experiments should involve inducing EMT in LN18 cells, as well as other cells with an epithelial phenotype, and performing a gelatin-degradation assay to analyze patterns of degradation. Perhaps inducing EMT results in a shift from focal adhesion to invadopodia-mediated matrix degradation. Critical future experiments should also involve determining how cells balance between the adhesive and invasive properties of focal adhesions, and identifying which factors are important for switching between functions.

Most of the studies presented in **Chapter 3** and **Chapter 4** involve irradiating the tumour spheroids alone and then either performing *in vitro* invasion experiments or implanting the spheroids onto brain tissue to monitor *ex vivo* invasion, respectively. However, when GBM patients receive radiation therapy it is unlikely that only the tumour cells will be exposed. Notably, little is known about how normal brain cells (*i.e.* astrocytes, neurons, microglia) are altered in response to radiation and how changes in the brain microenvironment might impact the invasiveness of GBM cells. Previous literature has shown that ionizing radiation increases the expression of glial fibrillary acidic protein (GFAP), suggesting increased astrocyte activation (Berg et al., 2021). Furthermore, the authors state that irradiating the surrounding brain tissue results in a tumour-supportive environment. Using our advanced *ex vivo* brain slice invasion assay, it would be interesting to irradiate the murine brain tissue prior to harvest and then implant

non-irradiated versus irradiated tumour spheroids onto the irradiated brain slices to determine how tumour cells interact with normal brain cells post-irradiation and how this impacts GBM invasion. Preliminary data from our lab has shown in some instances GFP-tagged GBM cells interact with α SMA-positive vasculature (Figure 5.2A) and GFAP-positive astrocytes (Figure 5.2B) within *ex vivo* murine brain tissue. Future *ex vivo* experiments investigating the interactions between non-irradiated versus irradiated GBM cells with nearby astrocytes and vasculature may help to further inform how the tumour microenvironment contributes to GBM invasiveness.

Despite GBM being a highly invasive tumour type, GBM cells rarely cross the blood-brain-barrier and metastasize to distant organs. More often, GBM cells locally invade within 1-2 cm of the primary tumour boarder typically by invading along pre-existing vasculature in the brain (Liu et al., 2019; Mair et al., 2018; Scherer, 1938; Turner et al., 2016). It is also well known that invadopodia are protrusive structures that secrete matrix metalloproteinases to help cancer cells invade through physical barriers (*i.e.* intravasation and extravasation) (Gligorijevic et al., 2012; Leong et al., 2014; Williams et al., 2019). Since GBM cells rarely intravasate into the vasculature, it seems unlikely that these cells require the use of invadopodia to invade. It seems more plausible that GBM cells primarily use focal adhesions to invade along pre-existing brain structures to invade further into brain tissue since focal adhesion structures typically facilitate motility across substrates (Burrige, 2017). To test this hypothesis, future experiments would involve implanting GBM spheroids fluorescently tagged for TKS5 (invadopodia) and vinculin (focal adhesions) onto brain slices to determine if either structure associates with blood vessels. Furthermore, it would be useful to inhibit either focal adhesion or invadopodia

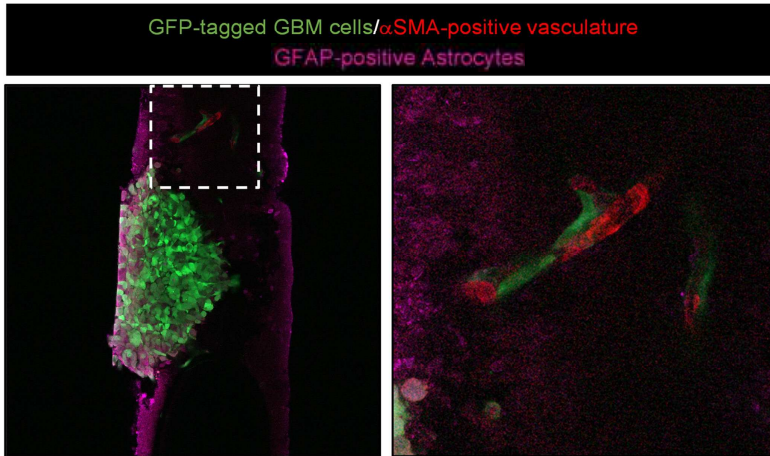
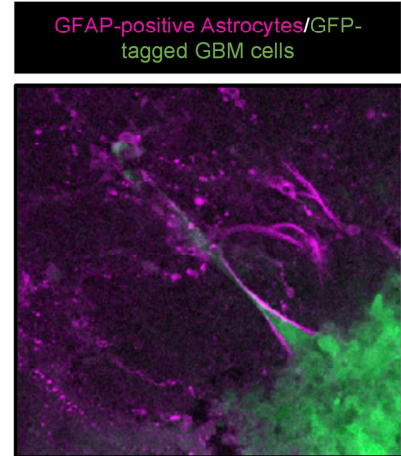
A**B**

Figure 5.2. Representative images displaying interactions between GFP-expressing GBM cells and alpha-smooth muscle actin (α SMA)-positive vasculature or glial fibrillary acidic protein (GFAP)-positive astrocytes within the surrounding brain environment.

(A) High resolution confocal images of GFP-expressing LN229 GBM spheroids invading into murine brain tissue sections stained for GFAP (astrocytes, pink) and α SMA (vasculature, red). The boxed region is enlarged to the right of the image. (B) High resolution confocal images of GFP-expressing LN229 GBM spheroids invading into murine brain tissue sections stained for GFAP (astrocytes, pink).

formation in GBM cells and implant these mutated cells as spheroids onto the *ex vivo* brain slices to determine which structure primarily regulates GBM cell invasion. Together, these important experiments will help to advance our current knowledge of the mechanisms that regulate glioblastoma invasion.

The most common treatment plan for patients diagnosed with GBM involves maximal surgical resection, radiation in combination with temozolomide (TMZ), and lastly adjuvant TMZ treatment (Mason et al., 2007; Stupp et al., 2005). Apart from TMZ, another commonly used therapeutic agent is Bevacizumab (Avastin), a vascular endothelial growth factor (VEGF) inhibitor, which has been used to prevent tumour angiogenesis and slow tumour growth (Fisher and Adamson, 2021). However, there have been several reports that show TMZ treatment (Mao et al., 2018) and anti-VEGF therapy (Falchetti et al., 2019; Otani et al., 2017; Thompson et al., 2011) may also induce the invasiveness of glioma cells. Therefore, it would be informative to investigate the role of radiation treatment in combination with TMZ/Avastin in facilitating GBM invasion as well as the interaction between GBM cells and the surrounding brain environment using our *ex vivo* brain slice invasion assay.

In summary, my work (i) reveals PTP α as a novel intrinsic regulator of TNBC cell invasion *in vitro* and *in vivo* (**Chapter 2**), (ii) identifies focal adhesion structures, rather than invadopodia, as important structures for facilitating GBM cell invasion *in vitro* (**Chapter 3**), (iii) describes a novel technique for studying GBM cell invasion *ex vivo* (**Chapter 4**), and (iv) utilizes our advanced *ex vivo* brain slice invasion assay to show ionizing radiation is a potential extrinsic regulator of GBM cell invasion when cells are in the presence of the brain microenvironment (**Chapter 4**). Advancing these findings by performing the experiments highlighted in **Chapter 5**

will undoubtedly increase our current knowledge of the complexities of cancer metastasis and may lead to increased patient outcomes.

References

- Abram, C.L., Seals, D.F., Pass, I., Salinsky, D., Maurer, L., Roth, T.M., Courtneidge, S.A., 2003. The adaptor protein Fish associates with members of the ADAMs family and localizes to podosomes of Src-transformed cells. *Journal of Biological Chemistry* 278, 16844–16851.
- Adachi, T., Zhao, W., Minami, K., Yokoyama, Y., Okuzaki, D., Kondo, R., Takahashi, Y., Tamari, K., Seo, Y., Isohashi, F., Yamamoto, H., Koizumi, M., Ogawa, K., 2021. Chk1 suppression leads to a reduction in the enhanced radiation-induced invasive capability on breast cancer cells. *Journal of Radiation Research* 62, 764–772.
- Al-Mahmood, S., Sapiezynski, J., Garbuzenko, O.B., Minko, T., 2018. Metastatic and triple-negative breast cancer: challenges and treatment options. *Drug Delivery and Translational Research* 8, 1483–1507.
- Alexander, N.R., Branch, K.M., Parekh, A., Clark, E.S., Iwueke, I.C., Guelcher, S.A., Weaver, A.M., 2008. Extracellular matrix rigidity promotes invadopodia activity. *Current Biology* 18, 1295–1299.
- Alieva, M., Leidgens, V., Riemenschneider, M.J., Klein, C.A., Hau, P., van Rheenen, J., 2019. Intravital imaging of glioma border morphology reveals distinctive cellular dynamics and contribution to tumor cell invasion. *Scientific Reports* 2019 9:1 9, 1–11.
- Allen Reference Atlas - Mouse Brain, n.d. . [brain atlas]. Available from atlas.brain-map.org.
- Alonso, A., Sasin, J., Bottini, N., Friedberg, Ilan, Friedberg, Iddo, Osterman, A., Godzik, A., Hunter, T., Dixon, J., Mustelin, T., 2004. Protein tyrosine phosphatases in the human genome. *Cell* 117, 699–711.
- Andersen, J.N., Jansen, P.G., Echwald, S.M., Mortensen, O.H., Fukada, T., Del Vecchio, R., Tonks, N.K., Møller, N.P.H., 2004. A genomic perspective on protein tyrosine phosphatases: gene structure, pseudogenes, and genetic disease linkage. *The FASEB Journal* 18, 8–30.
- Annabi, B., Lachambre, M.-P., Bousquet-Gagnon, N., Page, M., Gingras, D., Beliveau, R., 2001. Localization of membrane-type 1 matrix metalloproteinase in caveolae membrane domains. *Biochemical Journal* 353, 547–553.
- Ardini, E., Agresti, R., Tagliabue, E., Greco, M., Aiello, P., Yang, L.-T., Ménard, S., Sap, J., 2000. Expression of protein tyrosine phosphatase alpha (RPTP α) in human breast cancer correlates with low tumor grade and inhibits tumor cell growth in vitro and in vivo. *Oncogene* 19, 4979–4987.
- Ariel, P., 2017. A beginner's guide to tissue clearing. *The International Journal of Biochemistry & Cell Biology* 84, 35.
- Artym, V.V., Zhang, Y., Seillier-Moiseiwitsch, F., Yamada, K.M., Mueller, S.C., 2006. Dynamic interactions of cortactin and membrane type 1 matrix metalloproteinase at invadopodia: Defining the stages of invadopodia formation and function. *Cancer Research* 66, 3034–3043.
- Axpe, E., Orive, G., Franze, K., Appel, E.A., 2020. Towards brain-tissue-like biomaterials. *Nature Communications* 11, 1–4.
- Baik, M., French, B., Chen, Y.C., Byers, J.T., Chen, K.T., French, S.W., Díaz, B., 2019. Identification of invadopodia by TKS5 staining in human cancer lines and patient tumor samples. *MethodsX* 6, 718–726.
- Baskar, R., Lee, K.A., Yeo, R., Yeoh, K.W., 2012. Cancer and radiation therapy: Current

- advances and future directions. *International Journal of Medical Sciences* 9, 193–199.
- Beatty, B.T., Condeelis, J., 2014. Digging a little deeper: The stages of invadopodium formation and maturation. *European Journal of Cell Biology* 93, 438–444.
- Beatty, B.T., Sharma, V.P., Bravo-Cordero, J.J., Simpson, M.A., Eddy, R.J., Koleske, A.J., Condeelis, J., 2013. β 1 integrin regulates Arg to promote invadopodial maturation and matrix degradation. *Molecular Biology of the Cell* 24, 1661–1675.
- Benninger, R.K.P., Piston, D.W., 2013. Two-Photon Excitation Microscopy for the Study of Living Cells and Tissues. *Current Protocols in Cell Biology* 59, 4.11.1-4.11.24.
- Bentires-Alj, M., Neel, B.G., 2007. Protein-Tyrosine Phosphatase 1B Is Required for HER2/Neu-Induced Breast Cancer. *Cancer Research* 67, 2420–2424.
- Berg, T.J., Marques, C., Pantazopoulou, V., Johansson, E., von Stedingk, K., Lindgren, D., Pietras, E.J., Bergström, T., Swartling, F.J., Governa, V., Bengzon, J., Belting, M., Axelson, H., Squatrito, M., Pietras, A., 2021. The irradiated brain microenvironment supports glioma stemness and survival via astrocyte-derived Transglutaminase 2. *Cancer Research* 81, 2101–2115.
- Bhandari, V., Lim, K.L., Pallen, C.J., 1998. Physical and functional interactions between receptor-like protein-tyrosine phosphatase alpha and p59fyn. *The Journal of Biological Chemistry* 273, 8691–8.
- Biau, J., Chautard, E., Verrelle, P., Dutreix, M., 2019. Altering DNA Repair to Improve Radiation Therapy: Specific and Multiple Pathway Targeting. *Frontiers in Oncology* 9, 1009.
- Bjorge, J.D., Jakymiw, A., Fujita, D.J., 2000. Selected glimpses into the activation and function of Src kinase. *Oncogene* 19, 5620–5635.
- Blouw, B., Patel, M., Iizuka, S., Abdullah, C., You, W.K., Huang, X., Li, J.-L., Diaz, B., Stallcup, W.B., Courtneidge, S.A., 2015. The invadopodia scaffold protein Tks5 is required for the growth of human breast cancer cells in vitro and in vivo. *PLOS ONE* 10, e0121003.
- Blouw, B., Seals, D.F., Pass, I., Diaz, B., Courtneidge, S.A., 2008. A role for the podosome/invadopodia scaffold protein Tks5 in tumor growth in vivo. *European Journal of Cell Biology* 87, 555–67.
- Boivin, B., Chaudhary, F., Dickinson, B.C., Haque, A., Pero, S.C., Chang, C.J., Tonks, N.K., 2013. Receptor protein-tyrosine phosphatase α regulates focal adhesion kinase phosphorylation and ErbB2 oncoprotein-mediated mammary epithelial cell motility. *The Journal of Biological Chemistry* 288, 36926–35.
- Bollu, L.R., Mazumdar, A., Savage, M.I., Brown, P.H., 2017. Molecular pathways: Targeting protein tyrosine phosphatases in cancer. *Clinical Cancer Research* 23, 2136–2142.
- Borrego-Soto, G., Ortiz-López, R., Rojas-Martínez, A., 2015. Ionizing radiation-induced DNA injury and damage detection in patients with breast cancer. *Genetics and Molecular Biology* 38, 420–432.
- Bouchard, G., Therriault, H., Geha, S., Bujold, R., Saucier, C., Paquette, B., 2017. Radiation-induced lung metastasis development is MT1-MMP-dependent in a triple-negative breast cancer mouse model. *British Journal of Cancer* 116, 479–488.
- Branch, K.M., Hoshino, D., Weaver, A.M., 2012. Adhesion rings surround invadopodia and promote maturation. *Biology Open* 1, 711–722.
- Braunstein, S., Badura, M.L., Xi, Q., Formenti, S.C., Schneider, R.J., 2009. Regulation of Protein Synthesis by Ionizing Radiation. *Molecular and Cellular Biology* 29, 5645–5656.

- Brown, J.M., 1999. Special Lecture The Hypoxic Cell: A Target for Selective Cancer Therapy- Eighteenth Bruce F. Cain Memorial Award Lecture 1. *Cancer Research* 59, 5863–5870.
- Buccione, R., Caldieri, G., Ayala, I., 2009. Invadopodia: specialized tumor cell structures for the focal degradation of the extracellular matrix. *Cancer and Metastasis Reviews* 28, 137–149.
- Burridge, K., 2017. Focal adhesions: a personal perspective on a half century of progress. *FEBS Journal* 284, 3355–3361.
- Caires-dos-Santos, L., Silva, S.V. da, Smuczek, B., Siqueira, A.S. de, Cruz, K.S.P., Barbuto, J.A.M., Augusto, T.M., Freitas, V.M., Carvalho, H.F., Jaeger, R.G., 2020. Laminin-derived peptide C16 regulates Tks expression and reactive oxygen species generation in human prostate cancer cells. *Journal of Cellular Physiology* 235, 587–598.
- Camphausen, K., Moses, M.A., Ménard, C., Sproull, M., Beecken, W.-D., Folkman, J., O'reilly, M.S., 2003. Radiation abscopal antitumor effect is mediated through p53. *Cancer Research* 63, 1990–1993.
- Cao, H., Eppinga, R.D., Razidlo, G.L., Krueger, E.W., Chen, J., Qiang, L., McNiven, M.A., 2016. Stromal fibroblasts facilitate cancer cell invasion by a novel invadopodia-independent matrix degradation process. *Oncogene* 35, 1099–1110.
- Castro-Castro, A., Marchesin, V., Monteiro, P., Lodillinsky, C., Rossé, C., Chavrier, P., 2016. Cellular and molecular mechanisms of MT1-MMP-dependent cancer cell invasion. *Annual Review of Cell and Developmental Biology* 32, 555–576.
- Cathcart, J., Pulkoski-Gross, A., Cao, J., 2015. Targeting matrix metalloproteinases in cancer: Bringing new life to old ideas. *Genes and Diseases* 2, 26–34.
- Cha, J., Kim, P., 2017. Biomimetic strategies for the glioblastoma microenvironment. *Frontiers in Materials* 4, 45.
- Chan, K.T., Cortesio, C.L., Huttenlocher, A., 2009. FAK alters invadopodia and focal adhesion composition and dynamics to regulate breast cancer invasion. *The Journal of Cell Biology* 185, 357–70.
- Chan, R.J., Feng, G.-S., 2007. PTPN11 is the first identified proto-oncogene that encodes a tyrosine phosphatase. *Blood* 109, 862–867.
- Chen, B., Chen, C., Zhang, Y., Xu, J., 2021. Recent incidence trend of elderly patients with glioblastoma in the United States, 2000–2017. *BMC Cancer* 21, 1–10.
- Chen, M., Chen, S.C., Pallen, C.J., 2006. Integrin-induced tyrosine phosphorylation of protein-tyrosine phosphatase-alpha is required for cytoskeletal reorganization and cell migration. *The Journal of Biological Chemistry* 281, 11972–80.
- Chen, Q.K., Lee, K.A., Radisky, D.C., Nelson, C.M., 2013. Extracellular matrix proteins regulate epithelial-mesenchymal transition in mammary epithelial cells. *Differentiation* 86, 126–132.
- Chen, W. -T, 1989. Proteolytic activity of specialized surface protrusions formed at rosette contact sites of transformed cells. *Journal of Experimental Zoology* 251, 167–185.
- Chen, W., Wang, J., 1999. Specialized surface protrusions of invasive cells, invadopodia and lamellipodia, have differential MT1-MMP, MMP-2, and TIMP-2 localization. *Annals New York Academy of Sciences* 878, 361–371.
- Chen, Y.C., Baik, M., Byers, J.T., Chen, K.T., French, S.W., Díaz, B., 2019a. TKS5-positive invadopodia-like structures in human tumor surgical specimens. *Experimental and Molecular Pathology* 106, 17–26.
- Chen, Y.C., Baik, M., Byers, J.T., Chen, K.T., French, S.W., Díaz, B., 2019b. Experimental

- supporting data on TKS5 and Cortactin expression and localization in human pancreatic cancer cells and tumors. *Data in Brief* 22, 132–136.
- Choucair, A.K., Levin, V.A., Gutin, P.H., Davis, R.L., Silver, P., Edwards, M.S., Wilson, C.B., 1986. Development of multiple lesions during radiation therapy and chemotherapy in patients with gliomas. *Journal of Neurosurgery* 65, 654–658.
- Chuang, H.N., Lohaus, R., Hanisch, U.K., Binder, C., Dehghani, F., Pukrop, T., 2013. Coculture system with an organotypic brain slice and 3D spheroid of carcinoma cells. *J. Vis. Exp* 50881.
- Claes, A., Idema, A.J., Wesseling, P., 2007. Diffuse glioma growth: A guerilla war. *Acta Neuropathologica* 114, 443–458.
- Clark, E.S., Brown, B., Whigham, A.S., Kochaishvili, A., Yarbrough, W.G., Weaver, A.M., 2009. Aggressiveness of HNSCC tumors depends on expression levels of cortactin, a gene in the 11q13 amplicon. *Oncogene* 28, 431–444.
- Clark, E.S., Whigham, A.S., Yarbrough, W.G., Weaver, A.M., 2007. Cortactin is an essential regulator of matrix metalloproteinase secretion and extracellular matrix degradation in invadopodia. *Cancer Research* 67, 4227–35.
- Cohen-Sharir, Y., Kuperman, Y., Apelblat, D., den Hertog, J., Spiegel, I., Knobler, H., Elson, A., 2019. Protein tyrosine phosphatase alpha inhibits hypothalamic leptin receptor signaling and regulates body weight in vivo. *FASEB Journal* 33, 5101–5111.
- Committee, C.C.S.A., 2019. Canadian Cancer Statistics 2019.
- Cordes, N., Hansmeier, B., Beinke, C., Meineke, V., Van Beuningen, D., 2003. Irradiation differentially affects substratum-dependent survival, adhesion, and invasion of glioblastoma cell lines. *British Journal of Cancer* 89, 2122–2132.
- Cramer, J.M., Zimmerman, M.W., Thompson, T., Homanics, G.E., Lazo, J.S., Lagasse, E., 2014. Deletion of Ptp4a3 reduces clonogenicity and tumor-initiation ability of colitis-associated cancer cells in mice. *Stem Cell Research* 13, 164–171.
- Croft, C.L., Futch, H.S., Moore, B.D., Golde, T.E., 2019. Organotypic brain slice cultures to model neurodegenerative proteinopathies. *Molecular Neurodegeneration* 14.
- Cuddapah, V.A., Robel, S., Watkins, S., Sontheimer, H., 2014. A neurocentric perspective on glioma invasion. *Nature reviews. Neuroscience* 15, 455–465.
- Cui, N., Hu, M., Khalil, R.A., 2017. Biochemical and biological attributes of matrix metalloproteinases. *Progress in Molecular Biology and Translational Science* 147, 1–73.
- Daum, G., Regenass, S., Sap, J., Schlessinger, J., Fischer, E.H., 1994. Multiple forms of the human tyrosine phosphatase RPTP α . Isozymes and differences in glycosylation. *Journal of Biological Chemistry* 269, 10524–10528.
- David-Pfeuty, T., Singer, S.J., 1980. Altered distributions of the cytoskeletal proteins vinculin and α -actinin in cultured fibroblasts transformed by Rous sarcoma virus. *Proceedings of the National Academy of Sciences of the United States of America* 77, 6687–6691.
- Davies, W.A., Stossel, T.P., 1977. Peripheral hyaline blebs (podosomes) of macrophages. *Journal of Cell Biology* 75, 941–955.
- Dawson, S.J., Provenzano, E., Caldas, C., 2009. Triple negative breast cancers: Clinical and prognostic implications. *European Journal of Cancer* 45, 27–40.
- Delaney, G., Jacob, S., Featherstone, C., Barton, M., 2005. The role of radiotherapy in cancer treatment. *Cancer* 104, 1129–1137.
- den Hertog, J., Pals, C.E., Peppelenbosch, M.P., Tertoolen, L.G., Laat, S.W. de, Kruijer, W.,

1993. Receptor protein tyrosine phosphatase alpha activates pp60c-src and is involved in neuronal differentiation. *The EMBO Journal* 12, 3789–3798.
- Desouky, O., Ding, N., Zhou, G., 2015. Targeted and non-targeted effects of ionizing radiation. *Journal of Radiation Research and Applied Sciences* 8, 247–254.
- Diaz, B., Shani, G., Pass, I., Anderson, D., Quintavalle, M., Courtneidge, S.A., 2009. Tks5-dependent, Nox-mediated generation of reactive oxygen species is necessary for invadopodia formation. *Science Signaling* 2, ra53.
- Díaz, B., Yuen, A., Iizuka, S., Higashiyama, S., Courtneidge, S.A., 2013. Notch increases the shedding of HB-EGF by ADAM12 to potentiate invadopodia formation in hypoxia. *The Journal of Cell Biology* 201, 279–92.
- Dillekås, H., Rogers, M.S., Straume, O., 2019. Are 90% of deaths from cancer caused by metastases? *Cancer Medicine* 8, 5574–5576.
- Dongre, A., Weinberg, R.A., 2019. New insights into the mechanisms of epithelial–mesenchymal transition and implications for cancer. *Nature Reviews Molecular Cell Biology* 20, 69–84.
- Donya, M., Radford, M., Elguindy, A., Firmin, D., Yacoub, M.H., 2014. Radiation in medicine: Origins, risks and aspirations. *Global Cardiology Science and Practice* 57.
- Du, Y., Grandis, J.R., 2015. Receptor-type protein tyrosine phosphatases in cancer. *Chinese Journal of Cancer* 34, 61–9.
- Eckert, M.A., Lwin, T.M., Chang, A.T., Kim, J., Danis, E., Ohno-Machado, L., Yang, J., 2011. Twist1-induced invadopodia formation promotes tumor metastasis. *Cancer Cell* 19, 372–386.
- Eckert, M.A., Yang, J., 2011. Targeting invadopodia to block breast cancer metastasis. *Oncotarget* 2, 562–8.
- Eddy, R.J., Weidmann, M.D., Sharma, V.P., Condeelis, J.S., 2017. Tumor cell invadopodia: Invasive protrusions that orchestrate metastasis. *Trends in Cell Biology* 27, 595–607.
- Egeblad, M., Werb, Z., 2002. New functions for the matrix metalloproteinases in cancer progression. *Nature Reviews Cancer* 2, 161–174.
- Eisemann, T., Costa, B., Strelau, J., Mittelbronn, M., Angel, P., Peterziel, H., 2018. An advanced glioma cell invasion assay based on organotypic brain slice cultures. *BMC Cancer* 18, 103.
- Elson, A., 1999. Protein tyrosine phosphatase ϵ increases the risk of mammary hyperplasia and mammary tumors in transgenic mice. *Oncogene* 18, 7535–7542.
- Elson, A., Leder, P., 1995. Protein-tyrosine phosphatase ϵ . An isoform specifically expressed in mouse mammary tumors initiated by v-Ha-ras OR neu. *Journal of Biological Chemistry* 270, 26116–26122.
- Esmaili, M., Stensjøen, A.L., Berntsen, E.M., Solheim, O., Reinertsen, I., 2018. The direction of tumour growth in glioblastoma patients. *Scientific Reports* 8, 1199.
- Falchetti, M.L., D'Alessandris, Q.G., Pacioni, S., Buccarelli, M., Morgante, L., Giannetti, S., Lulli, V., Martini, M., Larocca, L.M., Vakana, E., Stancato, L., Ricci-Vitiani, L., Pallini, R., 2019. Glioblastoma endothelium drives bevacizumab-induced infiltrative growth via modulation of PLXDC1. *International Journal of Cancer* 144, 1331.
- Fares, J., Fares, M.Y., Khachfe, H.H., Salhab, H.A., Fares, Y., 2020. Molecular principles of metastasis: a hallmark of cancer revisited. *Signal Transduction and Targeted Therapy* 5, 28.
- Fisher, D.R., Fahey, F.H., 2017. Appropriate use of effective dose in radiation protection and risk assessment. *Health Phys* 113, 102–109.

- Fisher, J.P., Adamson, D.C., 2021. Current FDA-approved therapies for high-grade malignant gliomas. *Biomedicines* 9, 324.
- Fisher, K.E., Pop, A., Koh, W., Anthis, N.J., Saunders, W.B., Davis, G.E., 2006. Tumor cell invasion of collagen matrices requires coordinate lipid agonist-induced G-protein and membrane-type matrix metalloproteinase-1-dependent signaling. *Molecular Cancer* 5, 69.
- Fridolfsson, H.N., Roth, D.M., Insel, P.A., Patel, H.H., 2014. Regulation of intracellular signaling and function by caveolin. *FASEB Journal* 28, 3823–3831.
- Frittoli, E., Palamidessi, A., Disanza, A., Scita, G., 2011. Secretory and endo/exocytic trafficking in invadopodia formation: The MT1-MMP paradigm. *European Journal of Cell Biology* 90, 108–114.
- Gálvez, B.G., Matías-Román, S., Yáñez-Mó, M., Vicente-Manzanares, M., Sánchez-Madrid, F., Arroyo, A.G., 2004. Caveolae are a novel pathway for membrane-type 1 matrix metalloproteinase traffic in human endothelial cells. *Molecular Biology of the Cell* 15, 678–87.
- Geng, J.G., 2001. Directional migration of leukocytes: Their pathological roles in inflammation and strategies for development of anti-inflammatory therapies. *Cell Research* 11, 85–88.
- Gialeli, C., Theocharis, A.D., Karamanos, N.K., 2011. Roles of matrix metalloproteinases in cancer progression and their pharmacological targeting. *FEBS Journal* 278, 16–27.
- Gianni, D., Diaz, B., Taullet, N., Fowler, B., Courtneidge, S.A., Bokoch, G.M., 2009. Novel p47phox-related organizers regulate NADPH oxidase 1 (Nox1) activity and localization. *Science Signaling* 2, ra54.
- Gianni, D., Taullet, N., DerMardirossian, C., Bokoch, G.M., 2010. c-Src-mediated phosphorylation of NoxA1 and Tks4 induces the reactive oxygen species (ROS)-dependent formation of functional invadopodia in human colon cancer cells. *Molecular Biology of the Cell* 21, 4287–4298.
- Gil-Henn, H., Elson, A., 2003. Tyrosine Phosphatase-ε Activates Src and Supports the Transformed Phenotype of Neu-induced Mammary Tumor Cells. *Journal of Biological Chemistry* 278, 15579–15586.
- Gkretsi, V., Stylianopoulos, T., 2018. Cell adhesion and matrix stiffness: Coordinating cancer cell invasion and metastasis. *Frontiers in Oncology* 8, 145.
- Gligorijevic, B., Wyckoff, J., Yamaguchi, H., Wang, Y., Roussos, E.T., Condeelis, J., 2012. N-WASP-mediated invadopodium formation is involved in intravasation and lung metastasis of mammary tumors. *Journal of Cell Science* 125, 724–34.
- Gobin, E., Bagwell, K., Wagner, J., Mysona, D., Sandirasegarane, S., Smith, N., Bai, S., Sharma, A., Schleifer, R., She, J.X., 2019. A pan-cancer perspective of matrix metalloproteases (MMP) gene expression profile and their diagnostic/prognostic potential. *BMC Cancer* 19, 581.
- Goetze, K., Scholz, M., Taucher-Scholz, G., Mueller-Klieser, W., 2007. The impact of conventional and heavy ion irradiation on tumor cell migration in vitro. *International Journal of Radiation Biology* 83, 889–896.
- Gómez-Gaviro, M.V., Sanderson, D., Ripoll, J., Desco, M., 2020. Biomedical applications of tissue clearing and three-dimensional imaging in health and disease. *iScience* 23, 101432.
- Grabiec, U., Hohmann, T., Hammer, N., Dehghani, F., 2017. Organotypic hippocampal slice cultures as a model to study neuroprotection and invasiveness of tumor cells. *Journal of Visualized Experiments* 2017, e55359.

- Gray, L.H., Conger, A.D., Ebert, M., Hornsey, S., Scott, O.C., 1953. The concentration of oxygen dissolved in tissues at the time of irradiation as a factor in radiotherapy. *The British Journal of Radiology* 26, 638–648.
- Gritsenko, P., Leenders, W., Friedl, P., 2017. Recapitulating in vivo-like plasticity of glioma cell invasion along blood vessels and in astrocyte-rich stroma. *Histochemistry and Cell Biology* 148, 395–406.
- Gritsenko, P.G., Friedl, P., 2018. Adaptive adhesion systems mediate glioma cell invasion in complex environments. *Journal of Cell Science* 131.
- Gu, Z., Fang, X., Li, C., Chen, C., Liang, G., Zheng, X., Fan, Q., 2017. Increased PTPRA expression leads to poor prognosis through c-Src activation and G1 phase progression in squamous cell lung cancer. *International Journal of Oncology* 51, 489–497.
- Haeger, A., Krause, M., Wolf, K., Friedl, P., 2014. Cell jamming: Collective invasion of mesenchymal tumor cells imposed by tissue confinement. *Biochimica et Biophysica Acta (BBA) - General Subjects* 1840, 2386–2395.
- Hagedorn, E.J., Ziel, J.W., Morrissey, M.A., Linden, L.M., Wang, Z., Chi, Q., Johnson, S.A., Sherwood, D.R., 2013. The netrin receptor DCC focuses invadopodia-driven basement membrane transmigration in vivo. *Journal of Cell Biology* 201, 903–913.
- Hale, A.J., ter Steege, E., den Hertog, J., 2017. Recent advances in understanding the role of protein-tyrosine phosphatases in development and disease. *Developmental Biology* 428, 283–292.
- Hama, H., Hioki, H., Namiki, K., Hoshida, T., Kurokawa, H., Ishidate, F., Kaneko, T., Akagi, T., Saito, T., Saido, T., Miyawaki, A., 2015. ScaleS: an optical clearing palette for biological imaging. *Nature Neuroscience* 18, 1518–1529.
- Hama, H., Kurokawa, H., Kawano, H., Ando, R., Shimogori, T., Noda, H., Fukami, K., Sakaue-Sawano, A., Miyawaki, A., 2011. Scale: a chemical approach for fluorescence imaging and reconstruction of transparent mouse brain. *Nature Neuroscience* 14, 1481–1488.
- Han, W., Ngok Yu, K., 2009. Response of cells to ionizing radiation. In: *Advances in Biomedical Sciences and Engineering*. pp. 204–262.
- Hardy, S., Kostantin, E., Hatzihristidis, T., Zolotarov, Y., Uetani, N., Tremblay, M.L., 2018. Physiological and oncogenic roles of the PRL phosphatases. *The FEBS Journal* 285, 3886–3908.
- Hotary, K., Li, X.Y., Allen, E., Stevens, S.L., Weiss, S.J., 2006. A cancer cell metalloprotease triad regulates the basement membrane transmigration program. *Genes & Development* 20, 2686–2686.
- Hotary, K.B., Allen, E.D., Brooks, P.C., Datta, N.S., Long, M.W., Weiss, S.J., 2003. Membrane type I matrix metalloproteinase usurps tumor growth control imposed by the three-dimensional extracellular matrix. *Cell* 114, 33–45.
- Hsu, K.S., Otsu, W., Li, Y., Wang, H.C., Chen, S., Tsang, S.H., Chuang, J.Z., Sung, C.H., 2019. CLIC4 regulates late endosomal trafficking and matrix degradation activity of MMP14 at focal adhesions in RPE cells. *Scientific Reports* 9, 1–17.
- Humpel, C., 2015. Organotypic brain slice cultures: A review. *Neuroscience* 305, 86–98.
- Iizuka, S., Abdullah, C., Buschman, M.D., Diaz, B., Courtneidge, S.A., 2016. The role of Tks adaptor proteins in invadopodia formation, growth and metastasis of melanoma. *Oncotarget* 7, 78473.
- Inda, M. del M., Bonavia, R., Seoane, J., 2014. Glioblastoma multiforme: A look inside its

- heterogeneous nature. *Cancers* 6, 226–239.
- Iyer, R.P., Patterson, N.L., Fields, G.B., Lindsey, M.L., 2012. The history of matrix metalloproteinases: Milestones, myths, and misperceptions. *American Journal of Physiology - Heart and Circulatory Physiology* 303, H919–H930.
- Jackson, S.P., 2002. Sensing and repairing DNA double-strand breaks. *Carcinogenesis* 23, 687–696.
- Jacob, A., Jing, J., Lee, J., Schedin, P., Gilbert, S.M., Peden, A.A., Junutula, J.R., Prekeris, R., 2013. Rab40b regulates trafficking of MMP2 and MMP9 during invadopodia formation and invasion of breast cancer cells. *Journal of Cell Science* 126, 4647–4658.
- Jacob, A., Prekeris, R., 2015. The regulation of MMP targeting to invadopodia during cancer metastasis. *Frontiers in Cell and Developmental Biology* 3, 1–4.
- Jiang, X., Seo, Y.D., Sullivan, K.M., Pillarisetty, V.G., 2019. Establishment of slice cultures as a tool to study the cancer immune microenvironment. *Methods in Molecular Biology* 1884, 283–295.
- Jiang, Y., Liu, X.-Q., Rajput, A., Geng, L., Ongchin, M., Zeng, Q., Taylor, G.S., Wang, J., 2011. Phosphatase PRL-3 is a direct regulatory target of TGF β in colon cancer metastasis. *Cancer Research* 71, 234–244.
- Julien, S., Dubé, N., Read, M., Penney, J., Paquet, M., Han, Y., Kennedy, B., Muller, W., Tremblay, M., 2007. Protein tyrosine phosphatase 1B deficiency or inhibition delays ErbB2-induced mammary tumorigenesis and protects from lung metastasis. *Nature Genetics* 39, 338–346.
- Jung, S., Kim, H.W., Lee, J.H., Kang, S.S., Rhu, H.H., Jeong, Y. Il, Yang, S.Y., Chung, H.Y., Bae, C.S., Choi, C., Shin, B.A., Kim, K.K., Ahn, K.Y., 2002. Brain tumor invasion model system using organotypic brain-slice culture as an alternative to in vivo model. *Journal of Cancer Research and Clinical Oncology* 2002 128:9 128, 469–476.
- Kabilan, U., Graber, T.E., Alain, T., Klokov, D., 2020. Ionizing radiation and translation control: A link to radiation hormesis? *International Journal of Molecular Sciences* 21, 6650.
- Kaksonen, M., Peng, H.B., Rauvala, K., 2000. Association of cortactin with dynamic actin in lamellipodia and on endosomal vesicles. *Journal of Cell Science* 113, 4421–4426.
- Kalluri, R., Weinberg, R.A., 2009. The basics of epithelial-mesenchymal transition. *Journal of Clinical Investigation* 119, 1420–1428.
- Kaplan, H.S., Murphy, E.D., 1949. The effect of local roentgen irradiation on the biological behavior of a transplantable mouse carcinoma; increased frequency of pulmonary metastasis. *Journal of the National Cancer Institute* 9, 407–13.
- Karaman, S., Detmar, M., 2014. Mechanisms of lymphatic metastasis. *The Journal of Clinical Investigation* 124, 922–928.
- Ke, M.T., Fujimoto, S., Imai, T., 2013. SeeDB: a simple and morphology-preserving optical clearing agent for neuronal circuit reconstruction. *Nature Neuroscience* 2013 16:8 16, 1154–1161.
- Kegelman, T.P., Wu, B., Das, S.K., Talukdar, S., Beckta, J.M., Hu, B., Emdad, L., Valerie, K., Sarkar, D., Furnari, F.B., Cavenee, W.K., Wei, J., Purves, A., De, S.K., Pellicchia, M., Fisher, P.B., 2017. Inhibition of radiation-induced glioblastoma invasion by genetic and pharmacological targeting of MDA-9/Syntenin. *Proceedings of the National Academy of Sciences of the United States of America* 114, 370–375.
- Keller, R., 2005. Cell migration during gastrulation. *Current Opinion in Cell Biology* 17, 533–

- Kelley, L.C., Ammer, A.G., Hayes, K.E., Martin, K.H., Machida, K., Jia, L., Mayer, B.J., Weed, S.A., 2010. Oncogenic Src requires a wild-type counterpart to regulate invadopodia maturation. *Journal of Cell Science* 123, 3923–3932.
- Khanna, K.K., Jackson, S.P., 2001. DNA double-strand breaks: signaling, repair and the cancer connection. *Nature Genetics* 27, 247–254.
- Kim, R.K., Cui, Y.H., Yoo, K.C., Kim, I.G., Lee, M., Choi, Y.H., Suh, Y., Lee, S.J., 2015. Radiation promotes malignant phenotypes through SRC in breast cancer cells. *Cancer Science* 106, 78–85.
- Kim, W., Lee, S., Seo, D., Kim, D., Kim, K., Kim, E., Kang, J., Seong, K.M., Youn, H., Youn, B., 2019. Cellular stress responses in radiotherapy. *Cells* 8, 1105.
- Kolli-Bouhafs, K., Sick, E., Noulet, F., Gies, J.P., De Mey, J., Rondé, P., 2014. FAK competes for Src to promote migration against invasion in melanoma cells. *Cell Death and Disease* 5, e1379–e1379.
- Kousidou, O.C., Roussidis, A.E., Theocharis, A.D., Karamanos, N.K., 2004. Expression of MMPs and TIMPs in human breast cancer epithelial cells depends on cell culture conditions and is associated with their invasive potential. *Anticancer Research* 24, 4025–4030.
- Krdijja, D., Schmid, H., Eismann, J.-L., Lothar, U., Adler, G., Oswald, F., Seufferlein, T., von Wichert, G., 2010. Substrate stiffness and the receptor-type tyrosine-protein phosphatase alpha regulate spreading of colon cancer cells through cytoskeletal contractility. *Oncogene* 29, 2724–2738.
- Krueger, N.X., Streuli, M., Saito, H., 1990. Structural diversity and evolution of human receptor-like protein tyrosine phosphatases. *The EMBO Journal* 9, 3241–52.
- Kudlik, G., Takács, T., Radnai, L., Kurilla, A., Szeder, B., Koprivanacz, K., Merő, B.L., Buday, L., Vas, V., 2020. Advances in understanding TKS4 and TKS5: Molecular scaffolds regulating cellular processes from podosome and invadopodium formation to differentiation and tissue homeostasis. *International Journal of Molecular Sciences* 21, 8117.
- Laronha, H., Caldeira, J., 2020. Structure and Function of Human Matrix Metalloproteinases. *Cells* 9, 8117.
- Lau, L.W., Cua, R., Keough, M.B., Haylock-Jacobs, S., Yong, V.W., 2013. Pathophysiology of the brain extracellular matrix: a new target for remyelination. *Nature Reviews Neuroscience* 14, 722–729.
- Lauffenburger, D.A., Horwitz, A.F., 1996. Cell migration: A physically integrated molecular process. *Cell* 84, 359–369.
- Leong, H.S., Robertson, A.E., Stoletov, K., Leith, S.J., Chin, C.A., Chien, A.E., Hague, M.N., Ablack, A., Carmine-Simmen, K., McPherson, V.A., Postenka, C.O., Turley, E.A., Courtneidge, S.A., Chambers, A.F., Lewis, J.D., 2014. Invadopodia are required for cancer cell extravasation and are a therapeutic target for metastasis. *Cell Reports* 8, 1558–1570.
- Li, S., Seitz, R., Lisanti, M.P., 1996. Phosphorylation of Caveolin by Src Tyrosine Kinases: The α -isoform of caveolin is selectively phosphorylated by v-Src in vivo. *Journal of Biological Chemistry* 271, 3863–3868.
- Lim, K.L., Kolatkar, P.R., Peng Ng, K., Hoe Ng, C., Pallen, C.J., 1998. Interconversion of the kinetic identities of the tandem catalytic domains of receptor-like protein-tyrosine phosphatase PTP alpha by two point mutations is synergistic and substrate-dependent. *The*

- Journal of Biological Chemistry 273, 28986–28993.
- Lin, C., Xin, S., Huang, X., Zhang, F., 2020. PTPRA facilitates cancer growth and migration via the TNF- α -mediated PTPRA-NF- κ B pathway in MCF-7 breast cancer cells. *Oncology Letters* 20, 1–1.
- Linder, S., 2009. Invadosomes at a glance. *Journal of Cell Science* 122, 3009–3013.
- Linder, S., Scita, G., 2015. RABGTPases in MT1-MMP trafficking and cell invasion: Physiology versus pathology. *Small GTPases* 6, 145–152.
- Liu, C.J., Shamsan, G.A., Akkin, T., Odde, D.J., 2019. Glioma cell migration dynamics in brain tissue assessed by multimodal optical imaging. *Biophysical Journal* 117, 1179–1188.
- Liu, P., Rudick, M., Anderson, R.G.W., 2002. Multiple functions of caveolin-1. *The Journal of Biological Chemistry* 277, 41295–8.
- Lock, P., Abram, C., Gibson, T., Courtneidge, S., 1998. A new method for isolating tyrosine kinase substrates used to identify fish, an SH3 and PX domain-containing protein, and Src substrate. *EMBO J* 17, 4346–4357.
- Lohmer, L.L., Kelley, L.C., Hagedorn, E.J., Sherwood, D.R., 2014. Invadopodia and basement membrane invasion in vivo. *Cell Adhesion & Migration* 8, 246–55.
- Lü, X., De La Peña, L., Barker, C., Camphausen, K., Tofilon, P.J., 2006. Radiation-induced changes in gene expression involve recruitment of existing messenger RNAs to and away from polysomes. *Cancer Research* 66, 1052–1061.
- Mader, C.C., Oser, M., Magalhaes, M.A.O., Bravo-Cordero, J.J., Condeelis, J., Koleske, A.J., Gil-Henn, H., 2011. An EGFR-Src-Arg-cortactin pathway mediates functional maturation of invadopodia and breast cancer cell invasion. *Cancer Research* 71, 1730–41.
- Mair, D.B., Ames, H.M., Li, R., 2018. Mechanisms of invasion and motility of high-grade gliomas in the brain. *Molecular Biology of the Cell* 29, 2509–2515.
- Maksumova, L., Le, H.T., Muratkhodjaev, F., Davidson, D., André Veillette, A., Pallen, C.J., 2005. Protein Tyrosine Phosphatase α regulates Fyn activity and Cbp/PAG phosphorylation in thymocyte lipid rafts. *Journal of Immunology* 175, 7947–7956.
- Mao, L., Whitehead, C.A., Paradiso, L., Kaye, A.H., Morokoff, A.P., Luwor, R.B., Stylli, S.S., 2018. Enhancement of invadopodia activity in glioma cells by sublethal doses of irradiation and temozolomide. *J Neurosurg* 129, 598–610.
- Martin, K.H., Hayes, K.E., Walk, E.L., Ammer, A.G., Markwell, S.M., Weed, S.A., 2012. Quantitative measurement of invadopodia-mediated extracellular matrix proteolysis in single and multicellular contexts. *Journal of Visualized Experiments: JoVE* e4119.
- Martin, O.A., Anderson, R.L., Narayan, K., MacManus, M.P., 2017. Does the mobilization of circulating tumour cells during cancer therapy cause metastasis? *Nature Reviews Clinical Oncology* 14, 32–44.
- Martin, O.A., Anderson, R.L., Russell, P.A., Ashley Cox, R., Ivashkevich, A., Swierczak, A., Doherty, J.P., Jacobs, D.H.M., Smith, J., Siva, S., Daly, P.E., Ball, D.L., Martin, R.F., MacManus, M.P., 2014. Mobilization of viable tumor cells into the circulation during radiation therapy. *International Journal of Radiation Oncology Biology Physics* 88, 395–403.
- Martínez-Meza, S., Díaz, J., Sandoval-Bórquez, A., Valenzuela-Valderrama, M., Díaz-Valdivia, N., Rojas-Celis, V., Contreras, P., Huilcaman, R., Ocaranza, M.P., Chiong, M., Leyton, L., Lavandero, S., Quest, A.F.G., 2019. AT2 receptor mediated activation of the tyrosine phosphatase PTP1B blocks caveolin-1 enhanced migration, invasion and metastasis of

- cancer cells. *Cancers* 11, 1299.
- Martinou, M., Giannopoulou, E., Malatara, G., Argyriou, A.A., Kalofonos, H.P., Kardamakis, D., 2011. Ionizing radiation affects epidermal growth factor receptor signalling and metalloproteinase secretion in glioma cells. *Cancer Genomics & Proteomics* 8, 33–8.
- Mason, W.P., Maestro, R. Del, Eisenstat, D., Forsyth, P., Fulton, D., Laperrière, N., Macdonald, D., Perry, J., Thiessen, B., Canadian GBM Recommendations Committee, 2007. Canadian recommendations for the treatment of glioblastoma multiforme. *Current Oncology* 14, 110–7.
- McNiven, M.A., 2013. Breaking away: matrix remodeling from the leading edge. *Trends in Cell Biology* 23, 16–21.
- Md Hashim, N.F., Nicholas, N.S., Dart, A.E., Kiriakidis, S., Paleolog, E., Wells, C.M., 2013. Hypoxia-induced invadopodia formation: a role for β -PIX. *Open Biology* 3, 120159.
- Menassa, D.A., Gomez-Nicola, D., 2018. Microglial dynamics during human brain development. *Frontiers in Immunology* 9, 1014.
- Meyer, D.S., Aceto, N., Sausgruber, N., Brinkhaus, H., Müller, U., Pallen, C.J., Bentires-Alj, M., 2014. Tyrosine phosphatase PTP α contributes to HER2-evoked breast tumor initiation and maintenance. *Oncogene* 33, 398–402.
- Moncharmont, C., Levy, A., Guy, J.-B., Falk, A.T., Guilbert, M., Trone, J.-C., Alphonse, G., Gilormini, M., Ardail, D., Toillon, R.-A., Rodriguez-Lafrasse, C., Magné, N., 2014. Radiation-enhanced cell migration/invasion process: A review. *Critical Reviews in Oncology/Hematology* 92, 133–142.
- Monsky, W.L., Kelly, T., Lin, C.-Y., Yeh, Y., Stetler-Stevenson, W.G., Mueller, S.C., Chen, W.-T., 1993. Binding and localization of Mr 72,000 matrix metalloproteinase at cell surface invadopodia. *Cancer Research* 53, 3159–3164.
- Monteiro, P., Rossé, C., Castro-Castro, A., Irondelle, M., Lagoutte, E., Paul-Gilloteaux, P., Desnos, C., Formstecher, E., Darchen, F., Perrais, D., Gautreau, A., Hertzog, M., Chavrier, P., 2013. Endosomal WASH and exocyst complexes control exocytosis of MT1-MMP at invadopodia. *Journal of Cell Biology* 203, 1063–1079.
- Moodley, S., Bai, X.H., Kapus, A., Yang, B., Liu, M., 2015. XB130/Tks5 scaffold protein interaction regulates Src-mediated cell proliferation and survival. *Molecular Biology of the Cell* 26, 4492–4502.
- Motiwala, T., Jacob, S.T., 2006. Role of protein tyrosine phosphatases in cancer. *Progress in Nucleic Acid Research and Molecular Biology* 81, 297–329.
- Moynahan, M.E., Jasin, M., 2010. Mitotic homologous recombination maintains genomic stability and suppresses tumorigenesis. *Nature Reviews Molecular Cell Biology* 11, 196–207.
- Mueller, S.C., Ghersi, G., Akiyama, S.K., Sang, Q.X.A., Howard, L., Pineiro-Sanchez, M., Nakahara, H., Yeh, Y., Chen, W.T., 1999. A novel protease-docking function of integrin at invadopodia. *Journal of Biological Chemistry* 274, 24947–24952.
- Mundy, D.I., Li, W.P., Luby-Phelps, K., Anderson, R.G.W., 2012. Caveolin targeting to late endosome/lysosomal membranes is induced by perturbations of lysosomal pH and cholesterol content. *Molecular Biology of the Cell* 23, 864–880.
- Murphy, D.A., Courtneidge, S.A., 2011. The “ins” and “outs” of podosomes and invadopodia: characteristics, formation and function. *Nature Reviews Molecular Cell Biology* 12, 413–26.

- Nakahara, H., Howard, L., Thompson, E.W., Sato, H., Seiki, M., Yeh, Y., Chen, W.T., 1997. Transmembrane/cytoplasmic domain-mediated membrane type 1-matrix metalloprotease docking to invadopodia is required for cell invasion. *Proceedings of the National Academy of Sciences of the United States of America* 94, 7959–7964.
- Narayanan, I.V., Paulsen, M.T., Bedi, K., Berg, N., Ljungman, E.A., Francia, S., Veloso, A., Magnuson, B., Di Fagagna, F.D.A., Wilson, T.E., Ljungman, M., 2017. Transcriptional and post-transcriptional regulation of the ionizing radiation response by ATM and p53. *Scientific Reports* 2017 7:1 7, 1–11.
- Neve, A., Kumar, K.S., Tripolitsioti, D., Grotzer, M.A., Baumgartner, M., 2017. Investigation of brain tissue infiltration by medulloblastoma cells in an ex vivo model. *Scientific Reports* 2017 7:1 7, 1–12.
- Ohnishi, T., Matsumura, H., Izumoto, S., Hiraga, S., Hayakawa, T., 1998. A novel model of glioma cell invasion using organotypic brain slice culture. *Cancer Research* 58, 2935–2940.
- Oikawa, T., Oyama, M., Kozuka-Hata, H., Uehara, S., Udagawa, N., Saya, H., Matsuo, K., 2012. Tks5-dependent formation of circumferential podosomes/invadopodia mediates cell–cell fusion. *Journal of Cell Biology* 197, 553–568.
- Östman, A., Hellberg, C., Böhmer, F.D., 2006. Protein-tyrosine phosphatases and cancer. *Nature Reviews Cancer* 6, 307–320.
- Otani, Y., Ichikawa, T., Kurozumi, K., Inoue, S., Ishida, J., Oka, T., Shimizu, T., Tomita, Y., Hattori, Y., Uneda, A., Matsumoto, Y., Michiue, H., Date, I., 2017. Fibroblast growth factor 13 regulates glioma cell invasion and is important for bevacizumab-induced glioma invasion. *Oncogene* 2018 37:6 37, 777–786.
- Pallen, C.J., 2003. Protein Tyrosine Phosphatase alpha (PTP alpha): A Src family kinase activator and mediator of multiple biological effects. *Current Topics in Medicinal Chemistry* 3, 831–835.
- Park, C., Park, M., Kwak, H., Lee, H., Kim, M., Lee, S., Park, I., Rhee, C., Hong, S., 2006. Ionizing radiation enhances matrix metalloproteinase-2 secretion and invasion of Glioma cells through Src/Epidermal Growth Factor Receptor–Mediated p38/Akt and phosphatidylinositol 3-kinase/Akt signaling pathways. *Cancer Research* 66, 8511–19.
- Parthymou, A., Kardamakias, D., Pavlopoulos, I., Papadimitriou, E., 2004. Irradiated C6 glioma cells induce angiogenesis in vivo and activate endothelial cells in vitro. *International Journal of Cancer* 110, 807–814.
- Paterson, E.K., Courtneidge, S.A., 2018. Invadosomes are coming: new insights into function and disease relevance. *The FEBS Journal* 285, 8–27.
- Paz, H., Pathak, N., Yang, J., 2014. Invading one step at a time: The role of invadopodia in tumor metastasis. *Oncogene* 33, 4193–4202.
- Peláez, R., Pariente, A., Pérez-Sala, Á., Larrayoz, I.M., 2019. Integrins: Moonlighting proteins in invadosome formation. *Cancers* 11, 615.
- Pelkmans, L., Bürli, T., Zerial, M., Helenius, A., 2004. Caveolin-stabilized membrane domains as multifunctional transport and sorting devices in endocytic membrane traffic. *Cell* 118, 767–780.
- Pencheva, N., de Gooijer, M.C., Vis, D.J., Wessels, L.F.A., Würdinger, T., van Tellingen, O., Bernards, R., 2017. Identification of a druggable pathway controlling glioblastoma invasiveness. *Cell Reports* 20, 48–60.
- Petrone, A., 2003. Receptor protein tyrosine phosphatase is essential for hippocampal neuronal

- migration and long-term potentiation. *The EMBO Journal* 22, 4121–4131.
- Pignatelli, J., Bravo-Cordero, J.J., Roh-Johnson, M., Gandhi, S.J., Wang, Y., Chen, X., Eddy, R.J., Xue, A., Singer, R.H., Hodgson, L., Oktay, M.H., Condeelis, J.S., 2016. Macrophage-dependent tumor cell transendothelial migration is mediated by Notch1/Mena INV -initiated invadopodium formation. *Scientific Reports* 6, 37874.
- Planchon, D., Rios Morris, E., Genest, M., Comunale, F., Vacher, S., Biè Che, I., Denisov, E. V., Tashireva, L.A., Perelmuter, V.M., Linder, S., Chavrier, P., Bodin, S.S., Cécile Gauthier-Rouvière, C., 2018. MT1-MMP targeting to endolysosomes is mediated by upregulation of flotillins. *Journal of Cell Science* 131, jcs218925.
- Poincloux, R., Lizárraga, F., Chavrier, P., 2009. Matrix invasion by tumour cells: a focus on MT1-MMP trafficking to invadopodia. *Journal of Cell Science* 122, 3015–24.
- Pollard, E.C., Davis, S.A., 1970. The action of ionizing radiation on transcription (and translation) in several strains of *Escherichia coli*. *Radiation Research* 41, 375–399.
- Ponniah, S., Wang, D.Z., Lim, K.L., Pallen, C.J., 1999. Targeted disruption of the tyrosine phosphatase PTPalpha leads to constitutive downregulation of the kinases Src and Fyn. *Current Biology* 9, 535–8.
- Revach, O.-Y., Geiger, B., 2014. The interplay between the proteolytic, invasive, and adhesive domains of invadopodia and their roles in cancer invasion. *Cell Adhesion & Migration* 8, 215–25.
- Rieken, S., Habermehl, D., Mohr, A., Wuerth, L., Lindel, K., Weber, K., Debus, J., Combs, S.E., 2011. Targeting $\alpha v \beta 3$ and $\alpha v \beta 5$ inhibits photon-induced hypermigration of malignant glioma cells. *Radiation Oncology* 6, 132.
- Rieken, S., Habermehl, D., Wuerth, L., Brons, S., Mohr, A., Lindel, K., Weber, K., Haberer, T., Debus, J., Combs, S.E., 2012. Carbon ion irradiation inhibits Glioma cell migration through downregulation of integrin expression. *Radiation Oncology Biology* 83, 394–399.
- Roa, W., Brasher, P.M.A., Bauman, G., Anthes, M., Bruera, E., Chan, A., Fisher, B., Fulton, D., Gulavita, S., Hao, C., Husain, S., Murtha, A., Petruk, K., Stewart, D., Tai, P., Urtasun, R., Cairncross, J.G., Forsyth, P., 2004. Abbreviated course of radiation therapy in older patients with glioblastoma multiforme: A prospective randomized clinical trial. *Journal of Clinical Oncology* 22, 1583–1588.
- Sabeh, F., Ota, I., Holmbeck, K., Birkedal-Hansen, H., Soloway, P., Balbin, M., Lopez-Otin, C., Shapiro, S., Inada, M., Krane, S., Allen, E., Chung, D., Weiss, S.J., 2004. Tumor cell traffic through the extracellular matrix is controlled by the membrane-anchored collagenase MT1-MMP. *The Journal of Cell Biology* 167, 769–781.
- Sabeh, F., Shimizu-Hirota, R., Weiss, S.J., 2009. Protease-dependent versus-independent cancer cell invasion programs: Three-dimensional amoeboid movement revisited. *Journal of Cell Biology* 185, 11–19.
- Sahai, E., Marshall, C.J., 2003. Differing modes of tumour cell invasion have distinct requirements for Rho/ROCK signalling and extracellular proteolysis. *Nature Cell Biology* 5, 711–719.
- Sahin, M., Dowling, J.J., Hockfield, S., 1995. Seven protein tyrosine phosphatases are differentially expressed in the developing rat brain. *Journal of Comparative Neurology* 351, 617–631.
- Saini, P., Courtneidge, S.A., 2018. Tks adaptor proteins at a glance. *Journal of Cell Science* 131, jcs203661–6.

- Sakurai-Yageta, M., Recchi, C., Le Dez, G., Sibarita, J.B., Daviet, L., Camonis, J., D'Souza-Schorey, C., Chavrier, P., 2008. The interaction of IQGAP1 with the exocyst complex is required for tumor cell invasion downstream of Cdc42 and RhoA. *Journal of Cell Biology* 181, 985–998.
- Salvi, A., Thanabalu, T., 2017. Expression of N-WASP is regulated by HIF1 α through the hypoxia response element in the N-WASP promoter. *Biochemistry and Biophysics Reports* 9, 13–21.
- Samayawardhena, L.A., Pallen, C.J., 2008. Protein-tyrosine phosphatase alpha regulates stem cell factor-dependent c-Kit activation and migration of mast cells. *The Journal of Biological Chemistry* 283, 29175–85.
- Sap, J., D'Eustachio, P., Givol, D., Schlessinger, J., 1990. Cloning and expression of a widely expressed receptor tyrosine phosphatase. *Proceedings of the National Academy of Sciences of the United States of America* 87, 6112.
- Scherer, H.J., 1938. Structural development in gliomas. *The American Journal of Cancer* 34, 333–351.
- Schoumacher, M., Goldman, R.D., Louvard, D., Vignjevic, D.M., 2010. Actin, microtubules, and vimentin intermediate filaments cooperate for elongation of invadopodia. *Journal of Cell Biology* 189, 541–556.
- Scully, O.J., Bay, B.-H., Yip, G., Yu, Y., 2012. Breast cancer metastasis. *Cancer Genomics & Proteomics* 9, 311–20.
- Seals, D.F., Azucena, E.F., Pass, I., Tesfay, L., Gordon, R., Woodrow, M., Resau, J.H., Courtneidge, S.A., 2005. The adaptor protein Tks5/Fish is required for podosome formation and function, and for the protease-driven invasion of cancer cells. *Cancer Cell* 7, 155–165.
- Seals, D.F., Courtneidge, S.A., 2003. The ADAMs family of metalloproteases: multidomain proteins with multiple functions. *Genes & Development* 17, 7–30.
- Seiler, C., Davuluri, G., Abrams, J., Byfield, F.J., Janmey, P.A., 2012. Smooth muscle tension induces invasive remodeling of the zebrafish intestine. *PLoS Biol* 10, 1001386.
- Semple, B.D., Blomgren, K., Gimlin, K., Ferriero, D.M., Noble-Haeusslein, L.J., 2013. Brain development in rodents and humans: Identifying benchmarks of maturation and vulnerability to injury across species. *Progress in Neurobiology* 0, 1–16.
- Sharma, V.P., Eddy, R., Entenberg, D., Kai, M., Gertler, F.B., Condeelis, J., 2013. Tks5 and SHIP2 regulate invadopodium maturation, but not initiation, in breast carcinoma cells. *Current Biology* 23, 2079–2089.
- Shih, Y., Ly, P.T.T., Wang, J., Pallen, C.J., 2017. Glial and neuronal protein tyrosine phosphatase alpha (PTP α) regulate oligodendrocyte differentiation and myelination. *Journal of Molecular Neuroscience* 62, 329–343.
- Skelton, M.R., Ponniah, S., Wang, D.Z.-M., Doetschman, T., Vorhees, C. V, Pallen, C.J., 2003. Protein tyrosine phosphatase alpha (PTP α) knockout mice show deficits in Morris water maze learning, decreased locomotor activity, and decreases in anxiety. *Brain Research* 984, 1–10.
- Smith T, Yuan Y, Walker EV, Davis FG, 2019. Brain Tumour Registry of Canada (BTRC): Survival Report 2010-2015. A Surveillance Research Collaborative.
- Spinardi, L., Rietdorf, J., Nitsch, L., Bono, M., Tacchetti, C., Way, M., Marchisio, P.C., 2004. A dynamic podosome-like structure of epithelial cells. *Experimental Cell Research* 295, 360–374.

- Strong, M.S., Vaughan, C.W., Kayne, H.L., Aral, I.M., Ucmakli, A., Feldman, M., Healy, G.B., 1978. A randomized trial of preoperative radiotherapy in cancer of the oropharynx and hypopharynx. *The American Journal of Surgery* 136, 494–500.
- Strouthos, I., Karagiannis, E., Zamboglou, N., Ferentinos, K., 2022. High-dose-rate brachytherapy for prostate cancer: Rationale, current applications, and clinical outcome. *Cancer Reports* 5.
- Stuelten, C.H., Parent, C.A., Montell, D.J., 2018. Cell motility in cancer invasion and metastasis: insights from simple model organisms. *Nature Reviews Cancer* 18, 296–312.
- Stupp, R., Mason, W.P., van den Bent, M.J., Weller, M., Fisher, B., Taphoorn, M.J.B., Belanger, K., Brandes, A.A., Marosi, C., Bogdahn, U., Curschmann, J., Janzer, R.C., Ludwin, S.K., Gorlia, T., Allgeier, A., Lacombe, D., Cairncross, J.G., Eisenhauer, E., Mirimanoff, R.O., 2005. Radiotherapy plus Concomitant and Adjuvant Temozolomide for Glioblastoma. *New England Journal of Medicine* 352, 987–996.
- Stylli, S.S., Stacey, T.T.I., Verhagen, A.M., Xu, S.S., Pass, I., Courtneidge, S.A., Lock, P., 2009. Nck adaptor proteins link Tks5 to invadopodia actin regulation and ECM degradation. *Journal of Cell Science* 122, 2727–2740.
- Su, J., Muranjan, M., Sap, J., 1999. Receptor protein tyrosine phosphatase alpha activates Src-family kinases and controls integrin-mediated responses in fibroblasts. *Current Biology* 9, 505–11.
- Sun, G., Cheng, S.Y.S., Chen, M., Lim, C.J., Pallen, C.J., 2012. Protein tyrosine phosphatase α phosphotyrosyl-789 binds BCAR3 to position Cas for activation at integrin-mediated focal adhesions. *Molecular and Cellular Biology* 32, 3776–89.
- Sundahl, N., Duprez, F., Ost, P., De Neve, W., Mareel, M., 2018. Effects of radiation on the metastatic process. *Molecular Medicine* 24, 16.
- Sverdlov, M., Shajahan, A.N., Minshall, R.D., 2007. Tyrosine phosphorylation-dependence of caveolae-mediated endocytosis. *Journal of Cellular and Molecular Medicine* 11, 1239–1250.
- Tabiti, K., Smith, D.R., Goh, H.-S., Pallen, C.J., 1995. Increased mRNA expression of the receptor-like protein tyrosine phosphatase α in late stage colon carcinomas. *Cancer Letters* 93, 239–248.
- Tarone, G., Cirillo, D., Giancotti, F.G., Comoglio, P.M., Marchisio, P.C., 1985. Rous sarcoma virus-transformed fibroblasts adhere primarily at discrete protrusions of the ventral membrane called podosomes. *Experimental Cell Research* 159, 141–157.
- Tartaglia, M., Niemeyer, C.M., Fragale, A., Song, X., Buechner, J., Jung, A., Hählen, K., Hasle, H., Licht, J.D., Gelb, B.D., 2003. Somatic mutations in PTPN11 in juvenile myelomonocytic leukemia, myelodysplastic syndromes and acute myeloid leukemia. *Nature Genetics* 34:2 34, 148–150.
- Thompson, E.M., Neuwelt, E.A., Frenkel, E.P., 2011. The paradoxical effect of bevacizumab in the therapy of malignant gliomas. *Neurology* 76, 87.
- Tonks, N.K., 2006. Protein tyrosine phosphatases: From genes, to function, to disease. *Nature Reviews Molecular Cell Biology* 7, 833–846.
- Tonks, N.K., 2013. Protein tyrosine phosphatases: From housekeeping enzymes to master-regulators of signal transduction. *The FEBS Journal* 280, 346–378.
- Tonks, N.K., Diltz, C.D., Fischer, E.H., 1988. Purification of the major protein-tyrosine-phosphatases of human placenta. *Journal of Biological Chemistry* 263, 6722–6730.

- Turner, S.G., Ahmad, M., Toms, S.A., 2016. Mechanisms of Glioma Cell Invasion. In: Neurooncology - Newer Developments. InTech.
- van Eekelen, M., Runtuwene, V., Overvoorde, J., den Hertog, J., 2010. RPTP α and PTP ϵ signaling via Fyn/Yes and RhoA is essential for zebrafish convergence and extension cell movements during gastrulation. *Developmental Biology* 340, 626–639.
- van Zijl, F., Krupitza, G., Mikulits, W., 2011. Initial steps of metastasis: Cell invasion and endothelial transmigration. *Mutation Research/Reviews in Mutation Research* 728, 23–34.
- Vilalta, M., Rafat, M., Giaccia, A.J., Graves, E.E., 2014. Recruitment of circulating breast cancer cells is stimulated by radiotherapy. *Cell Reports* 8, 402–409.
- Vilalta, M., Rafat, M., Graves, E.E., 2016. Effects of radiation on metastasis and tumor cell migration. *Cellular and Molecular Life Sciences* 73, 2999–3007.
- Vollmann-Zwerenz, A., Leidgens, V., Feliciello, G., Klein, C.A., Hau, P., 2020. Tumor Cell Invasion in Glioblastoma. *International Journal of Molecular Sciences* 21.
- von Essen, C.F., 1991. Radiation enhancement of metastasis: a review. *Clinical & Experimental Metastasis* 9, 77–104.
- Von Wichert, G., Jiang, G., Kostic, A., De Vos, K., Sap, J., Sheetz, M.P., 2003. RPTP-acts as a transducer of mechanical force on α 3-integrin-cytoskeleton linkages. *Journal of Cell Biology* 161, 143–153.
- Walker, C., Mojares, E., Del Río Hernández, A., 2018. Role of extracellular matrix in development and cancer progression. *International Journal of Molecular Sciences* 19, 3028.
- Wang, J., Liu, B., Chen, X., Su, L., Wu, P., Wu, J., Zhu, Z., 2011. PTP1B expression contributes to gastric cancer progression. *Medical Oncology* 29, 948–956.
- Wang, P.-S., Wang, J., Zheng, Y., Pallen, C.J., 2012. Loss of protein-tyrosine phosphatase α (PTP α) increases proliferation and delays maturation of oligodendrocyte progenitor cells. *Journal of Biological Chemistry* 287, 12529–12540.
- Wang, P.S., Wang, J., Xiao, Z.C., Pallen, C.J., 2009. Protein-tyrosine phosphatase α acts as an upstream regulator of Fyn signaling to promote oligodendrocyte differentiation and myelination. *Journal of Biological Chemistry* 284, 33692–33702.
- Wang, X., Ma, D., Keski-Oja, J., Pei, D., 2004. Co-recycling of MT1-MMP and MT3-MMP through the trans-Golgi network: Identification of DKV582 as a recycling signal. *Journal of Biological Chemistry* 279, 9331–9336.
- Wang, Y., McNiven, M.A., 2012. Invasive matrix degradation at focal adhesions occurs via protease recruitment by a FAK-p130Cas complex. *Journal of Cell Biology* 196, 375–85.
- Wang, Y., Pallen, C.J., 1991. The receptor-like protein tyrosine phosphatase HPTP α has two active catalytic domains with distinct substrate specificities. *EMBO Journal* 10, 3231–3237.
- Wank, M., Schilling, D., Reindl, J., Meyer, B., Gempt, J., Motov, S., Alexander, F., Wilkens, J.J., Schlegel, J., Schmid, T.E., Combs, S.E., 2018a. Evaluation of radiation-related invasion in primary patient-derived glioma cells and validation with established cell lines: impact of different radiation qualities with differing LET. *Journal of Neuro-Oncology* 139, 583–590.
- Wank, M., Schilling, D., Schmid, T., Meyer, B., Gempt, J., Barz, M., Schlegel, J., Liesche, F., Kessel, K., Wiestler, B., Bette, S., Zimmer, C., Combs, S., Wank, Michaela, Schilling, D., Schmid, T.E., Meyer, B., Gempt, J., Barz, M., Schlegel, J., Liesche, F., Kessel, K.A., Wiestler, B., Bette, S., Zimmer, C., Combs, S.E., 2018b. Human Glioma migration and infiltration properties as a target for personalized radiation medicine. *Cancers* 10, 456.
- Ward, J.F., 1991. DNA Damage and Repair, Basic Life Sciences. Springer, Boston, MA.

- Weaver, A.M., 2009. Regulation of cancer invasion by reactive oxygen species and Tks family scaffold proteins. *Science signaling* 2, pe56.
- Wei, S.C., Fattet, L., Tsai, J.H., Guo, Y., Pai, V.H., Majeski, H.E., Chen, A.C., Sah, R.L., Taylor, S.S., Engler, A.J., Yang, J., 2015. Matrix stiffness drives epithelial-mesenchymal transition and tumour metastasis through a TWIST1-G3BP2 mechanotransduction pathway. *Nature Cell Biology* 17, 678–688.
- Weidmann, M.D., Surve, C.R., Eddy, R.J., Chen, X., Gertler, F.B., Sharma, V.P., Condeelis, J.S., 2016. MenaINV dysregulates cortactin phosphorylation to promote invadopodium maturation. *Scientific Reports* 6, 1–18.
- Whitehead, C.A., Nguyen, H.P.T., Morokoff, A.P., Luwor, R.B., Paradiso, L., Kaye, A.H., Mantamadiotis, T., Stylli, S.S., 2018. Inhibition of radiation and temozolomide-induced invadopodia activity in Glioma cells using FDA-approved drugs. *Translational Oncology* 11, 1406–1418.
- Wild-Bode, C., Weller, M., Rimner, A., Dichgans, J., Wick, W., 2001. Sublethal irradiation promotes migration and invasiveness of Glioma cells: Implications for radiotherapy of human Glioblastoma. *Cancer Research* 61, 2744–2750.
- Williams, K.C., Cepeda, M.A., Javed, S., Searle, K., Parkins, K.M., Makela, A. V., Hamilton, A.M., Soukhtehzari, S., Kim, Y., Tuck, A.B., Ronald, J.A., Foster, P.J., Chambers, A.F., Leong, H.S., 2019. Invadopodia are chemosensing protrusions that guide cancer cell extravasation to promote brain tropism in metastasis. *Oncogene* 38, 3598–3615.
- Williams, K.C., Coppolino, M.G., 2011. Phosphorylation of membrane type 1-matrix metalloproteinase (MT1-MMP) and its vesicle-associated membrane protein 7 (VAMP7)-dependent trafficking facilitate cell invasion and migration. *Journal of Biological Chemistry* 286, 43405–43416.
- Wisdom, K.M., Adebowale, K., Chang, J., Lee, J.Y., Nam, S., Desai, R., Rossen, N.S., Rafat, M., West, R.B., Hodgson, L., Chaudhuri, O., 2018. Matrix mechanical plasticity regulates cancer cell migration through confining microenvironments. *Nature Communications* 9, 4144.
- Wolf, K., Mazo, I., Leung, H., Engelke, K., Von Andrian, U.H., Deryugina, E.I., Strongin, A.Y., Bröcker, E.B., Friedl, P., 2003. Compensation mechanism in tumor cell migration: mesenchymal–amoeboid transition after blocking of pericellular proteolysis. *The Journal of Cell Biology* 160, 267–277.
- Wu, C.W., Kao, H.L., Li, A.F.Y., Chi, C.W., Lin, W. chang, 2006. Protein tyrosine-phosphatase expression profiling in gastric cancer tissues. *Cancer Letters* 242, 95–103.
- Xu, R., Yu, Y., Zheng, S., Zhao, X., Dong, Qinghua, He, Z., Liang, Y., Lu, Q., Fang, Y., Gan, X., Xu, X., Zhang, S., Dong, Qi, Zhang, X., Feng, G.-S., 2005. Overexpression of Shp2 tyrosine phosphatase is implicated in leukemogenesis in adult human leukemia. *Blood* 106, 3142–3149.
- Yamaguchi, H., Lorenz, M., Kempiak, S., Sarmiento, C., Coniglio, S., Symons, M., Segall, J., Eddy, R., Miki, H., Takenawa, T., Condeelis, J., 2005. Molecular mechanisms of invadopodium formation: The role of the N-WASP-Arp2/3 complex pathway and cofilin. *Journal of Cell Biology* 168, 441–452.
- Yamaguchi, H., Takeo, Y., Yoshida, S., Kouchi, Z., Nakamura, Y., Fukami, K., 2009. Lipid rafts and caveolin-1 are required for invadopodia formation and extracellular matrix degradation by human breast cancer cells. *Cancer Research* 69, 8594–8602.

- Yao, H., Zeng, Z.Z., Fay, K.S., Veine, D.M., Staszewski, E.D., Morgan, M., Wilder-Romans, K., Williams, T.M., Spalding, A.C., Ben-Josef, E., Livant, D.L., 2011. Role of $\alpha 5\beta 1$ integrin up-regulation in radiation-induced invasion by human pancreatic cancer cells. *Translational Oncology* 4, 282–292.
- Yoneda, T., Williams, P.J., Hiraga, T., Niewolna, M., Nishimura, R., 2001. A bone-seeking clone exhibits different biological properties from the MDA-MB-231 parental human breast cancer cells and a brain-seeking clone in vivo and in vitro. *Journal of Bone and Mineral Research* 16, 1486–1495.
- Yoo, K.C., Suh, Y., An, Y., Lee, H.J., Jeong, Y.J., Uddin, N., Cui, Y.H., Roh, T.H., Shim, J.K., Chang, J.H., Park, J.B., Kim, M.J., Kim, I.G., Kang, S.G., Lee, S.J., 2018. Proinvasive extracellular matrix remodeling in tumor microenvironment in response to radiation. *Oncogene* 37, 3317–3328.
- Yuan, Y., Shi, Q., Li, M., Nagamuthu, C., Andres, E., Davis, F.G., 2016. Canadian brain cancer survival rates by tumour type and region: 1992-2008. *Can J Public Health* 107, 37–42.
- Zeng, L., Si, X., Yu, W.-P., Le, H.T., Ng, K.P., Teng, R.M.H., Ryan, K., Wang, D.Z.-M., Ponniah, S., Pallen, C.J., 2003. PTP alpha regulates integrin-stimulated FAK autophosphorylation and cytoskeletal rearrangement in cell spreading and migration. *Journal of Cell Biology* 160, 137–46.
- Zeng, Q., Dong, J.-M., Guo, K., Li, J., Tan, H.-X., Koh, V., Pallen, C.J., Manser, E., Hong, W., 2003. PRL-3 and PRL-1 promote cell migration, invasion, and metastasis. *Cancer Research* 63, 2716–2722.
- Zhang, X., Wang, X., Xu, R., Ji, J., Xu, Y., Han, M., Wei, Y., Huang, B., Chen, A., Zhang, Q., Li, W., Wang, J., Li, X., Qiu, C., 2018. YM155 decreases radiation-induced invasion and reverses epithelial-mesenchymal transition by targeting STAT3 in glioblastoma. *Journal of Translational Medicine* 16, 79.
- Zhao, P., Xu, Y., Wei, Y., Qiu, Q., Chew, T.L., Kang, Y., Cheng, C., 2016. The CD44s splice isoform is a central mediator for invadopodia activity. *Journal of Cell Science* 129, 1355–1365.
- Zheng, X., Resnick, R.J., Shalloway, D., 2008. Apoptosis of estrogen-receptor negative breast cancer and colon cancer cell lines by PTP alpha and src RNAi. *International Journal of Cancer* 122, 1999–2007.
- Zheng, X.M., Wang, Y., Pallen, C.J., 1992. Cell transformation and activation of pp60 c-src by overexpression of a protein tyrosine phosphatase. *Nature* 359, 336–339.
- Zhou, X., Coad, J., Ducatman, B., Agazie, Y.M., Coad, Z.X., Agazie, D.B., 2008. SHP2 is up-regulated in breast cancer cells and in infiltrating ductal carcinoma of the breast, implying its involvement in breast oncogenesis. *Histopathology* 53, 389–402.
- Zhu, S., Bjorge, J.D., Fujita, D.J., 2007. PTP1B contributes to the oncogenic properties of colon cancer cells through Src activation. *Cancer Research* 67, 10129–10137.
- Zimmerman, M.W., Homanics, G.E., Lazo, J.S., 2013. Targeted deletion of the metastasis-associated phosphatase Ptp4a3 (PRL-3) suppresses murine colon cancer. *PLoS ONE* 8, e58300.
- Zimnicka, A.M., Husain, Y.S., Shajahan, A.N., Sverdlov, M., Chaga, O., Chen, Z., Toth, P.T., Klomp, J., Karginov, A. V., Tirupathi, C., Malik, A.B., Minshall, R.D., 2016. Src-dependent phosphorylation of caveolin-1 Tyr-14 promotes swelling and release of caveolae. *Molecular Biology of the Cell* 27, 2090–2106.

Appendix: Supplemental Tables

A1. List of investigated cell lines.

Cell Line	Tumour Type	Patient Age	Sex	Year Established	Catalog Number
MDA-MB-231	Breast Adenocarcinoma	51	Female	n.s.	ATCC, #HTB-26
LN229	Glioblastoma	60	Female	1979	ATCC, #CRL-2611
U87-MG	Glioblastoma	n.s.	Male	1966	ATCC, #HTB-14
LN18	Glioblastoma	65	Male	1976	ATCC, #CRL-2610
U251-MG	Glioblastoma	75	Male	n.s.	---
U343-MG	Glioblastoma	54	Male	n.s.	---

* n.s. = information not stated.

** U251 and U343 cell lines were a gift from Dr. Stephen Yip's lab at BC Cancer, Vancouver, Canada.

A2. Troubleshooting guide for the *ex vivo* brain slice spheroid invasion assay.

Issue	Possible Causes	Solutions
Large cuts along sides of the brain slices.	(i) Cutting into the side of the brain during removal.	(i) Use curved scissors to cut along the side of the skull pointing outward to avoid the brain.
Brain slices fall apart during transfer steps.	(i) Incorrect placement of the spatula.	(i) Use a spatula with a wide, flat end to scoop up the brain slice. Be sure to place the spatula directly in the center of the slice before lifting.
Fragmented z-sections.	(i) The agar block was glued to the platform at an angle resulting in the blade skipping. (ii) One side of the brain slice is too close to the edge of the agar block. (iii) The z-section is too thin and is falling apart.	(i) Remove the agar block from the platform and re-glue such that the top of the block is perfectly perpendicular to the platform. (ii) Ensure there is sufficient agar on the top and bottom of the brain slice when embedding into agar block. (iii) Increase the thickness of each z-slice.
Spheroid appears too small.	(i) Imaging the edge of the spheroid.	(i) When z-sectioning the brain slice, parts of the same spheroid will appear in multiple z-sections. Thus, if the spheroid appears too small, image the surrounding z-sections to get a more representative sample.
Spheroid is too large and fills the entire z-section of brain slice.	(i) Spheroid too large for the thickness of the brain slice. (ii) Tumour type is highly invasive. (iii) Slice is too thin for the size of the spheroid.	(i) Decrease the initial size of the spheroids. (ii) Decrease the length of the invasion assay. (iii) Increase the slice thickness to 400 μm to create more space.
Spheroid appears out of focus when imaging.	(i) A bubble formed around the spheroid when placing coverslip over z-sections.	(i) Remove the coverslip, blot excess PBS with a Kimwipe™, and replace coverslip to remove bubbles.